AD-A128 721 A REVIEW OF FATIGUE CRACK GROWTH IN METALLICS AT LOW STRESS INTENSITIES(U) FINMET CONSULTANTS EDGBASTON (ENGLAND) C J BEEVERS 01 JAN 83 EOARD-TR-83-10 1/2

UNCLASSIFIED F49620-82-C-0088 F/G 20/11 NL

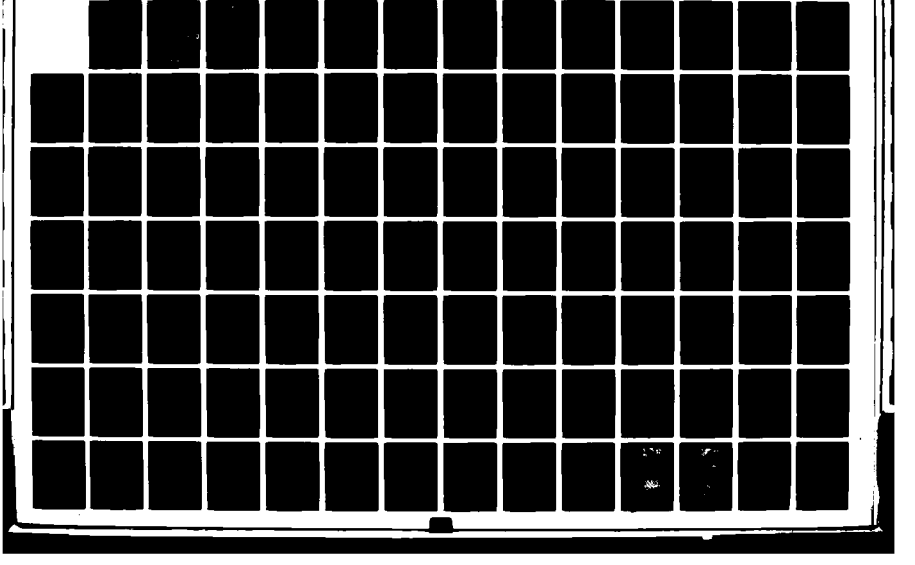

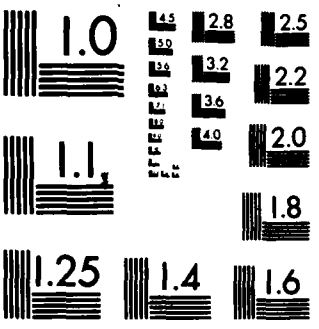

MICROCOPY RESOLUTION TEST CHART
NATIONAL BUREAU OF STANDARDS-1963-A

F 49620-82-C-0088

A REVIEW OF FATIGUE CRACK GROWTH IN METALLICS AT LOW STRESS INTENSITIES

C.J. BEEVERS

Finmet Consultants,
104, Carpenter Road,
Birmingham, B15 2JU,
U.K.

1st January, 1983.

Final Scientific Report (1st July 1982 - 31st December 1982).

Prepared for

EUROPEAN OFFICE OF AEROSPACE RESEARCH AND DEVELOPMENT

London, England.

SECURITY CLASSIFICATION OF THIS PAGE (When Data Entered)

REPORT DOCUMENTATION PAGE

READ INSTRUCTIONS BEFORE COMPLETING FORM

1. REPORT NUMBER: F 49620-82-C-0088
2. GOVT ACCESSION NO.: -
3. RECIPIENT'S CATALOG NUMBER: FM-A3

EOARD-TR-83-06

4. TITLE (and Subtitle): A Review of Fatigue Crack Growth in Metallics at Low Stress Intensities.

5. TYPE OF REPORT & PERIOD COVERED: Final Scientific Report (1 July 1982 - 31 December 1982).

6. PERFORMING ORG. REPORT NUMBER: -

7. AUTHOR(s): C.J. Beevers.

8. CONTRACT OR GRANT NUMBER(s): -

9. PERFORMING ORGANIZATION NAME AND ADDRESS: Finmet Consultants, 104, Carpenter Road, Birmingham, B15 2JU, U.K.

10. PROGRAM ELEMENT, PROJECT, TASK AREA & WORK UNIT NUMBERS: -

11. CONTROLLING OFFICE NAME AND ADDRESS: Major J. Marsh, European Office of Aerospace Research and Development, London, U.K.

12. REPORT DATE: 1st January, 1983.

13. NUMBER OF PAGES: 113

14. MONITORING AGENCY NAME & ADDRESS (if different from Controlling Office): AFOSR, Bolling 410, Bolling AFB, DC 20332.

15. SECURITY CLASS. (of this report): Unclassified

15a. DECLASSIFICATION/DOWNGRADING SCHEDULE -

16. DISTRIBUTION STATEMENT (of this Report)

DISTRIBUTION STATEMENT A
Approved for public release;
Distribution Unlimited

17. DISTRIBUTION STATEMENT (of the abstract entered in Block 20, if different from Report): -

18. SUPPLEMENTARY NOTES: -

19. KEY WORDS (Continue on reverse side if necessary and identify by block number)

Fatigue crack growth (fcg) Stress Intensity, Fatigue Thresholds, Metals Crack Length, Aluminium Alloys, Steels, Titanium Alloys.

20. ABSTRACT (Continue on reverse side if necessary and identify by block number)

This review is concerned with the fatigue crack growth response of metallics at low stress intensities. In particular the fatigue threshold e.g. the stress intensity at which cracks can arrest is considered in detail. The fatigue crack growth rates and the fatigue threshold stress intensity

DD FORM 1 JAN 73 1473 EDITION OF 1 NOV 65 IS OBSOLETE

SECURITY CLASSIFICATION OF THIS PAGE (When Data Entered)

ΔK_{th} are considered in relation to the following variables, mean stress, yield stress, test temperature, test frequency, fatigue crack closure, microstructure, environment and crack length. The mechanisms, models and formulations derived to represent fatigue crack growth at low stress intensities and the fatigue threshold are also reviewed. The measurement of fatigue crack growth rates and fatigue thresholds is outlined and the desirability of obtaining ΔK_{eff} data is highlighted. The main characteristics of aluminium alloys, steels and titanium alloys with respect to fatigue crack growth and fatigue thresholds are presented.

A conservative view of the fcg resistance of metals and alloys is developed which allows the identification of the minium fatigue threshold and maximum fcg rates that can be experienced for a particular set of test conditions.

PREFACE

This document looks at a small part of a much larger problem, namely, how to live successfully with cyclic loading. Much of the life of surface initiated and small subsurface cracks is spent where the stress intensity is below the knee in the fatigue crack growth curve. Thus an improvement in our understanding, modelling and predictive capability in this area should be helpful in determining the "life" of a defective component.

The review develops the role of yield stress, mean stress, microstructure, environment, test temperature, frequency and fatigue crack closure in relation to fatigue crack growth. It was not possible, mainly due to the interactive nature of many of the above variables to present a unified model for fatigue crack growth at low stress intensities. However, a conservative view on the fatigue crack growth resistance of materials is developed. This involves a clear understanding of the role of fatigue crack closure and the presentation of information in a form which exhibits the minimum fatigue threshold and maximum fatigue crack growth rates that can be experience in a grain set of conditions.

TABLE OF CONTENTS

LIST OF ILLUSTRATIONS

LIST OF TABLES

LIST OF SYMBOLS

a	Crack length.
B	Specimen thickness.
b	Asperity width.
C	Distance from asperity to crack tip.
COD	Crack opening displacement.
da/dN	Fatigue crack growth rate.
D	Grain diameter.
E	Young's modulus.
e	Compression of asperity.
FCG	Fatigue crack growth.
FCP	Fatigue crack propagation
G	Rigidity modulus.
K	Stress intensity factor
K_I	Total stress intensity factor.
$K_{I(local)}$	Stress intensity from local force.
$K_{I(global)}$	Stress intensity from external force.
K_{max}	Maximum stress intensity.
K_{min}	Minimum stress intensity
K_{CL}	K_I when $K_{I(global)} = 0$.
k'	Cyclic strain hardening coefficient.
L	Aperity height.
LCF	Low cycle fatigue.
MDZ	Microstructural deformation zone.
n'	Cyclic strain hardening exponent.
N	Number of cycles.
N_f	Number of cycles to failure

P	Local crack face force.
Q, Q_{max}, Q_{min}	General load, maximum and minimum points in applied load range.
Q^1, $Q^1_{(open)}$	Opening load for fully elastic case.
Q^2, $Q^2_{(open)}$	Opening load for plasticity corrected case.
Q^3, $Q^3_{(open)}$	Observed opening load.
R	Stress ratio.
R_p	Plastic zone radius.
RPZ	Reverse plastic zone.
r	Polar co-ordinate distance.
$U_2(r,)$, $U_2(c)$, $U_2(global)$ $U_2(local)$	Vertical displacements.
$\Delta\varepsilon$	Total strain range.
$\Delta\varepsilon_p$	Plastic range ahead of the crack tip for a continuum.
$\Delta\bar{\varepsilon}_e$	Elastic component of the strain $\Delta\bar{\varepsilon}$.
$\Delta\varepsilon_p$	Plastic component of the strain $\Delta\bar{\varepsilon}$.
$\Delta\varepsilon_{pn}$	Plastic strain range for the n-th echelon of MDZ.
$\Delta\varepsilon_{pth}$	Threshold plastic strain range.
ΔK	Stress intensity factor range.
ΔK_{th}	Threshold stress intensity.
$\Delta\sigma$	Applied stress range.
ε_f	Monotonic fracture strain.
ε_y	Cyclic yield strain.

ρ^*	Microstructural parameter from the Majumdar and Morrow equation.
ρ'	Size of an MDZ.
$\bar{\rho}_n'$	Average size of the MDZs in the n-th echelon
w	Specimen width.
θ	Polar co-ordinate angle.
ν	Poisson's ratio.
σ_y	Yield stress.
σ_{yc}	Cycled yield stress.

I. INTRODUCTION

The influence on fatigue crack growth rate of the cyclic stress intensity range ΔK is characterised by a three stage curve (Fig. 1). This report is concerned specifically with region A, namely the lower fatigue crack rates region and the fatigue threshold ΔK_{th}. The existence of an absolute threshold ΔK for crack arrest is undoubtably of academic interest but for the purpose of this report and for most practical applications the fatigue threshold can be considered as the ΔK associated with a fatigue crack growth rate of 10^{-8} mm/cycle. The shape of the log da/dN vs log ΔK curve in region A will determine to a large extent the lifetime of many growing fatigue cracks. The position of the curve is primarily determined by the lower bound ΔK_{th} and the magnitude of ΔK at which reverse plasticity dominated fcg (fatigue crack growth) occurs. Superimposed upon these two factors are variables such as environment and test temperature, which can substantially influence the shape of the curve in the intervening ΔK range of region A. As the plasticity dominated fcg regime (region B) is relatively insensitive to many tests and material variables attention is naturally focussed on the factors influencing ΔK_{th}.

The report considers variables such as mean stress, environment, microstructure, yield strength, crack closure, test temperature, frequency, loading modes, crack length. The threshold concept and the development of fcg laws incorporating ΔK_{th} are presented. The particular characteristics of aluminium alloys steels and titanium alloys are then considered in separate sections.

II. THE CHARACTERISTICS OF FCG AT LOW STRESS INTENSITIES

In region B (Fig. 1) fatigue crack growth is characterised by extensive reverse plasticity at the crack tip which in some aluminium alloys results in a striated fatigue fracture surface. The crack face opening displacement are generally of a similar mode to that imposed externally upon the specimen, for most cases this is Mode I. The crack front remains macroscopically uniform and the crack faces relatively smooth except for shear lip formation. Providing that the crack tip plasticity remains effectively contained within the specimen LEFM offers a good route for data analysis and rationalisation. In region A (Fig. 1) the lower ΔK values lead to crack tip plastic zone sizes approaching the microstructural element size and the growth rate becomes sufficiently slow for extensive environmental activity to occur.

The containment of the reverse plastic zone within say individual grains has the following consequences. The plasticity at the crack tip is highly anisotropic and dependent upon the orientation of the grain with respect to the principal stress axis. Where an alternating slip mechanism for crack extension operates e.g. {111} slip leading to separation on {001} planes the {001} plane orientation to the stress axis will be determined by the grain orientation. Thus, in the circumstances where the grain orientations are random along the crack front the crack advances with a substantial mode II component. Thus a macroscopic non-coplanar crack front can develop with different modes of growth and growth rates in individual grains. These particular features are well illustrated in titanium alloys (1.2).

Figure 2 represents the three principal orientations that can be presented to the crack front by individual grains in α-titanium. In the growth rate range of 10^{-5} mm/cycle the three orientations lead to quite different modes of crack extension. For orientation (a) striations are found (Fig. 3). The striation spacing being equal to the measured fatigue crack growth rate. For orientation (b) a furrow mode of crack growth was observed (Fig. 4). The mode of growth involved extensive plastic flow with the upper ridges representing regions of plastic tearing. For orientation (c) separation occured on the basal plane (0001) Fig. 5. This form of separation has been given several different terminologies, pseudo-cleavage, fatigue cleavage, fatigue facets, the latter name will be used in this report. In other metals and alloys faceting also occurs on crystallographic planes e.g. aluminium alloys separate on {111} and {100} planes. The occurrence of these crystallographic facets during transgranular fatigue crack growth is reviewed in (3).

The results of crystallographic plane identification are presented in Table I. In the fcc metals, aluminium and nickel, planes of the {001} and {111} type are reported whilst in close packed hexagonal titanium the planes are dominantly (0001). In body centred cubic iron the facet plane was reported as {001}.

The overall consequence of these faceted modes of crack growth is that an irregular crack trajectory develops which in association with Mode II displacements can lead to extensive crack closure (4). The extent of the faceting can be enhanced by active environments and reduced by inert environments such as a vacuum of 5×10^{-6} torr.

In steels with a dominantly ferritic or austenitic grain structure the occurrence of faceting has been reported (5). For quenched and tempered steels the observations are somewhat different. Intergranular separation along the prior austenite grain boundaries is observed (Fig. 6) with associated regions of ductile tearing. The variation in the extent of intergranular separation with ΔK is illustrated in Figure 7. In active environments, e.g. laboratory air, corrosion deposits on the fatigue fracture surface of these steels have been reported (6). Recent studies have reported the measurements of oxide layer thickness in air and hydrogen environments and concluded that the oxide build up results in substantial crack closure (7).

In conclusion, fatigue crack growth at low ΔK's results in some highly identifiable features on the fracture surfaces. The microstructural and environmental interactions lead to crack closure becoming significant in this regime. Thus, the observed fatigue crack growth rates and thresholds can be expected to be influenced by mean stress levels, microstructure and testing environments.

III. THE ROLE OF MEAN STRESS

The mean stress level or R ratio ($\sigma_{min}/\sigma_{max}$) can have a marked effect upon the fcg rates and fatigue thresholds. In general, the fcg is sustained to lower ΔK levels and ΔK_{th} is decreased as R increases. This feature is illustrated in Figure 8 for a high strength aluminium zinc-magnesium alloy (7075T351) tested in laboratory air and vacuum (8). The

observations in Figures 9 and 10 show the R dependence in laboratory air and vacuum for high strength aluminium alloys and for a high strength steel (6,8). These observations and others of a similar nature (9,10) have led to the suggestion that the R dependence originates from environmental factors. The alternative viewpoint is that the phenomena is created by the occurrence of crack closure (11).

The representation of the mean stress effect was initially proposed by Lukas and Klesnil (12)

$$\Delta K_{th} = \Delta K_{th(o)} \ (1-R)^{\gamma} \qquad \ldots (1)$$

where $\Delta K_{th(o)}$ is the nominal value of ΔK_{th} at R=0. The values of γ for a range of alloys and test conditions are presented in Table 2. The main trend to be noted is that γ tends to zero in vacuum, that is the threshold condition occurs at a constant value of ΔK independent of mean stress. In laboratory air the value of γ can approach unity which indicates threshold is achieved at a constant value of K_{max}.

A series of relationships between ΔK_{th} and R have been developed and reported. For BS 15 (13) the following relationship was considered appropriate.

$$\Delta K_{th} = \Delta K_{th(o)} \left[(-R^2)\right]^{\frac{1}{2}} \qquad \ldots (2)$$

In HY 130 tested in salt water Vosikovsky (14) showed the following relationship to fit the data; when B is a material constant

$$\Delta K_{th} = \Delta K_{th(o)} + BR \qquad \ldots (3)$$

An alternative relationship suggested by Barsom (15) is presented in Equation 4.

$$\Delta K_{th} = \Delta K_{th(o)} \ (1-\beta R) \qquad \ldots (4)$$

where β is a constant.

Other relationships between ΔK_{th} and R have been developed in recent years. McEvily (16) proposed the following formulation

$$\Delta K_{th} = \Delta K_{th(o)} \left[\frac{(1-R)}{(1+R)}\right]^{\frac{1}{2}} \qquad \ldots (5)$$

Wei and McEvily (17) suggested the relationship in Equation 6.

$$\Delta K_{th} = \frac{\Delta K_{th(o)} K_c (1-R)}{(1-R)K_c + R\Delta K_{th(o)}} \qquad \ldots (6)$$

The formulation in Equation 7 was proposed by Davenport and Brook (18)

$$\Delta K_{th} = \Delta K_{th(o)} \left[\frac{(K_c - K_{max})(1-R)}{K_c - \Delta K_{th(o)}}\right]^{\alpha} \qquad \ldots (7)$$

The relationship in Equations 1 to 7 predict a decrease in ΔK_{th} with increasing values of R. The physical processes which lead to this dependence were mentioned earlier and include crack closure, environmental effects and the detailed failure process in the crack tip zone. Thus, the precise form of the R dependence of ΔK_{th} will depend upon these parameters. The variation of the R dependence for steels is illustrated in Figure 11 (19). The spread in the data is considerable and to

be expected in view of the wide range of alloys involved. The effect of environment (CO_2 and vacuum) on the ΔK_{th} values for a mild steel and weld metal are presented in Fig. 12 (20). The vacuum data is relatively insensitive to R whilst in CO_2 data is strongly R dependent. A further example of environmental influence is presented in Fig. 13 (21). The authors attribute the higher ΔK_{th} at lower R ratios to the more active environments and to the formation of oxide debris with increased levels of crack closure. The R dependence of ΔK_{th} can also be influenced by grain size (22,23) as illustrated in Fig. 14 for results obtained from AlSl 316 stainless steel. The plot would indicate a higher γ value for the coarser grain sized material.

The plots and data so far have been presented in a form which assumes γ is constant in say equation 1 over the whole range of R. The results of Usami (19) show that for $R>0.75$, ΔK_{th} no longer exhibits a linear relationship with R. The data presented in Fig. 15 shows results obtained from a wide range of metal and alloys including steels, aluminium alloys and titanium alloys. The data, as might be expected is partly normalised by dividing ΔK_{th} by Youngs Modulus E.

It may be observed that a relationship as in Equations 1-5 will describe the R dependence of ΔK_{th} over a limited R range and γ will be influenced by such factors as microstructure, environment and the occurrence and extent of crack closure.

If a wider R range has to be encompassed and particularly for $R>0.75$ then a relationship of the form in Equations 6 and 7 is desirable. In this case α will be susceptible to the same variables as γ in Equation 1.

IV. THE EFFECT OF ENVIRONMENT

In discussing the role of environment it is worthwhile considering some of the basic aspects in what is a complex situation. Environmental factors can influence both ΔK^{i}_{th} (the intrinsic contribution to ΔK_{th}) and ΔK^{c}_{th} (the crack closure contribution to ΔK_{th}). The two components contribute to the measured value of ΔK_{th} (29).

$$\Delta K_{th\,(measured)} = \Delta K^{i}_{th} + \Delta K^{c}_{th} \qquad \ldots (8)$$

in the general literature the relationship in Equation 9 is

$$\Delta K_{eff} = \Delta K - \Delta K_{CL} \qquad \ldots (9)$$

often used to represent the active ΔK at the crack tip, namely ΔK_{eff}. ΔK^{i}_{th} is then the effective ΔK at the crack tip under threshold conditions.

Both ΔK^{i}_{th} and ΔK^{c}_{th} can be influenced by environmental situations involving the access of embrittling agents into the crack tip process zone. A classical embrittling agent such as hydrogen may be involved but other gases and liquids can also reduce the effective surface energy for crack extension and hence the ΔK^{i} level required to sustain crack growth is also reduced. A consequence of the embrittlement is to encourage separation on close packed crystallographic planes as discussed in section 2. The consequence of this embrittlement may be the occurrence of crack branching and out of plane crack trajectories which could increase the closure component ΔK^{c}. Thus, whilst ΔK^{i}_{th} may be reduced by environmental activity ΔK^{c}_{th} can be increased and the resulting balance namely, ΔK_{th} is difficult to predict with any certainty.

In order to understand more fully the environmental factors several authors have tested in vacuum ($<10^{-5}$ torr) to establish an inert environment (6,8,9,20,25,26,27). A typical example of the results of these tests is presented in Figure 16 for a high strength steel. For da/dN > 10^{-6} mm/cycle the fcg rate in laboratory air is a factor of 10 faster than in vacuum. This can probably be accounted for by a lower ΔK^i in laboratory air compared with vacuum and ΔK^c being fairly small at the ΔK level. Below a fcg rate of 10^{-6} mm/cycle the data converges and the indications are that the growth rate is faster in vacuum than air for the low R condition. A possible explanation for this is the increased environmental activity at the low growth rates in air leading to microstructural sensitive growth and oxide formation with a resultant increase in the ΔK^c component and a decrease in the fcg rate. It should be noted that where a high mean stress is imposed and the closure contribution is small the fcg rate in air remains substantially higher than in vacuum.

The mean stress effect considered in section 3 was strongly linked to the environmental factor and the results in Table II show the effect on γ in Equation 1 of the test environment. It may well be appropriate to use the fcg data obtained from vacuum tests when assessing the behaviour of defects initiated and growing within the internal regions of a structure.

The role of different gases on the fcg rates and ΔK_{th} has been reported by Stewart (26), Priddle (20), Suresh et al. (7) and Petit and Zeghloul (28). The effects of gaseous environments such as dry air, dry hydrogen, lab air, water vapour and steam are illustrated in Figure 13. The more hostile environments showed a stronger R dependence and this arose mainly from higher

ΔK_{th} values at the lower R regions. The results in Figure 17 show the relative influences of hydrogen, vacuum and water vapour on a 4130 steel (29). The results of Priddle (20) show the substantial range of ΔK_{th} that can result from testing over a range of temperatures in a Co_2 environment. Petit and Zeghloul (28) studied the influence of air, vacuum and nitrogen environments on the fcg and ΔK_{th} behaviour of several high strength aluminium alloys. These authors and others (7,26,30) in their consideration of the results discuss the role of corrosion debris and its influence on crack closure. Suresh et al. (7) have shown that the oxide layer builds up more substantially in air than in hydrogen. The closure contribution from the oxide build up may explain the difference in fcg and ΔK_{th} observed in air and hydrogen.

The specific effect of a particular environment is difficult to predict due to the interactive nature of ΔK^{i}_{th} and ΔK^{c}_{th}. At high mean stresses R (>0.5) non-inert environments can lead to substantial increases in fcg rates and the lowering of ΔK_{th}. At low mean stresses the resulting behaviour is more complex.

The ΔK^{c} contribution can be influenced by the asperities which form as a result of faceted fcg and the development of oxide layers. These physical features might be expected to reduce the access of active environments to the crack tip and hence also lead to an increase ΔK^{i}_{th}. To illustrate the complexity of this problem the results of Suresh et al. (7) show the reverse of the above statement, namely that much more oxide debris build up occurs at low compared with high mean stresses.

V. THE INFLUENCE OF METALLURGICAL VARIABLES

5.1 Grain Size

It has been observed that grain size can have a marked influence on fcg rates at low ΔK's and ΔK_{th} in a wide range of metals and alloys (1,2,3,22,23,25,30,31).

In general the effect is significant where the fcg is dominantly transgranular in a metal or alloy with a well defined grain structure.

In most instances the relationship

$$\Delta K_{th} = \Delta K_o + kd^{\frac{1}{2}} \qquad \ldots (10)$$

is observed, where ΔK_o is the fatigue threshold ΔK_{th} at a nominal zero grain size, k is a constant and d is the grain size. The Hall-Petch relationship between yield stress σ_y and grain size d is

$$\sigma_y = \sigma_o + k_y d^{-\frac{1}{2}} \qquad \ldots (11)$$

where σ_o is the yield when $d \to \infty$ and k_y is a material constant. Thus, whilst the yield stress decreases with increasing grain size the ΔK_{th} increases. This point is worth examining a little further. The value of σ_y is controlled by the elastic/plastic transition or yielding of a substantial number of grains in a polycrystalline aggregate. At ΔK_{th} in almost all metals and alloys the plastic zone ahead of the crack tip is smaller than the containing grain size. Thus, the crack tip plasticity does not experience any first order grain size effects. Thus, the parameter most likely to influence the yielding at the crack tip is σ_o in Equation 11 and not k_y.

The results of Priddle (22) in Figure 14 and the observations of Masounave and Bailon (23) indicate an increasing γ value in Equation 1 for the coarser grain size material. Examination of the data shows that γ is not as sensitive to grain size as the lines indicate. Some recent data on nickel alloys (32) shows that γ is virtually independent of grain size.

In a study of the fatigue of α-titanium the author (1) came to the conclusion that in the low fcg region where facet formation predominated, the mode of crack extension was bi-modal with the formation of ligaments behind the crack front. On average the coarser the grain size the larger the ligament size and a higher ΔK^i required to sustain crack growth. A similar view on the role of ligaments has also been presented by Gerberich and Moody (33).

For coarser grain size material with a facet formation mode of fcg the extent of out of plane crack trajectory increases with the possibility of a greater crack closure contribution to ΔK_{th}. Thus, for long crack configurations (crack length > 5-10 grain diameter) there are two possible contributions to the grain size effect on ΔK_{th}. The results of Taira et al. (34) illustrate this point from tests on low carbon steel (Figure 18). The major contribution to ΔK_{th} comes from ΔK^c_{th}. If Equation 10 is represented in the form

$$\Delta K^i_{th} = \Delta K^i_o + k^i . d^{\frac{1}{2}} \qquad \ldots (12)$$

$$\Delta K^c_{th} = \Delta K^c_o + k^c \, d^{\frac{1}{2}} \qquad \ldots (13)$$

then $\Delta K^c_o > \Delta K^i_o$ and $k^c > k^i$. These results suggest that grain size has a more progressive influence on the closure contribution than the ligament factor in determining ΔK_{th}.

Conventionally refining the grain size improves the static yield strength and the fatigue limit. In so far as the fatigue limit is associated with a crack initiation process involving the probability of nucleating cracks through slip activity the above correlation is acceptable. If ΔK_{th} is related to the arrest of a propagating crack then the grain size trend is also understandable and there is no real conflict in the opposing trends for ΔK_{th} and the fatigue limit with grain size.

5.2 Other Microstructural Features

In high strength (σ_y > 1000 MPa) 300 M steels the tempering temperature has a marked influence on the low fcg rates and ΔK_{th}. This effect is more marked at R=0.1 than R=0.7. (Figures 19a and 19b (35)). The ΔK_{th} value increased with increasing tempering temperature but decreased with increasing yield stresses.

In steels with duplex microstructure it has been shown (36) that a continuous martensitic phase with island ferrite leads to higher ΔK_{th} values than if the ferrite is continuous.

The role of inclusions is not fully understood. In mild steels where the inclusions can be heavily aligned in the rolling direction the steel can exhibit a marked anisotropy of ΔK_{th}, in medium strength steels the results are not so consistent (37,38). For cases where the yield stress increases with a constant grain size, ΔK_{th} increases with yield strength (39,40).

VI. INFLUENCE OF YIELD STRENGTH ON ΔK_{th}

There are several aspects of the influence of yield strength on fcg and ΔK_{th} to be considered.

If the extension of a crack is controlled by the crack tip opening displacement (CTOD) then

$$\Delta(\text{CTOD}) = \frac{B\Delta K^m}{4\sigma_y E} \qquad \ldots (14)$$

the above relationship would indicate, other factors being constant, that with increasing Youngs Modulus E, and yield stress σ_y, the Δ(CTOD) would decrease and hence the related fcg rate. This feature has been illustrated for a range of metals and alloys and in particular by the normalisation of $\Delta K/E$ versus da/dN curves.

If the threshold condition is that a critical Δ(CTOD) must be exceeded for crack growth then

$$\Delta K_{th} \sim B'(E\sigma_y)^{\frac{1}{2}} \qquad \ldots (15)$$

That is, the fatigue threshold is increased as E and σ_y increases. The author (41) has shown this to be the case for a range of metals and alloys (Figure 20). It should be noted that the ΔK_{th} incorporated in Figure 24 is ΔK^i_{th} where

$$\Delta K^i_{th} \simeq \Delta K_{th(\text{measured})} - K_{CL} \qquad \ldots (16)$$

The results in Figure 20 were obtained from metals and alloys which exhibit dominantly transgranular modes of crack growth. Results obtained from pearlitic steels (42) and titanium alloys (1) show that if the yield stress is increased by solid solution

hardening or by refining the pearlite spacing then the strength increase is accompanied by an increase in ΔK_{th}.

For high strength steels and aluminium alloys a different pattern of behaviour emerges. The results in Figure 21 show a trend of ΔK_{th} decreasing with σ_y increasing for 2XXX, 5XXX, 7XXX and powder route aluminium alloys (43). For a range of steels, with varying yield stress and microstructure, ΔK_{th} decreased with increasing yield stress (Figure 22) (43). Two further features are significant in Figure 21. The $\Delta K_{th(eff)}$ or ΔK^i_{th} does not change significantly with yield stress and secondly, the substantial improvements in ΔK_{th} are being derived from increases in ΔK^c_{th}, namely the closure contribution to ΔK_{th}. The results in Figure 23, show the influence of yield stress on ΔK_{th} for a range of R ratios (19). At the higher R ratios (0.5 and 0.9) where ΔK^c_{th} is small the value of $\Delta K_{th} \simeq \Delta K^i_{th} \simeq \Delta K_{theff}$ the values of ΔK_{th} are similar in both Figures 23 and 22.

A more general plot of data for steels, aluminium and titanium alloys is presented in Figure 24 with ΔK_{th} decreasing with increasing yield stress (43).

There are many factors involved in this ΔK_{th} dependence on strength level. From the preceding results it seems that higher ΔK_{th} values are obtained in lower yield strength steels as a consequence of the increase in the closure component. This could be a reflection of the changing microstructure and fcg mode. The occurrence of faceted fcg and substantial out of plane crack trajectories in the lower yield strength steels probably accounts for the majority of the increase in ΔK_{th} through ΔK^c_{th}. The presence of oxide films is clearly a contributor to ΔK^c_{th} for steels, but for most cases plays a minor role.

VII. THE ROLE OF CRACK CLOSURE

As shown in the previous sections fatigue crack closure can be a major influence on the magnitude of ΔK_{th} and the rate of fcg at low stress intensities. In a fully reversed fatigue cycle R=-1: it would be expected that the crack faces would come together over the compressive part of the cycle. During the tensile part of the cycle we would expect the crack faces to remain open. This later statement does not take account of the presence of plastic zones at the crack tip, plastic wakes and surface roughness and irregularities.

Elber (44) studied fatigue crack growth in aluminium alloy sheet specimens. Visible deformation associated with closure lead to an investigation using strain gauges anddirect visual observations. The results showed the cracks tobe open for only part of the tensile load cycle even for R=O. The residual tensile plastic deformation was considered to wedge the crack open. Subsequent tests on 2024-T3 alloys was carried out using a sensitive clip gauge (45). The form of the stress-displacement curve obtained in this type of experiment is shown in Figure 25. Region AB has the same slope as an uncracked sample, region CD is also linear and reflects the behaviour of a fully opened crack. Region BC is a transition from a fully closed to fully open crack. The concept of an effective stress range, $(\Delta\sigma_{eff})$, was suggested by Elber

$$\Delta\sigma_{eff} = \sigma_{max} - \sigma_{op} \qquad \ldots (15)$$

together with an effective stress range factor U.

$$U = \frac{\sigma_{max} - \sigma_{op}}{\sigma_{max} - \sigma_{min}} = \frac{\Delta\sigma_{eff}}{\Delta\sigma} \quad \ldots (16)$$

Then the conventional crack growth relationship becomes

$$\frac{da}{dN} = B(\Delta K_{eff})^m = B(U.\Delta K)^m \quad \ldots (17)$$

U was found to be a function of the mean stress R, for the aluminium alloy studied

$$U = 0.5 + 0.4\ R \quad \ldots (18)$$

7.1 Measurement of Crack Closure

Various techniques have been used to assess the extent of crack closure including strain gauges (46), crack tip opening using laser interferometry (47,48), ultrasonic Rayleigh waves (49,50,51). These investigations revealed that U increased with K_{max} but the changes with R varied from material to material with specimen geometry. The length over which the crack faces closed was also estimated and appears to be of a similar extent to the plastic zone ahead of the crack tip.

Observations on Ti-6Al-4V (52,53), using a high sensitivity extensometer at the crack tip showed U to increase with K_{max} to a value of 0.9 for a $K_{max} = 28\ MNm^{-3/2}$. In high strength steels a clip gauge attached to the mouth of WOL specimens showed a tendency for closure to increase with decreasing thickness (23 mm to 6 mm) (54). A metallographic sectioning technique (55) showed that for thin specimens (6.8 mm) slant fractures resulted in much of the crack surfaces coming together. In thicker samples (>7.7 mm) at minimum load the central region (plane strain) remained open

whilst the surface regions (plane stress) were observed to be touching.

Potential difference techniques using d.c. and a.c. have been used to investigate closure (55,56,57). This technique has some limitations in that crack face touching does not necessarily lead to changes in potential difference. A comparison of COD and potential difference is shown in Figure 25.

In conclusion, the measurement of fatigue crack closure, should involve a method in which the whole of the crack face interactions are investigated. Crack mouth opening displacement (CMOD), crack tip opening displacement (CTOD) and back face strain (BFS) will give reliable measurements of the magnitude of crack closure.

7.2 Influence of Specimen Geometry

In a recent review (58) it was concluded that there was no general trend of the extent of closure with thickness. The thickness of a specimen can influence the proportion of plane stress and plane strain, and hence closure, providing that the plastic zone sizes are of a significant proportion of the thickness. Thus in intermediate to high ΔK regions, the closure may well increase as the specimen thickness decreases. On the other hand, at low ΔK's and near the threshold region the stress state is dominantly plane strain and any thickness effects due to Elber type closure would not be expected. This point was recently emphasised in some work on titanium alloys (59).

7.3 Mechanisms of Fatigue Crack Closure

There are several mechanisms proposed to account for the closure process. All of them are concerned with crack faces touching over the reducing part of the load cycle.

a) The Elber model is concerned with a plastic wake formed by the crack tip plastic zone. The plastically extended material at the fracture surface holds the main crack front open as the load is reduced. For this mechanism to be operative, the reverse plastic zone size should be at least 10-20% of the specimen thickness. Thus, this mechanism will be operative only in the intermediate and high ΔK regions except for very low yield strength metals and alloys.

b) At intermediate to low ΔKs the advent of microstructurally controlled fatigue crack growth occurs (1). For many materials this particular condition is achieved when the reverse plastic zone size is equal to or less than the grain size or equivalent microstructural element. Thus, the crack tip plasticity in most specimens for this condition is very much less than the specimen thickness.

In a recent paper the author came to the following conclusion regarding crack closure in α-titanium (4). Crack closure is a result of deviations of the crack trajectory associated with a transgranular mode of crack growth. As the crack faces approach one another on the reducing half of the load cycle small amounts of in-plane shear produce points of contact which tend to wedge the crack open and prevent the stress intensity from falling to that associated with the minimum load. This surface roughness model has been shown to be operative in a wide range of materials

where the fatigue failure mode is dominantly transgranular (60).

c) A wedging open of the crack faces by corrosion products, fretting debris and oxide layers has been identified as a closure mechanism (61,62,63).

d) In non-uniform or random loading conditions the introduction of a peak overload can lead to the retardation of subsequent crack growth as a consequence of crack closure. In this instance the closure mechanism can be directly related to the residual compressive stresses associated with the peak load cycles.

In a recent report Newman (64) has used the closure concept to model and predict the fcg behaviour in non-uniform loading conditions.

7.4 Factors Influencing Crack Closure

In K increasing tests, ΔK and K_{max} increase with a/w. It is observed that the closure contribution increases with K_{max}. For a given a/w and ΔK as the R ratio is increased and K_{min} is raised, the closure contribution decreases.

The strength of the metal or alloy will influence the closure behaviour through the size of the crack tip plastic zones in relation to specimen thickness and microstructure.

In the low fcg rate regime and near threshold the microstructure can influence the closure contribution through the extent of surface roughness. It is observed that coarser microstructures lead to higher ΔK_{th} values. This can be directly attributed to an increase in the ΔK^{c}_{th} contribution to ΔK_{th}.

Texture may also be expected to play a role in the extent of surface roughness depending upon the operative crack growth mechanism.

The influence of test frequency on closure was illustrated by tests on low alloy steels at 550°C (63) where a decrease from 10 Hz to 10^{-2} Hz doubled the observed ΔK_{th}. This effect was attributed to a greater build up of the oxide layer during the crack growth preceding the ΔK_{th} condition. The role of environment as indicated previously is complex but the generation of faceted fcg and or corrosion debris can be expected to raise the "closure" component ΔK^{c}.

7.5 A Model for Crack Closure

Recently a model for crack closure (65) has been developed for the case of a single asperity near the crack tip under mode I loading and dominantly plane strain conditions.

Methods for determining the global component, as expressed in terms of the stress intensity factor, are well known, so primary emphasis in this section will be on the development of an analysis for determining the local component, (Figure 26a).

Since the loading across the crack faces occurs as discrete contacts at interfering asperities, the stress analysis problem involved is actually three dimensional in character.

For a properly loaded fracture mechanics specimen, however, the distribution of the asperities is essentially uniform across the specimen thickness. This suggests the possibility of representing the distribution of asperities through the thickness by an effective precompressed spring which makes line contact

across the thickness. It should be noted here, incidently, that in the case of oxide build-up on the crack face, the line contact very nearly represents the actual situation. The model will be applied to an analysis of data from cases for both discrete asperities and oxide build-up in a subsequent section.

The line contact representation permits the problem to be treated as a two dimensional one, and methods for analysing the effect of crack face loading can be used. Equations for determining stress intensity factors due to crack face pressure loading are available (66). From these, the stress intensity factor produced by concentrated, opposing line loads on the crack faces can be determined. The opening mode stress intensity factor for plane strain for this case is†

$$K_I(\text{local}) = \left(\frac{2}{\pi C}\right)^{\frac{1}{2}} \frac{P}{B}, \qquad \ldots (19)$$

where C is the distance from the crack tip to the line load. P is the total, local crack face force and B is the specimen thickness.

The contribution of the external load will be represented by K_I (global). By superposition, the total stress intensity factor

$$K_I = K_I(\text{local}) + K_I(\text{global}) \qquad \ldots (20)$$

The development of the equations for the model can be followed by reference to Fig. 26. The presence of both externally

---

† This result is for an infinite body with a semi-infinite crack. In the present application the distance from the crack tip to the crack face force is very much smaller than typical specimen dimensions. The local state given by Eq. 19 should, therefore, apply.

applied forces and crack face forces are illustrated in Fig. 26a. The details of the proposed model are indicated in Fig. 26b. Only the upper crack face is shown and a force P is developed by an asperity which is at a distance C from the crack tip. The dimension L represents the magnitude of the interference produced by the asperity. Until the external loads are sufficient to eliminate contact of the upper asperity with the lower asperity, there will be a compression of the amount e. The effective width of the asperity is b.

The vertical displacement of any point on the upper crack face (at r and at $\theta = \pi$) may be written as

$$U_2(r,\pi) = U_2(\text{global}) + U_2(\text{local}) \qquad \ldots (21)$$

By use of stress intensity factors for these two cases, we can write the displacement at $r = C$, $\theta = \pi$ (66).

$$U_2(C,\pi) = \frac{2}{G}\left(\frac{C}{2\pi}\right)^{\frac{1}{2}}(1-\nu)K_I(\text{global}) + \frac{2}{\pi G}(1-\nu)\frac{P}{B} \qquad \ldots (22)$$

The compression of the asperity is

$$e = \frac{PL}{EbB} \qquad \ldots (23)$$

The displacement of the crack face may then be written as

$$U_2(C,\pi) = (L-e) = \frac{2}{\pi G}(1-\nu)\frac{P}{B} + \frac{2}{G}\left(\frac{C}{2\pi}\right)^{\frac{1}{2}}(1-\nu)K_I(\text{global}) \qquad \ldots (24)$$

The quantities e and P can be determined by use of Equations 23 and 24. The quantities C, L and b are related to the micro-fracture details for a given material.

The stress intensity factor with no external load and the stress intensity factor for the case in which the external load reduces the local contact load to zero can be determined as special cases of the above equations. There are referred to as the closure and opening stress intensity factors, respectively.

For the case of zero external load,

K_I(global) = 0, and the use of Equations 19, 23 and 2 gives

$$K_I = K_I(\text{local}) = \left(\frac{2}{\pi C}\right)^{\frac{1}{2}} \left[\frac{1}{Eb} + \frac{2}{\pi GL}\ (1-\nu)\right]^{-1} \qquad \ldots (25)$$

where E is Young's modulus

G is the rigidity modulus

and ν is the Poisson's ratio.

In the case in which the external load is just sufficient to remove the asperity pressure, P=0 and e=0. The Equation 24 yields the result

$$K_I = K_I(\text{global}) = \frac{LG}{2(1-\nu)}\ \left(\frac{2\pi}{C}\right)^{\frac{1}{2}} \qquad \ldots (26)$$

For the external maximum loads applied, it can be expected that small plastic enclaves would form at the crack tip. Since this can result in a relaxation of the stress state at the crack tip, an estimate of the magnitude of this effect was made. The concept of an effective crack length, as proposed by Irwin, was applied to increase the distance from the crack tip to the asperity. Thus, C was increased by the radius of the plastic zone. For plane strain, an estimate of this radius is (67)

$$R_p = \frac{1}{6\pi}\ \left(\frac{K_{max}}{\sigma_y}\right)^2 \qquad \ldots (27)$$

Incorporating Equation (27) into Equations (25) and (26) gives

$$K_I(\text{local}) = \left(\frac{2}{\pi(C+R_p)}\right)^{\frac{1}{2}} \left[\frac{1}{Eb} + \frac{2}{\pi GL}(1-\nu)\right]^{-1} \quad \ldots (28)$$

$$K_I(\text{global}) = \frac{LG}{2(1-\nu)} \left(\frac{2\pi}{C+R_p}\right)^{\frac{1}{2}} \quad \ldots (29)$$

An example of the application of the model is illustrated in Fig. 27. The variation of stress intensity factor versus external load Q is presented for a CTS specimen of a nickel alloy where a/w = 0.44, B the specimen thickness = 13 mm, w the specimen width = 26 mm, C = 28 μm and L = 0.125 μm and the yield stress σ_y = 350 MNm^{-2}.

The closure stress intensity factor for a completely elastic response is given by Equation (25) and it is shown as point A. The opening load is given by Equation (26) and it is shown as point B. The response between points A and B is linear. The difference in the values of stress intensity factor at A and B is determined by the magnitude of the parameter b, the effective width of the asperities. As b decreases, the closure stress intensity factor decreases. The value of the stress intensity factor at B is independent of b.

The experimental maximum, minimum and opening external loads for the given example are also indicated in Fig. 27. Clearly, the effective range of the stress intensity factor is decreased by closure.

The presence of a plastic zone would effectively increase C, the distance from the asperity to the crack tip. For this particular case in Fig. 27, C would be increased from 28 μm to 38.5 μm using the plastic correction factor in Equation 27.

The closure and opening stress intensity factors then appear as points A' and B' respectively in Figure 27.

7.5.1 Microstructural asperities

A wrought nickel alloy N901 with a grain size of 375 μm and a yield stress of 350 MNm^{-2} was used in this investigation. CTS specimens were subjected to cyclic loading leading to an evaluation of the fatigue crack growth and fatigue threshold characteristics in laboratory air at a frequency of ∿100 Hz and at R = 0.1. In the course of these tests the following procedure was adopted. At particular crack length increments both the crack tip profiles and the load versus crack opening displacements curves were obtained.

Crack tip profiles were examined by taking plastic replicas of the surface with the specimen in situ at minimum loads. A small piece of cellulose acetate, 4 mm thick, had one side moistened with a few drops of acetone and the partially dissolved plastic was then pressed firmly onto the surface. Bubbles may be trapped between the specimen and the plastic and as the plastic sets the sheet may peel away from the surface - if either of these events occurred in the area of interest the procedure was repeated. When after 15-20 minutes the solvent had evaporated the plastic was separated from the surface. This negative replica was examined at low magnifications on an optical microscope and then for high resolution work further preparation was done.

The replicas in this experiment had a fine layer of gold evaporated onto them where to avoid shadowing the replicas had

to be on a rapidly revolving table while the evaporation took place. It has since been found that sputter coating is a more efficient procedure giving a more uniform layer and less heating effects. A supporting layer of copper ∿0.3mm thick was then electroplated onto the gold and the metal positive replica separated from the negative plastic replica and washed. Washing included a long soak in acetone to dissolve any cellulose acetate stuck in the crevice of the replica crack.

This experimental approach presented measurement of the extent to which the crack faces were wedged open and also the distance from the crack tip to the asperity. An example of such a crack tip profile is presented in Figure 28.

The load-crack face opening displacement curves were obtained at the same crack length as the replicas. The stress intensity at which the crack was open was taken as the intercept of the fully open and fully closed portions of the curve.

Examination of the fatigue fracture surfaces revealed extensive facetting and out of plane fatigue crack growth as reported previously for other alloys. An example of microstructural sensitive fatigue crack growth in this nickel alloy is presented in Fig. 29.

The information obtained from three different tests was used to compute the results in Table 3. All these sets of data refer to fatigue cracks in the near threshold region. Using values of $G=77\ GNm^{-2}$, $\nu=0.3$, $E=200\ GNm^{-2}$ the values of Q^1_{open} and Q^2_{open} were computed when Q^1 is the opening load for a fully elastic response and Q^2 is the opening load for the plasticity corrected case. Q^3 is the observed experimental opening load. A comparison of Q^2_{open} and Q^3_{open} reveals a

reasonable level of agreement between observed and predicted values of Q.

The agreement between observation and prediction is subjected to several limitations, although these may well be of secondary importance in the present application.

a) The model is two dimensional and requires that the load transfer across the faces occurs dominantly at the asperity immediately behind the crack tip.

b) The values of C and L were obtained from the specimen surface. Computed Q^2_{open} is then compared with Q^3_{open} obtained from the bulk response of the specimen.

c) No account is taken of crack front shape nor the possible effects of surface battering.

7.5.2 Oxide asperities

Examination of Equation 28 shows that the closure stress intensity factor is dependent upon L, the asperity height C, the distance from the crack tip to the asperity and also the rigidity of the asperity.

The influence of C on K_{CL} is illustrated in Fig. 30. The curves in this figure were computed using the following values $G = 77\ GNm^{-2}$, $\nu = 0.3$, $L = 0.2\ \mu m$ and $b = 0.5\ \mu m$. The family of curves represents the effects of different elastic moduli for the asperity. The upper curve is the case for a rigid asperity with $E \to \infty$. The lower curve is the case where the asperity has the same elastic modulus as the base material.

In a recent paper Suresh et al. (7) reported the results of fatigue crack growth and fatigue thresholds in a 2½ Cr 1 Mo steel tested at room temperature in a range of atmospheres. The results from an SA5423 steel tested at R = 0.05 showed that an oxide asperity built up on the fatigue fracture face, the height of the asperity was a maximum in the threshold region. The value of ΔK_{th} was 7.7 $MNm^{-3/2}$ at R = 0.05 and 3.2 $MNm^{-3/2}$ at at R = 0.7. If it is assumed that the closure contribution at R = 0.7 is negligible then the maximum value of K_{CL} at R = 0.05 is 4.5 $MNm^{-3/2}$.

The lower curve in Fig. 30 may be considered to approximate to the case of a steel with oxide asperities. For K_{max} = 8.1 $MNm^{-3/2}$ and σ_y = 500 MNm^{-2}, R_p = 13.9 μm. Thus for an asperity of height 0.2 μm and width 0.5 μm to result in a K_{CL} of 4.5 $MNm^{-3/2}$ it would have to be situated 7.1 μm behind the crack tip (Equation (29). Specific values of C are not available from the results reported by Suresh et al. (7). The present model places the asperity in a position compatible with crack growth rates in the threshold region.

In conclusion, crack closure can lead to significant increases in the resistance of a material to fcg. The modelling of crack closure is developing and the ability to predict closure contributions should be available in the near future.

VIII. THE EFFECTS OF TEST TEMPERATURE

There have been several investigations of the influence of test temperature on fcg rates and ΔK_{th} in steels and aluminium alloys (68-70).

The temperature effects are observed through changes in the mode of fcg and mechanical properties, a significant change in environment can also occur with varying temperature. An example of the influence of test temperature of a mill annealed Ti-6Al-4V alloy with an α-grain size of 8μm is illustrated in Fig. 31 (71). The value of ΔK_{th} is reduced by ∿30% for a change in test temperature from 20°C to 386°C. The major influence is on the form of the ΔK-da/dN curve and in particular the increases in fcg rate in the near threshold region. Fractographic studies showed that facet formation was increased markedly at 257°C (Fig. 32) with facet like regions extending over several α grain diameters.

The effect of lowering the test temperature could inhibit environmental activity and also lead to an increased strength level in some metals and alloys. It is possible that the latter effect which resulted in the increased ΔK_{th} values at 77°K compared to 293°K reported by Tscheg and Stanzl (70). The reasoning behind this conclusion is as follows. In the absence of an environmental dominating factor the fcg is related to the range of crack tip opening displacement ΔCTOD. The ΔCTOD is essentially determined by the relationship in Equation 14. Thus, for a given set of conditions and comparable ΔK's, raising the yield stress will decrease ΔCTOD and reduce the fcg rate.

This approach was confirmed by the results of Jatavalabula and Gerberich (72) who studied the fcg and ΔK_{th} characteristics of Ti-30% Mo, a β-titanium alloy over the temperature range 123°K to 375°K. At the lower temperature the alloy exhibited extensive cyclic cleavage. In spite of this apparent embrittlement the closure corrected fcg rates decreased and ΔK_{th} increased as the temperature decreased with the associated increase in yield stress.

IX. INFLUENCE OF TEST FREQUENCY AND LOADING MODE

Bathias et al. (73) found little effect of frequency (0.5Hz to 125Hz) on fcg rates and ΔK_{th} in aluminium alloys. For steels Mutz and Weiss (74) found the effect of frequency in the range 100 to 375 Hz to be minimal. Radan (75) for RR58 (7075) aluminium alloys indicated that frequency could influence both ΔK_{th} and low fcg rates. At 550°C a CrMoV steel exhibited higher ΔK_{th} values at lower frequencies (76). Lower frequencies may allow the build up of debris in the crack tip region and hence increase the closure contribution to ΔK_{th}. Nominal frequency ranges of 1.0 to 100 Hz for fcg and ΔK_{th} measurement at ambient temperatures can be expected to exhibit little influence. On the other hand at extremely low frequencies corrosion fatigue can dominate and under these circumstances fcg may occur to extremely low ΔK levels.

At the other end of the spectrum ultrasonic frequencies of up to 20 kHz have been employed in the testing of a wide range of metals and alloys in the growth rate range 10^{-5} to

10^{-11} mm/cycle (Table 4) (77). The ultrasonic test gives results similar to those obtained at lower frequencies for metals such as copper. The brevity of the test means that the environmental factor is more or less excluded from the test.

Implicit in the rest of the review is the statement that the crack face opening is mode I in character. Recent work (78-80) indicates that the loading mode does not have a significant influence on the appropriate ΔK_{th}. For example in steels tested at ambient temperatures $\Delta K_{IIth}/\Delta K_{th}$ and $\Delta K_{III}/\Delta K_{th}$ have values of 1.15 and 1.25 respectively.

X. THE INFLUENCE OF CRACK LENGTH ON FCG RATE AND ΔK_{th}

At "short" crack lengths there is a general view that crack growth rates increase and ΔK_{th} decreases. The definition of "short" in this instance is open to much debate but is probably of the order of a small multiple of the grain diameter or similar microstructural element.

The early work of Frost et al. (81,82) and Pearson (83) indicated there was a significant influence of crack length on ΔK_{th} and fcg rates for a range of materials and specimen geometries. The growth of short surface cracks in HT80 a low alloy steel showed that for cracks of length greater than 0.5 m ΔK_{th} was constant at a value of 4.8 $MNm^{-3/2}$ (84). For a Ni-Cr-Mo turbine rotor steel, the results show ΔK_{th} falling from $\sim$6 to 1 $MNm^{-3/2}$ for $a/w < 0.1$ (85). The lowest of the short crack length ΔK_{th} was of the same order as the long crack length ΔK_{th} for $R = 0.9$.

Recently Romaniv et al. (86) have reported some results on the short crack behaviour of mild steel, stainless steel and an aluminium magnesium manganese alloy, (Table 5 and Figure 33). The transition for short to long crack behaviour occurs at 0.5 to 1.0 mm. The authors conclude that

$$\Delta K_{th}^{sh} = \Delta K_{th} \left(\frac{A_s}{A^o_s}\right)^z \qquad \ldots (30)$$

where, A_s is the initial crack length, A^o_s critical initial surface crack length above which ΔK_{th} is independent of crack length, ΔK_{th}^{sh} is the ΔK_{th} obtained when the crack length is shorter than A^o_s, z, is the power exponent in the relationship. Fatigue crack growth in corner cracked tension-tension specimens has been investigated in a coarse grained IMI 685 alloy (87) with crack lengths up to 3.5 mm. The effect of crack length, frequency and dwell in corner cracked and compact tension specimens is illustrated in Figure 34. It can be seen that the fcg rate is an order of magnitude faster for the shorter cracks in the corner cracked specimens. The effect of a 2 minute dwell was to decrease the fcg rate. The short cracks were also arrested at colony boundaries and grain boundaries.

The authors Fig. 35 also ranked the short crack behaviour of titanium alloys, steels and aluminium alloys. The significance of such a plot is to draw attention to the marked influence of microstructure in this regime.

10.1 Models Related to Crack Length Effects

Smith (88) considered the minimum crack length for which continuum considerations should apply. The stress field can be

described in terms of K over a near crack tip stress field of a/10. This near crack tip field should be at least one grain diameter, thus for a 10 μm grain size a minimum size of 100 μm crack would be required. Smith also pointed out that the plastic zone at the crack tip should be well contained within the near crack tip elastic field. Alternatively the minimum plasticity unit associated with the crack tip could be a slip band contained in a subcell of size 0.5 μm, on this basis the minimum crack length was considered to be of the order of 25 μm or 0.025 mm. If Smith's analysis is correct then almost all short cracks investigated should be treatable by a continuum model and also that the changes in fcg rates and ΔK_{th} are not attributable to a breakdown of LEFM.

The control of failure by the fatigue limit or propagation of a crack is a feature to be considered in relation to "short cracks". As the crack length decreases $\Delta\sigma$ must increase for $\Delta K_{th} = \Delta\sigma(\pi\alpha a)^{\frac{1}{2}}$ to be satisfied. Clearly, there must be a crack length below which the crack remains arrested and the initiation and growth process pertaining to a plane bar specimen takes over.

Thus, if σ_e is the fatigue limit and ΔK_{th} the long fatigue crack threshold then a_o the crack length above which ΔK_{th} is independent of crack length will decrease as the fatigue limit increases

$$a_o = \left(\frac{\Delta K_{th}}{\sigma_e}\right)^2 \frac{1}{\pi\alpha} \qquad \ldots (31)$$

For mild steel $a_o \sim$ 1mm and for 4340 steel $\sim$0.02 mm.

The concept of an "effective" crack length was introduced by Topper and Haddad (89).

$$\Delta K = \Delta\sigma(\pi(\ell + \ell_o))^{\frac{1}{2}} \quad \ldots (32)$$

$$\ell_o = \left(\frac{\Delta K_{th}}{\sigma_e}\right)^2 \frac{1}{\pi\alpha} \quad \ldots (33)$$

As ℓ_o is the crack length associated with the fatigue limit it can be added to the existing crack length ℓ. Thus for a given $\Delta\sigma$, this leads to an increase in the "effective" ΔK leading to increased fcg rates and lower ΔK_{th}. Hudak (90) has reviewed the behaviour of short fatigue cracks and concluded that "short cracks" grow faster than "long cracks" and that this behaviour can be best described by applying an "effective crack" length concept as illustrated in Equations 32 and 33. This approach may well prove most satisfactory for the normalisation of data but it should be noted that the effective crack length procedure is retrospective rather than predictive.

Recent experimental and theoretical work has turned its attention to the case of applied stresses approaching the yield stress. In a recent paper (91) Zurek et al. considered the case of the growth of short cracks (20-500 μm) in a 7075-T6 aluminium alloy. For short semi-elliptical cracks having a depth to length ratio of 0.4.

$$\Delta K = 1.12\ \sigma_{max}\ (2a)^{\frac{1}{2}} \quad \ldots (34)$$

$$\Delta K_{eff} = 1.12\ (\sigma_{max} - \sigma_{cl})(2a)^{\frac{1}{2}} \quad \ldots (35)$$

Using an empirical value for σ_{cl}

$$\Delta K_{eff} = 1.12\ (\sigma_{max} - \frac{\alpha z}{\sqrt{2}}\ \sigma_{max})\ (2a)^{\frac{1}{2}} \qquad \ldots (36)$$

$$\Delta K_{eff} = \Delta K \left[1-\alpha z\ \left(\frac{1.12\ \sigma_{max}}{\Delta K}\right)^{2}\right] \qquad \ldots (37)$$

where α is a constant and z is approximately the grain diameter.

$$\frac{da}{dN} = A\Delta K^{n} \left[1-\alpha z\ \left(\frac{1.12\sigma_{max}}{\Delta K}\right)^{2}\right]^{n} \qquad \ldots (38)$$

The fcg results for two stress levels (195 and 140 MPa) are shown in Fig. 36 together with the predicted fcg rates from Equation 38. For a particular ΔK the shorter crack has the slower crack growth rate. A result which contrasts with much of the data in the section on crack length where the general trend was for faster fcg rates at shorter crack lengths. The authors (91) consider that plasticity induced crack tip closure occurs in these alloys and σ_{cl} is incorporated into their model (Eqn. 35) on this basis.

In conclusion, the evidence on balance favours faster fcg rates and lower ΔK_{th} for shorter cracks. With the regime of "short cracks" however, the magnitude of this effect may be modified by the overall stress level and by microstructural factors.

XI. MODELS FOR THE THRESHOLD CONDITION

Sadananda and Shahinian (92), developed a model based on the stress (τ_t) to nucleate a dislocation at the crack tip and

related τ_t to K by the relationship

$$\Delta K_{th} = \frac{(2\pi\rho)^{\frac{1}{2}}\tau_t}{f(\theta)} \quad \ldots (39)$$

ρ is the distance between the dislocation line and the crack tip, the minimum value of ρ is the Burgers vector b. Assumptions can be made for τ_t in terms of the shear modulus and leads to K_{max}/μ as a constant with a value of $\sim 1\text{x}10^{-13}$ $(cm^{\frac{1}{2}})$ for a range of metals and alloys. This model predicts the threshold at a constant K_{max} which is not always observed in practice.

In a study of the influence of grain size Taira et al. (93) measured the extent of the crack tip slip band zone and observed them to be limited by the grain boundaries. The assumption is made that the slip band is a linear extension of a Mode I crack and perpendicular to the boundary. By superposition

$$K_{th} = K^m_{crit} + K_{fr} \quad \ldots (40)$$

where K^m_{crit} is the microscopic stress intensity at the slip band tip, K_{fr} is due to the flow stress in the slip band and,

$$K_{th} = K^m_{crit} + 2\sqrt{2\sigma}_{fr} \left(\frac{0.2\ell}{\pi}\right)^{\frac{1}{2}} \quad \ldots (41)$$

In Equation 41, ℓ is the grain diameter and 0.2ℓ is the experimentally observed size of the slip bands. Thus the threshold is predicted to increase with grain size.

From a study of crystallographic crack growth in MarM200 single crystals ΔK^i_{th} was observed and projected with values of 1-2 $MNm^{-3/2}$ (94,95). Taylor (96) has predicted minimum values for ΔK_{th} from an energy balance analysis

$$\Delta K_{th} = \left[\frac{2\pi E\gamma}{1-\nu^2 - 0.47I}\right]^{\frac{1}{2}} \quad \ldots (42)$$

I varies from 1.0 to 1.2. A comparison of the observed with predicted values of ΔK_{th} are illustrated in Fig. 37. On the basis of plasticity spreading from the crack tip to the nearest grain boundary a grain size dependence of ΔK_{th} was also developed by Taylor (96)

$$\Delta K_{th} = \sigma_{yc}\left[\frac{2.8\pi d}{(1-\nu^2)}\right]^{\frac{1}{2}} \quad \ldots (43)$$

The correlation with observed values of ΔK_{th} is within 20%.

Weiss and Lal (97,98) developed a relationship for ΔK_{th} in terms of stress levels at the crack tip.

$$\Delta K_{th}^2 = \frac{3\pi}{2}(0.1E)^2\,\rho^* \quad \ldots (44)$$

ρ^* is the linear dimension of an element at the tip of the crack and a range of values of ρ^* from 0.02 to 0.1 μm was proposed however, a value of 0.25 μm gives good agreement with observed values of ΔK_{th}.

In a recent paper (24) the author suggested that the fatigue crack growth threshold was associated with a lower bound crack tip opening displacement range ΔCTOD, (Equation 14). For a range of metals and alloys a plot of ΔK_{th}^i versus $(\sigma_y E)^{\frac{1}{2}}$ showed a good linear response (Figure 20).

The present position is that in general ΔK_{th}, the fatigue threshold cannot be predicted with any degree of accuracy. However, given values of yield strength, Youngs modulus and grain size, values for ΔK_{th}^i can be attempted for some metals and alloys.

XII. FCG LAWS INCORPORATING ΔK_{th}

There have been several proposed models to account for fcg at low stress intensities. These equations have incorporated ΔK_{th} in recognition or the arrest of near arrest of the fatigue crack in this regime.

Klesnil and Lukas (99) proposed

$$\frac{da}{dN} = B(\Delta K^m - \Delta K_{th}^m) \qquad \ldots(45)$$

Equation 46 was developed for fcg just above ΔK_{th} for continuously increasing or decreasing ΔK

$$\frac{da}{dN} = C \{ \Delta K^m - \left[\Delta K_{th} \left(\frac{\Delta K_a}{\Delta K}\right)^{\frac{\alpha}{1-\alpha}} \right]^m \} \qquad \ldots(46)$$

$$\Delta K_{th} << \Delta K < \Delta K_a$$

The format of Equation 46 was developed by Ohta and Sasaki (100) to account for sudden underload conditions. ΔK_{th} is the intrinsic threshold, ΔK_a is the preceeding ΔK prior to a load decrease, α is a constant which is stress history dependent.

For high strength steels the influence of R can be accomodated by relationships of the form in Equation 47 and 48 (101)

$$\frac{da}{dN} = A \left(\frac{1}{1-R}\right)^{\gamma m} \left[\Delta K^m - \{(1-R)^{\gamma} (\Delta K_{th})_{R=0}\}^m \right] \qquad \ldots(47)$$

for $-1 \leq R \leq 0.33$, where γ characterises the asymmetry of the stress cycle; and

$$\frac{da}{dN} = A \left(\frac{1}{1-0.33}\right)^{\gamma m} \left[\Delta K^m - \{(1-R)^{\gamma} (\Delta K_{th})_{R=0}\}^m\right] \qquad \ldots(48)$$

for $0.33 \leqslant R \leqslant 0.8$.

In circumstances where a high R ratio is imposed the form of the fcg curve can be influenced by a toughness parameter K_c. Several expressions have been developed including the following (102)

$$\frac{da}{dN} = \frac{C(\Delta K^m - \Delta K_{th}{}^m)}{(1-R)\ K_c - \Delta K} \qquad \ldots(49)$$

Fcg laws have also been developed by McEvily et al. (103,104)

$$\frac{da}{dN} = \frac{4C'}{\pi \sigma_y E} (\Delta K^2 - \Delta K_{th}{}^2)\left(1 + \frac{\Delta K}{K_{IC} - K_{max}}\right) \qquad \ldots(50)$$

where C' is a dimensionless material constant which reflects an assumed proportionality between CTOD and the crack advance per cycle.

Equation 50 was later modified to a form given in equation 51 (105)

$$\frac{da}{dN} = \frac{A}{E^2} (\Delta K^2 - \Delta K_{th}{}^2)\ \left(1 + \frac{\Delta K}{K_{IC} - K_{max}}\right) \qquad \ldots(51)$$

Radon proposed a model based on a strain controlled fracture criterion and an effective ΔK:- (106)

$$\frac{da}{dN} = \frac{2^{1+n}(1-\nu^2)^{1+n}\ (\Delta K_{eff}{}^2 - \Delta K_{c,th}{}^2)}{4\ \alpha\ (1+n)\ \pi \sigma_{yc}{}^{1-n}\ E^{1+n}\ \varepsilon_f{}^{1+n}} \qquad \ldots(52)$$

where, $\Delta K_{c,th}$ is the minimum values of ΔK_{th} found with increasing R, n is the cyclic strain hardening exponent, σ_{yc} is the cyclic yield stress, ε_f is the true fracture strain and α is a constant.

The predicted growth rates were found to correlate well with experimental results for low alloy steel BS4360-50D, at R = 0.7 (presumed to be closure free conditions, i.e. $\Delta K = \Delta K_{eff}$).

Duggan (107) developed a model based on cumulative "damage" irreversible plastic strain) at the crack tip, which may be presented in the form:-

$$\frac{da}{dN} = \left(\frac{\pi}{32}\right)^{\frac{1}{2\alpha}} \frac{1}{\alpha} \frac{2}{\varepsilon_f' \, E(K_c - K_{max})} \left[\left(\frac{1 + \Delta K_{th}}{K_c}\right) - \left(\frac{\Delta K}{K_c} + \frac{\Delta K_{th}}{\Delta K}\right)\right]^{\frac{1}{\alpha}} (\Delta K)^{\frac{2}{\alpha}} \quad \ldots(53)$$

where α is the fatigue ductility exponent, ε_f' the fatigue ductility coefficient, E the elastic modulus, K_c the critical stress intensity factor for fast fracture and ΔK_{th} is the basic threshold level (unaffected by cyclic transient effects). This model was found to give a good prediction of mid-range fcg behaviour for four different alloys; steels 2S96D and FV535, nickel alloy INCO 901, and powder compact material Ferrotic C, all at R = 0 in room temperature air.

Bailon and Lanteige (108) have proposed the following crack growth law

$$da/dN = \frac{4}{\rho^{\frac{1}{\beta}-1}} \left[\frac{0.2(1-\nu^2)\ (\Delta K^2 - \Delta K_{th}^{\ 2})}{\pi\sqrt{3}\ C\ E\ \sigma_{ys}\ \varepsilon_f'}\right]^{1/\beta} \quad \ldots(54)$$

where

$$\Delta\varepsilon_p\ N_f^{\beta} = \frac{\varepsilon'_f}{2}$$

C is a triaxility factor, ν Poisson's ratio and ρ is the crack tip radius.

A predicted value of ΔK_{th} is also proposed

$$\Delta K_{th} \cong 12.4 \ (\rho\sigma_{ys} E \Delta\varepsilon_o)^{\frac{1}{2}} \qquad \ldots(55)$$

Where $\Delta\varepsilon_o$ is the strain range at the crack tip which does not contribute to damage.

Chakraborty (109) has studied the problem of predicting fcg rates using the cyclic ductility and cyclic strength of metals and alloys. It is assumed that for a ductile metal the fcg occurs by exhausting the ductility in the reverse plastic zone. The crack growth depends on cyclic stress-strain response. The model treats a series of ligaments ahead of the crack tip and provides the relationships shown in Fig. 38, $\bar{\rho}'n$ is the average size of the MDZ's in the n_{th} element and the MDZ is the microstructural deformation zone.

Recently this model has been modified (110) to take account of the threshold concept and predict fcg at low ΔKs. The threshold condition is related to the situation where persistent slip bands no longer form. As indicated in Figure 39 this can be associated with a particular plastic strain range Δεpth. The fcg relationship is now modified to

$$da/dN = 2 \ \Sigma \ \bar{\rho}'n \left[\left(\frac{\Delta\varepsilon pm - \Delta\varepsilon pth}{2\varepsilon'_f} \right) \right]^{-\frac{1}{c}} \qquad \ldots(56)$$

The application of the model to an aluminium-zinc-magnesium alloy is shown in Fig. 40. The model predicts faster growth rates than the observed values for nominal ΔK. However, if the data is closure corrected there is a reasonable correlation between observation and prediction.

Ritchie (35) modified the analysis of Weiss and Lal (97, 98) by assuming that, in high strength steels, hydrogen can decrease the local fracture stress $\sigma_f \cong E/10$ at the threshold by an amount $\Delta\sigma_H$. He obtained the following equation:

$$\Delta K_{th} \cong \left(\frac{3\pi}{2}\rho^*\right)^{\frac{1}{2}} \left\{\frac{\sigma_f - C_o \exp(B'\sigma_y)}{1 + \frac{\alpha C_o \rho^*}{(1-R)} B^* \exp(B'\sigma_y)}\right\} \quad \ldots(57)$$

with $B' = \bar{V}R_oT$ and $B^* = 2\alpha_2 \frac{\bar{V}}{R_oT} \frac{3\pi}{2}$

where

C_o = the equilibrium concentration of hydrogen in the unstressed lattice

α = a constant in the relationship between σ_f and the local hydrogen concentration

σ_y = the static yield strength

R_o = the perfect gas constant

T = the absolute temperature

$\bar{V}$ = the molar volume of hydrogen in iron

R = the load ratio

α_2 = an empirical constant.

As pointed out by Ritchie, the experimental confirmation of equation (56) is subject to the values chosen for ρ^* and αC_o.

When hydrogen is present, equation (56) predicts a complex influence of the R-ratio on ΔK_{th}, while, in the absence of hydrogen equation 56 predicts a ΔK_{th} which is insensitive to the R ratio, as experimentally observed in several studies in vacuum.

Clearly, the incorporation of ΔK_{th} in equation 56 into say equation 45 would then permit an assessment of fcg rates.

In conclusion, there is no generalised equation which can be used to predict fcg rates at low stress intensities. The conservative approach, i.e., lowest ΔK_{th} values and highest fcg rates is to assume the form of the log ΔK^i versus log da/dN curve. This would apply for the long crack and short crack case where the crack length is greater than 10 grain diameters. There is limited data available for ΔK^i but the format is illustrated in Figure 41 for a low carbon steel (34).

For the case where a crack is initiated in a single grain or single crystal and develops into a 'long' crack the growth rate/ΔK response may have the form projected in Figure 42. The curve A represents the case of a single crystal where there is little resistance to fcg except the intrinsic material properties. Curve C is the case of a finer grained material where arrest can occur for $\Delta K < \Delta K_1$. If crack arrest occurs ΔK_1 must be increased to ΔK_2 for crack propagation to be recommenced. Curve B represents an intermediate case where grain boundaries present some resistance to the grow out of cracks from the original grain but does not involve an arrest condition. As the crack in case B develops into a long crack the effects of crack closure reduce the fcg rate compared with the finer grained alloys.

XIII. MEASUREMENT OF FCG RATES AND ΔK_{th}

There have been several approaches to this measurement of ΔK_{th}. The initial work of Frost (13) involved precracking of S-N specimens, machining of the surface layer and determination of the fatigue limit stress of the pre-cracked specimen. With the advent of fracture mechanics and the characterisation of the threshold in terms of a stress intensity parameter, a different range of specimen geometries and test procedures were developed.

In the intermediate and high fcg rate regions the approach to data analysis and presentation is well reviewed by ASTM (111) and there is available a proposed standard method.

In the case of low fcg rates and ΔK_{th} it has proved more difficult to arrive at a generally agreed procedure. Readers are referred to the view of Russian workers (112) in this area and the conclusions reached by a panel of French researchers (113).

There are inconsistencies in the level of ΔK_{th} and the fcg rates for a particular material. One of the reasons for this is illustrated in Fig. 43. The results were obtained from a quenched and tempered steel (114) following tests at R = 0.1. The load decreasing curve exhibited a lower ΔK_{th} and higher fcg rates than the load increasing curve. The tests were carried out in laboratory air at 21°C and with a test frequency of 100 Hz. The specimen geometry was three point bend with w = 50 mm. The crack length short in terms of a/w was always greater than 2.5mm in length. The test procedure involved load decrements from an initiated crack, the length of crack

grown in each interval was based on the size of the preceeding maximum plastic zone size. Careful control of this step down procedure can minimise "stress history effects". The measurement of low fcg rates requires accurate crack length measurement to within 0.01 mm and the capability to apply large numbers of cycles over reliable load ranges. The data in Fig. 43 required a minimum of 10^7 cycles to establish the load decreasing ΔK_{th}. Any reliable procedure should be based on fcg rate measurement and not simply on an arrest situation. After cycling in the "threshold region" substantial increases in load were required to achieve further fcg. This hysteresis of the fcg behaviour has been observed in several materials investigated in the authors laboratory. The reason for this hysteresis is not entirely obvious at the present time although crack tip blunting and the build up of corrosion debris in the crack tip region may be involved.

It may well be that the problem of rationalising low stress intensity fcg data and ΔK_{th} values even for "long crack" configurations will not be resolved easily. The problem is in part "closure" related and more data in the form of log ΔK^i versus log da/dN would be helpful in the present situation.

XIV. ALUMINIUM ALLOYS

The purpose of this section is to highlight the major characteristics of fcg and threshold behaviour of aluminium alloys.

The fcg response is essentially dominated by the metallurgical contents and processing of the alloy together with the environmental and the mechanical aspects of loading such as mean stress overloads, random loading and crack closure.

High strength aluminium alloys exhibit a low resistance to fcg in the presence of an active environment (moist air) and a high mean stress. This feature is illustrated in Fig. 44, for a 2L93 alloy and 7075-T651 and 7075-T7351. The range of fcg rates varied by a factor of 10 depending on the alloy and mean stress. The lowest resistance to fcg was offered at the higher mean stress levels (115). As can be seen in Fig. 8 the ΔK_{th} approaches 1 $MNm^{-3/2}$ for a 7075 T 7351 alloy in laboratory air at ambient temperature. There should exist therefore, the possibility of some substantial improvement in ΔK_{th} and fcg resistance through control of composition, grain size, ageing treatment and crack closure.

14.1 Alloy Composition

Bretz et al (116) found no difference in the fcg response of a low and high purity 7075-T7 alloy. Intermetallic particle content could be expected to lower toughness and decrease fcg resistance at high ΔK's.

Li and Starke (117) concluded that the fcg rate decreases as the copper content decreases (3.1 to 1.1) in 7XXX series alloys. Bretz (116) found little influence of copper content on fcg in 7XXX series alloys for $\Delta K < 3.3$ $MNm^{-3/2}$ and some

beneficial effects in the intermediate ΔK regime. The additions of Cr and Zr to 7075 T7 alloys to introduce dispersoids has been investigated (116). Some improvement in the fcg resistance at low ΔK's is reported. The addition of manganese to an Al/Mg/Si alloy resulted in the presence of Al_2Mn_3Si dispersoids of dimension 0.1 to 0.2 μm in diameter (118). The resultant fatigue threshold ΔK_{th} was increased as was the fcg resistance with higher dispersoid content, (Fig. 45). The reason for this improvement with a larger volume fraction of dispersoids may be related to an increase in the level of crack closure.

14.2 Temper Condition

In Al 6Zn 2Mg and Cu alloys Lin and Starke (119) have shown that ΔK_{th} is higher, irrespective of environment for the T651 compared with the T7351 condition. This was related to the possibility of greater slip reversibility in the T651 condition. These results are in agreement with those reported by Kirby and Beevers (8). Bucci et al. (120) have concluded from a study of 7XXX series alloys that the T6 temper is beneficial under high mean stress conditions. However, the T7 temper gives greater fcg resistance for the higher ΔK regions. In a study of an Al 6Zn 2Mg 0.1Zr alloy, Heikemon et al. (121) showed that greater fcg resistance and high ΔK_{th} values were obtained in the underaged compared with the overaged condition (Fig. 46). The influence of ageing condition appears to have positive effects on fcg resistance but these are of a marginal character at least for the "long" crack configuration.

14.3 Grain Size

Some recent work on a 7475 alloy has shown that in vacuum increasing the grain size can increase the ΔK_{th} and the fcg resistance, (Fig. 47), (122). The results also show that a combination of underaging and coarser grain size give the most beneficial effect.

14.4 Yield Strength

With a particular family of alloys the lower yield stress of an underaged alloy will tend to give more fcg resistance at the lower yield strength. From one alloy to another the trend as illustrated in Fig. 21 is for ΔK_{th} to decrease as the yield stress increases.

14.5 Crack Closure

Wasudevan and Suresh (123) have studied the fcg of 2XXX and 7XXX series alloys. They found little evidence of fatigue crack closure due to oxide debris on the fracture faces of 2021 T6 and 2024 T3 alloys. In an overaged 7075 alloy an oxide layer near threshold built up to a thickness of $\sim$0.1 μm and probably resulted in significant crack closure. In the T6 fully aged condition oxide layers 0.01 μm in thickness were formed. The oxide asperities in this case were insignificant compared with the microstructural asperities which were produced by the faceted growth in the fully aged condition. The authors (123) also reported a significant influence of oxide asperities on the

fcg response of a P/M 7091 alloy.

The development of both microstructural and oxide asperities should as indicated in Section VII have a beneficial effect and improve the fcg resistance.

14.6 Short Cracks

In a recent paper Lankford (124) has reported results on the growth of short cracks (18 μm to 175 μm) in a 7075 T6 alloy. The direct observations of the crack growth in the SEM revealed grain boundaries as a particular region of resistance to crack extension and in particular for cracks formed in individual grains. It was considered that this resistance to the early growth of cracks by grain boundary regions could lead to the arrest of microcracks. The results and overall view developed by Lankford is presented in Figs. 48 and 49. In the microcrack (short crack) region growth was dominated by local plasticity and the resistance to fcg by the grain boundaries could lead to crack arrest. The potential for this arrest was greater the finer the grain size. Zurek et al. (91) studied the growth of short cracks in a 7075 T6 alloy. They also observed grain boundaries as regions of resistance to crack growth. A plasticity induced crack tip closure stress was introduced to model and predict the fcg rates; Equation 37, Figure 36. These authors confirm the view that fine grain sizes are beneficial to fcg resistance at short crack lengths.

The present position for aluminium alloys is that control of the alloy composition, ageing condition and microstructure can have a beneficial effect on the fcg resistance for both short and long crack configurations.

XV STEELS

In this section the main characteristics of the fatigue threshold and the fcg resistance of steels are highlighted. In general steels are susceptible to environmental attack and to hydrogen embrittlement. This feature tends to keep the intrinsic crack resistance ΔK^i_{th} at a low level.

15.1 Mean Stress

In air environments a wide range of steels exhibit a strong R dependence with fcg rates increasing and ΔK_{th} decreasing as the mean stress is raised. The R dependence is somewhat reduced with negative R ratios (101) and with increasing strength in tempered martensitic steels (61) and more or less completely removed in an inert environment (vacuum < 10^{-5} torr), (6,125). The influence of air and inert environments on the fatigue thresholds of a Ni-Cr-Mo steel designated En 24 are illustrated in Figure 50. The 500°C temper resulted in a yield strength of 1275 MNm^{-2} and the 200°C a yield strength of 1570 MNm^{-2}. Thus, the fatigue threshold in both air and vacuum decrease with increasing yield strength. The results at high R (> 0.7) assuming that crack closure is negligible show that ΔK^i_{th} is strongly influenced by environment. In both ferritic and pearlitic steels the R dependence of ΔK_{th} is strong with $\gamma \to 1$, ' Equation 1, (23,42).

15.2 Crack Length

This topic is under substantial investigation at the present time and reliable data should become available in the medium term. One or two general points however, can be made. As shown in section X (Figure 33) there is a general trend for ΔK_{th} to decrease and fcg rates to increase for cracks less than a critical length.

In low strength steels the formation of arrested microcracks is well established (126,127) and could lead to the form of log ΔK versus log da/dN shown in Figure 42. The complex interaction of microstructure, yield strength, grain size and applied stress level with fcg rate in the "short crack" regime is still to be resolved.

15.3 Yield Strength

The general trend in steels (Figures 22-24) is for ΔK_{th} to decrease with increasing yield strength. This is further illustrated in Figure 51 for a high strength 300 M steel when the ΔK_{th} at low R ratios decreases with increasing cyclic yield strength. It would appear that cyclic softening and the associated slip reversibility can be helpful in improving the crack growth resistance in high strength steels. This decrease in ΔK_{th} with yield strength may well reflect an increasing environmental sensitivity with yield strength. It is interesting to note that the higher ΔK_{th} values for low strength steels is related to the substantial ΔK_{th}^{C} (closure contributions) to ΔK_{th} (Figure 18). It is clearly not possible to compare directly steels with different microstructures and cyclic deformation responses, but it seems likely that variation

in both ΔK^{i}_{th} and ΔK^{c}_{th} with yield strength (and associated microstructures) have to be taken into account when interpreting the overall trends in this area.

15.4 Microstructure

The role of grain size was considered in section V. A comparison of the influence of ferritic and austenitic grain size is presented in Figure 52. If the results for a ferritic steel in Figure 18 are examined it is most likely that the substantial increases in ΔK_{th} for the ferritic steel (Figure 52) arise from the ΔK^{c}_{th} contribution to ΔK_{th}. The prior austenitic grain size has little influence on ΔK_{th} and in so far as the fine transformed microstructure would dominate the crack tip response this result might be expected.

Isothermally transformed 300M offers slightly higher ΔK_{th} values than the equivalent quenched and tempered microstructure. (Figure 51).

A similar effect of the presence of retained austenite marginally improving the ΔK_{th} response has been observed in a 9Ni-4Co 0.2C high strength steel (126) tested in air at ambient temperatures.

Two examples of the microstructure improving both the yield strength and ΔK_{th} have been reported (42,36). In a pearlitic steel (42) the refining of the pearlite spacing with increasing manganese content raised the yield stress from 434 to 590 MNm^{-2} and ΔK^{i}_{th} (R = 0.5) from 4.4 to 6.0 $MNm^{-3.2}$. In AISI 1618 duplex steel the ferrite with island martensite (σ_y = 290 MNm^{-2}) had a ΔK_{th} of $\sim$ 8 $MNm^{-3/2}$

whereas the martensite with island ferrite (σ_y = 452 MNm^{-2}) had a ΔK_{th} of 20 MNm^{-2}.

Both of these results (42,36) are consistent in principle with the results presented in Figure 20 and with the premise that ΔK^i_{th} increases proportionally with $(E\ \sigma_y)^{\frac{1}{2}}$ in the absence of strong environmental factors and crack closure.

The results of Ritchie and Suresh on high strength steels show that a build up of oxide near the crack tip can lead to substantial increases in ΔK_{th} at low R ratios through the ΔK^c_{th} component. In low and medium strength steels where a dominantly transgranular mode of fcg occurs there will be a contribution to the closure from both microstructural and oxide asperitus.

In conclusion, it is now obvious that there is little benefit to be gained from attempting to rationalise the fcg and ΔK_{th} response of steels over the whole strength and microstructural spectrum. The cyclic deformation characteristics and closure response of martensitic and ferritic and pearlitic microstructures are quite different and their potential fcg response at low ΔK's should be treated quite separately.

XVI. TITANIUM ALLOYS

The fcg characteristics of titanium alloys have been investigated over a wide range of microstructural, environmental and mean stress conditions, (1,2,4,9,31,41,59, 71,129-135,87,136-142).

Yield Strength

The general trend is for ΔK_{th} to decrease with increasing yield strength. However, for a particular group of alloys such as the α or α/β titaniums the reverse trend is observed (41). Whilst the fcg mode is dominantly a transgranular one with an α or near α microstructure ΔK_{th} increases with yield stress. If however as in the Ti-6Al-4V the fcg mode involves both α/β interface separation and transgranular fcg in the α grains then refining the microstructure leads to higher yield strengths and lower ΔK_{th}. In Ti-6Al-4V (mill annealed) ΔK_{th} can be less than $3 MNm^{-3/2}$ for a yield strength of 850 MNm^{-2} whilst in α-titanium ΔK_{th} can be $5 MNm^{-3/2}$ for a yield strength of 400 MNm^{-2}.

Because of the significant influences of microstructure and closure on ΔK_{th} and da/dN in these alloys it is not possible to predict these parameters on the basis of yield strength alone.

16.2 Microstructure

There have been many studies of the role of microstructure and the microstructure/environment interaction. There is evidence that ΔK^i the intrinsic element in ΔK is influenced by the basic microstructural/environmental condition at the crack tip. However, a detailed analysis of the role of microstructure is restricted by the lack of information with respect to both ΔK^i_{th} and ΔK^c_{th}. Only recently has information or ΔK^c_{th} become available and hence an evaluation of ΔK^i_{th} possible. The result of β-heat treatment of a mill annealed Ti 6Al-4V alloy was to improve the fcg resistance by a factor of 10 at a ΔK of 10 $MNm^{-3/2}$. This improvement was shown to be directly attributable to a coarser α-grain size increasing the closure component K^c (13), (Fig. 53). Recent results on Ti 6Al 4Zr 0.5Mo (IMI 685) with a range of prior β grain sizes (0.6 to 0.88 mm) and colony sizes (0.1 to 0.2 mm) exhibited room temperature/air ΔK_{th} values in the range 8 to 12 $MNm^{-3/2}$ for R = 0.1. From a detailed analysis of the crack closure behaviour it was shown that ΔK^i_{th} was in the range of 4 to 5 $MNm^{-3/2}$, independent of microstructure and R ratio. The fcg curves log ΔK^i (ΔK_{eff}) versus log da/dN were also superimposed upon one another for the ΔK^i range 5 to 20 and for the R ratio range 0.12 to 0.61. It would thus appear that in some cases at least that improvements in ΔK_{th} and fcg resistance are attributable the microstructural features increasing the closure contribution ΔK^c.

In a recent technical report Ward-Close et al. (143) have presented information on the intermediate and low fcg behaviour of a Ti 4Al 2Sn 4 Mo (IMI (550) alloy. Their results together

with other data for α/β alloys following various thermomechanical working and heat treatments are presented in Fig. 54. This information shows clearly that substantial differences (factors 10 to 20) in the fcg resistance of α/β and near α titanium alloys exist as a consequence of variable microstructures.

16.3 Crack Length

Brown and Smith (142) studied the fcg and threshold behaviour of Ti 6Al 4V containing "short cracks". The ΔK_{th} were in the range 4.5 to 6 $MNm^{-3/2}$ and increased with grain size. In a more recent study the growth of fatigue cracks in corner cracked specimens of IMI 685 has been reported (87). The prior β grain size was ∿5 mm and the colony size ∿1 mm. Thus, cracks of ∿1 mm in length behaved as "short crack" in this microstructure. The results of this study are presented in Fig. 35, and it can be seen that fcg rates in IMI 685 can be 20 to 50 faster than in a Ti 6Al 4V (Ti 318) or aluminium alloys or steels. These results indicate that where the crack length is less than the grain size relatively high fcg rates might be experienced with the range of microstructures in titanium alloys and the limited information available it is not possible at the present time to generalise the influence of crack length on ΔK_{th} or fcg rates.

The α/β and near α titanium alloys have been shown to exhibit substantial resistance to fcg and tolerably high ΔK_{th} levels through both the intrinsic and closure contributions to ΔK. Two microstructural conditions namely, coarse β grain sizes

(>2 mm) and fine grain sizes (<10 μm) can potentially lead to both high fcg rates and low threshold ΔK's.

XVII CONCLUDING REMARKS

This review has outlined some of the areas where a reasonable level of understanding has been achieved in relation to fcg at low stress intensities and ΔK_{th}. Considerable attention has been given to the occurrence and extent of fatigue crack closure. This reflects the growing awareness of the role of closure in determining fcg resistance. Closure is always benefical to fcg resistance and is a substantial contributer when the stress ratio R is less than 0.5. From an understanding of the closure process and the measurement of ΔK^c it is possible to obtain ΔK^i and present data in the form log da/dN v log ΔK^i. This permits an approach which is conservative in nature and identifies the minimum ΔK_{th} and the maximum fcg rates that the material can experience for a given set of conditions. Presently, this approach has been applied to data obtained under laboratory conditions and with the applied load range constant.

The "short" crack problem is presently under attack and is somewhat contraversial at the present time. Some resolution as to the role of microstructure, mean stress and applied stress in this regime should become available in the medium term.

In the preparation of a review of this nature there is a general tendency to try and rationalize the available data

It has not been possible, mainly due to the interactive nature of many of the variables to present a unified fcg model with the appropriate formulations. To some extent the review developed in the other direction and indicated that over simplification does not necessarily improve our understanding of, for example, the role of yield stress and microstructure in determing fcg rates. It is hoped that this document will provide a basic for current discussion and future research into fcg at low stress intensities in metals and their alloys.

REFERENCES

1. J.L. Robinson and C.J. Beevers, Metal Science Journal, 7, p 153 (1973).
2. C.M. Ward-Close and C.J. Beevers, Met. Trans. A. 1A p. 1007, (1980).
3. C.J. Beevers, Fracture 1, p. 239, (1977) ICF 4 Waterloo, Canada.
4. N.J. Walker and C.J. Beevers, Fatigue of Engineering Materials and Structures, 1 p. 135-148, (1980).
5. G. Birbeck et al. J. Metal Science, 6 p 319 (1971)
6. R.J. Cooke et al. Engineering Fracture Mechanics 7 69-77 (1975).
7. S. Suresh et al. Met Trans. 12A p. 1435 - 1443 (1981).
8. B.R. Kirby and C.J. Beevers, Fatigue of Engineering Materials and Structures, 1, p. 203-215, (1979)
9. P.E. Irving and C.J. Beevers, Met. Trans. A. 5 p. 391 (1974).
10. J.K. Musuva and J.C. Radon, Fatigue of Engineering Materials and Structures, 1 p. 457, (1979).
11. P.C. Paris, 1, p (1982) Fatigue Thresholds Stockholm June 1981. Editor J. Backlund et al. Pub. EMAS Warley. West Midlands, U.K.
12. M. Klesnil and P. Lukas, Material Science and Engineering, 9, p. 231 (1972).
13. N.E. Frost et al. Engineering Fracture Mechanics, 3, p. 109, (1971).

14. O. Vosikovsky, J. of Testing and Evaluation, 6, p. 175 (1977).

15. I.M. Bensor in W.R.C. Bulletin (1974).

16. A.J. McEvily Metal Science Journal, 11 p. 274 (1977).

17. R.P Wei and A.J. McEvily, Proceedings Corrosion Fatigue Conf. Stors. Conn. USA. 1971.

18. R.T. Davenport and R. Brook, Fatigue of Engineering Materials and Structures 1 p. 151 (1979).

19. S. Usami, Fatigue Thresholds, Stockholm, June 1981. 1, 205-238 (1982).

20. K.E. Priddle, Fatigue Thresholds, Stockholm, June 1981. 1, p. 581-600 (1982).

21. B.L. Freeman et al. Fatigue Thresholds, Stockholm June 1981, 1 p. 547-561, (1982).

22. K.E. Priddle, Scripta Met. 12, p 49, (1978)

23. J. Masounave and J.P. Bailon, Scripta Met. 10, p. 165-170 (1976).

24. C.J. Beevers, ICF5 Canus April (1981) Advances in Fracture. Pub. Pergamon Press.

25. P. Boisson et al. Mem. Sci. Rev. Met. 74, p. 427 (1977).

26. A.T. Stewart, Engineering Fracture Mechanics, 13 P. 463, (1980).

27. K.E. Priddle and C. Wiltshire. International Journal of Fracture. 1, p. 697, (1975).

28. J. Petit and A. Zeghloul. Fatigue Thresholds. Stockholm, June 1981, 1, p. 563-579, (1982).

29. R. Gangloff, Advances in Crack Length Measurement, Ed. C.J. Beevers. To be published 1983.

30. C.J. Beevers, Metal Science Journal, September p. 418-423 (1980).

31. M.D. Halliday and C.J. Beevers, American Society of Testing Materials, p. 195-201, (1981).

32. M. Chana, Ph.D. Thesis, University of Birmingham, 1981.

33. W.W. Gerberich and W.R. Moody, Fatigue Mechanisms, ASTM STP 675, p. 292 (1979).

34. S. Taira, Fatigue Mechanisms ASTM STP 675, p. 135, (1979)

35. R.O. Ritchie, Fatigue 1977, Univ. Cambridge, p.62 pub. Metals Society.

36. H. Suzuki and A.J. McEvily, Met. Trans. 10A, p. 475 (1979).

37. O.M. Romaniv et al Soviet Material Science, 1, p. 113 (1978).

38. G.J. Fowley, Material Science and Engineering, 39 p. 121, (1979).

39. J.P. Benson and D.V. Edmunds, Metal Science Journal 12, p. 123 (1978).

40. C.M. Austin et al, Met. Trans. 8A, p. 1621 (1977).

41. C.J. Beevers, Fatigue Thresholds Stockholm, June 1981, 1 p. 257, (1982).

42. R.J. Cooke and C.J. Beevers, Engineering Fracture Mechanics 5, p. 10, 61-1071, (1973).

43. K. Minakawa and A.J. McEvily, Fatigue Thresholds. Stockholm, June 1981, 1, p. 373 (1982).

44. W. Elber, Engineering Fracture Mechanics, 2, p. 37, (1970).

45. W. Elber, ASTM STP 486, p. 230.

46. R. Roberts and R.A. Schmidt, International J. of Fracture, 8, p. 469, (1972).

47. W.M. Sharpe and A.F. Grandt, AFML-TR-74-203, March (1975).

48. W.M. Sharpe et al. AFML-TR-75-77, August (1975).

49. O. Buck et al. ASTM STP 513, p. 280, (1972).

50. O. Buck et al. Engineering Fracture Mechanics, 5, p. 23, (1973).

51. C.L. Hoet, ASTM STP 536, p. 5 (1973).

52. V. Backman and D. Munz, International Journal of Fracture, 11, p. 73, (1975).

53. V. Backman and D. Munz, Fatigue Testing and Design, Society of Environmental Engineers, 2, p. 351, (1976).

54. A.M. Sullivan and T. Croker, Engineering Fracture Mechanics, 19, p. 749, (1977).

55. T.C. Lindley and C.E. Richards, Material Science and Engineering, 14, p. 281, (1974).

56. T.T. Shih and R.P. Wei, Engineering Fracture Mechanics, 16, p. 19, (1974).

57. P.E. Irving et al. Engineering Fracture Mechanics, 7, p. 169, (1975).

58. K. Sadananda and P. Shahinian, Characterisation of Materials for Service at Elevated Temperature. Montreal, Canada, p. 107, June (1978).

59. M.D. Halliday, ICF 5 (Pergamon Press, Advances in Fracture Research) p. 953, (1981).

60. C.J. Beevers and K. Bell, to be published.

61. R.O. Ritchie et al. J. Engineering Materials and Technology, 102, p. 293, (1980).

62. S. Suresh and R.O. Ritchie, ICF 5, (Pergamon Press) Advances in Fracture Research, p. 1873 (1981).

63. A.T. Stewart, Engineering Fracture Mechanics, 13, p. 463, (1980).

64. J.C. Newman, NASA Technical Memoranda 8194 and 81942.

65. C.J. Beevers et al. A Model for Fatigue Crack Closure - to be published.

66. J.R. Rice. Fracture of Solids, Ed. H. Liebowitz, Academic Press, 2 p. 218-221, (1969)

67. F.A. McClintock and G.R. Irwin, ASTM STP 381, p. 84, (1963).

68. T.L. Mackay, Engineering Fracture Mechanics, 11, p. 753, (1979).

69. R.J. Bucci et al. ASTM STP 536, p. 206, (1973)

70. E. Tschog and S. Stanzl, Acta Met. 29, p. 21, (1981).

71. C.J. Beevers, Tewksbury Symposium, Melbourne, p. 179, (1974).

72. K.J. Jatavallabula and W.W. Gerberich, J. Fatigue of Engineering Materials and Structures, 4, p. 173 (1981).

73. C. Bathias et al. ICF 4. Advances in Fracture Research Waterloo, Canada, 2, p. 1283 (1977).

74. J. Mautz and V. Weiss, ASTM STP 601, p. 154.

75. J.C. Radon, J. Metal Science, 18, p.441, (1981).

76. R.P. Skelton and J.R. Haigh, J. Material Science and Engineering, 36, p. 17, (1978).

77. R. Stickler and B. Weiss, Fatigue up to Ultrasonic Frequency Severn Springs, Oct. 1981.

78. L.P. Pook and J.K. Sharpes, International Journal of Fracture, 15, p. 223. (1979).

79. L.P. Pook and A.F. Green, NEL Report 654, (1978).

80. L.P. Pook and A.F. Green, ASTM-STP 677, p. 22 (1979).

81. N.E. Frost et al. Metal Fatigue, Clarendon Press, p. 44, (1974).

82. N.E. Frost et al. Engineering Fracture Mechanics, 3, p. 109, (1971).

83. S. Pearson, RAE Tech. Rep. 72236 (1973).

84. H. Kitagawa and S. Takahashi, Second Int. Conference on Mechanical Behaviour of Materials, Boston, 1976 p. 627-631.

85. P. Chauhan and B.W. Roberts, The Metallurgist and Metals Techologist, March, p. 131, (1979).

86. H. Romaniv et al. Fatigue Thresholds, Stockholm June 1981, 2 p.799-802, (1982).

87. C.W. Brown and M.A. Hicks "A study of the Short Fatigue Crack Growth Behaviour in Titanium Alloy IMI 685, To be published, Fatigue of Engineering Materials and Structures. 1983.

88. R.A. Smith, International Journal of Fracture, 13 p. 717, (1980).

89. T.H. Topper and M.H. El Haddad, Fatigue Thresholds, June 1981, Stockholm, 2 p. 777 (1982).

90. S.J. Hudak, J. Engineering Materials and Techology, 103, p. 26, (1981)

91. A.G. Zurek et al. The Effects of Grain Size on the Fatigue Crack Growth of Short Cracks. To be published, Met. Trans. (1983)

92. K. Sadananda and P. Shahinian, International. J. of Fracture, 13, p. 585, (1977).

93. S. Taira et al. ASTM STP 675 p. 135 (1979).

94. S. Purushothaman and J.K. Tien, Met. Trans. A. 9A, p. 351, (1978).

95. S. Purushothaman and J.K. Tien, Material Science and Engineering, 34, p. 241 (19-78).

96. D. Taylor, Fatigue Thresholds, June, 1981, Stockholm 1, p. 455, (1982).

97. V. Weiss and D.M. Lal. Met Trans. 5, p. 1496, (1974).

98. D.N. Lal, V. Weiss, Met Trans. 9A, p. 413, (1979).

99. M. Klesnil and P. Lukas, Engineering Fracture Mechanics, 4, p. 79, (1982).

100. A. Ohta and E. Sasaki, Engineering Fracture Mechanics, 9, p. 307-315, (1977).

101. A. Ohta and E. Sasaki, Engineering Fracture Mechanics, 9, p. 655, (1977).

102. M. Schutz, Engineering Fracture Mechanics, 11, p. 405 - 421, (1979).

103. R.J. Donahue et al. International J. of Fracture Mechanics, 8, p. 209, (1972).

104. A.J. McEvily. The Microstructure and Design of Alloys. Metals Society, London, (1974).

105. R.E. Bara, et al. Proc. 2nd International Conf. on Mechanical Behaviour of Materials Boston, (1976).

106. J.C. Radon, Fatigue Thresholds, Stockholm, June 1981, 1, p. 113, (1982)

107. T.V. Duggan, Engineering Fracture Mechanics, 9, p. 735, (1977).

108. J.T. Dickson, J.P. Bailon and J. Masounave. A Review on the Threshold Stress Intensity Range for Fatigue Crack Growth. To be published, Canadian Metallurgy Quarterly, 20, p. 317, 1981.

109. S.B. Chakraborty, Fatigue of Engineering Materials and Structures, 2, p. 331, (1980).

110. H.C. Heikemon and E.A. Starke, Scripta Met. 16, p.511-513, (1982).

111. ASTM STP 738, p. 321.

112. Determination of characteristics of Fatigue Crack Growth, Soviet Material Science, 3, p. 261-275, (1979).

113. Influence of Various Parameters on the Determination of the Fatigue Crack Growth About Threshold. Fatigue of Engineering Materials and Structures, 4, p. 1-13 (1981).

114. L. Grabowski, University of Birmingham. Private Communication.

115. C.J. Beevers, and J.L. Robinson, University of Birmingham, Reprint. (1973).

116. P.E. Bretz, Effects of Microstructure on 7XXX Aluminium Alloys Fatigue Crack Growth Behaviour Down to Near Threshold. Al coa Report, Oct. 30, 1981.

117. F.S. Lin and E.A. Starke, Material Science and Engineering, 43, p. 65, (1980).

118. L. Edwards and J.W. Martin, ICF 5 Cannes, April 1981, Advances in Fracture. Pub. Pergamon Press.

119. F.S. Lin and E.A. Starke, Materials Science and Engineering, 45, p. 153, (1980).

120. R.J. Bucci et al. ASTM STP 714, p. 411.

121. H.C. Heikemon, F.S. Lin and E.A. Starke, The Effect of Environment on the Low Cycle Fatigue and Fatigue Crack Propagation Behaviour of Al-6-Zn-2Mg 0.1Zr. Alloy, Georgia Tech. Report.

122. Private Communication, E.A. Starke.

123. A.K. Wasudevan and S. Suresh, Influence of Corrosion Deposits on Near Thresholds Fatigue Crack Growth Behaviour, in 2XXX and 7XXX Series Aluminium Alloys. submitted to Met. Trans. A.

124. J. Lankford, Fatigue of Engineering Materials and Structures, 5, p. 233, (1982).

125. P.E. Irving and A. Kunzfeld, Metal Science J., 12, p. 495, (1978).

126. H. Kitagawa and S. Takahashi, Proc. of Second International Conference on Mechanical Behaviour, of Metals, Boston, Aug. 1976, p. 67.

127. H. Kitagawa et al. ASTM STP 675, p. 420. (1978).

128. R.O. Ritchie et al. Fatigue of Engineering Materials and Structures, 1, (1979).

129. C.M. Ward-Close, Proceedings of the Fourth International Confernce on Titanium, 3, p. 1749-156, (1980).

130. A.W. Thompson and J.D. Federson, Metal Science Journal 9, p. 46-48, (1975).

131. G.R. Yodo et al Met Trans A, 9A p. 1413 (1978).

132. G.R. Yodo et al, Journal of Engineering Materials, and Technology, p. 313-318, (1977).

133. J.C. Chestnut et al AFML, Technical Report, TR-78-68 (1978).

134. D. Eylan and J.A. Hall, Met. Trans. 8A p. 981 (1977).

135. J.A. Rupen and A.J. McEvily, Fatigue of Engineering Materials and Structures 2, p. 63, (1979).

136. G.R. Yodo, Transactions of the ASME, 101, p. 86 (1979).

137. S.B. Chakraborty and E.A. Starke, Met. Trans 10A p.1901, (1979).

138. M.A. Hicks et al. Fatigue of Engineering Materials and Structures Slow Fatigue Crack Growth and Threshold Behaviour in IMI 685, To be published in Fatigue of Engineering Materials and Structures 1982/1983.

139. W.J. Evans and C.R. Gostelow, Met. Trans. 10A, p. 1837, (1979).

140. J.R. Wilcox and D.A. Koss, Crack Propagation along Crystallographic Slip Bands and Hydrogen Embrittlement. Third International Conference on Effects of Hydrogen on Behaviour of Materials, August (1980).

141. A. Gysler et al. Fatigue Thresholds, June 1981. 2, p. 655. (1982).

142. C.W. Brown and G.C. Smith, Fatigue Thresholds, June 1981. 1, p. 329, (1982).

143. C.M. Ward-Close et al. Effects of Interstitial Oxygen Content and Solution Heat Treatment Temperature on the Properties of Ti 4Al 4M 4Mo 2Sn 0.5 Si (IMI 550). RAE Farnborough Tech Report TR 81079.

TABLE 1 Crystallographic facets formed during microstructural sensitive fcg.

Reference	Material	Environment	$\Delta K \cdot \frac{da}{dN} \cdot N_f$	Facet Plane	Identification Technique
(a)	Al Zn Mg	Laboratory Air		(001)	Laué X-ray
(b)	Al Zn Mg	3% NaCl solution	10^3	(001)	Laué X-ray
(c)	Cu 47.6% Zn	Laboratory Air	10^5 ↓ 10^7	(110) ± 10°	Laué X-ray
(d)	Al 2024	Laboratory Air	5.5 ↓ 16.5	3° to 20° from (100)	Laué X-ray
(d)	Al 2024	Vacuum (3×10^{-3} torr)	5.5 ↓ 16.5	(001) ± 5° (111)	Laué X-ray
(e)	Nickel Superalloy	Laboratory Air	10^4 ↓ 10^7	(111)	Laué X-ray
(f)	Al 2219-T6	Laboratory Air		(111) ± 5°	Laué X-ray
(g)	Al 2024 - 7075 7178	Dry Air Wet Air Distilled Water	2.2 ↓ 11.0		

TABLE 1 Continued

Reference	Material	Environment	$\Delta K \cdot \frac{da}{dN} \cdot N_f$	Facet Plane	Identification Technique
(h)	Ti 8Al 1Mo 1V	3½% NaCl solution	1.1 ↓ 100	(0001) and 15° from (0001)	Laué X-ray
(h)	Ti 8Al 1Mo 1V	Vacuum (2×10^{-7} torr)	1.1 ↓ 100	two (11$\bar{2}$0) examples	Laué X-ray
(i)	Al 3% Cu	Laboratory Air	7 ↓ 30	(001) ± 5-10°	Laué X-ray
(j)	Ti 6Al 4V Ti 4Al 4Mo 2Sn 0.5Si	Dry Air Moist Air	10^7	15° from (0001) (10$\bar{1}$7)	Laué X-ray
(k)	316 Stainless Steel	Laboratory Air	5.5 ↓ 30.0	(111)	X-ray
(l)	α-Titanium	Laboratory Air	5	(0001) ± 5°	SACP, Selected Area Channelling Pattern
(m)	Fe 3%Si	Laboratory Air	10 ↓ 30	(001)	

(a) Forsyth, P.J.E., Stubbington, C.A. and Clark, D., J. Int. Metals, 90, 238, 1963.

(b) Stubbington, C.A., Metallurgia, 68, 109, 1963.

(c) Williams, H.D. and Smith, G.C., Phil. Mag., 13, 835, 1966.

(d) Meyn, D.A., Trans. ASM, 61, 52, 1968.

(e) Gell, M. and Leverant, G.R., Acta Met., 16, 553, 1968.

(f) Thompson, K.R.L. and Craig, J.V., Met. Trans., 1, 1042, 1970.

(g) Feeney, J., McMillan, J.C. and Wei, P.R., Met. Trans., 1, 1741, 1970.

(h) Meyn, D.A., Met. Trans., 2, 853, 1971.

(i) Garrett, G.G. and Knott, J.F., Acta Met., 23, 841, 1975.

(j) Neal, D.E. and Blenkinsop, P.A., Acta Met., 24, 59, 1976.

(k) Priddle, E.K. and Walker, P.E., J. Mat. Sci., 11, 386, 1976.

(l) Ward-Close, C.M., Private Communication.

(m) Richards, C.E., Acta Met., 19, 583, 1971.

TABLE 2

THE VARIATION OF THE PARAMETER γ (EQUATION 1)

WITH MATERIAL AND ENVIRONMENT

Material	Environment	γ	Reference
Aluminium alloys	Lab air	1.0	a
7075 Al alloy (T651)	lab air	1.0	b
2L93 Al alloy	Lab air	1.0	b
2618A Al alloy (T651)	Lab air	0.61	c
2618A Al alloy (T651)	Lab air	0.43	d
7075 Al alloy (T7351)	Lab air	1.0	b
	Vacuum	0	
Carbon Steels	Lab air	0.71	a
Pearlitic steels	Lab air	0.93,0.94	a, e
A533 and A508 steels	Lab air	0.82	f
En 24 steel	Lab air	0.17,0.47	a
	Vacuum	0	
Ferritic - pearlitic steels	Lab air	1	g
Low Carbon steel	Lab air	1	h
Ti steel	Lab air	0.2 to 0.8	i
HSLA steel	Lab air	0.33	j
316 stainless steel	Lab air	0.5	k
Ti - 6 Al - 4V	Vacuum	0	a
Ti alloy	Lab air	0.7	a

a) C.J. Beevers, Metal Science J. 11 p. 362 (1977).

b) B.R. Kirby and C.J. Beevers, Fatigue in Engineering Materials and Structures 1 p.203 (1979).

c) J. Lanteigne, Ph.D. Thesis Ecole Polytechnic Montreal Canada (1979).

d) C. Robin, Ph.D. Thesis University of Technology Compeigne (1978).

e) R.J. Cooke and C.J. Beevers, Engineering Fracture Mechanics 5 p.1061 (1973).

f) P.C. Paris et al. ASTM STP 513 p.141 (1972).

g) J. Masounauve and J.P. Bailon, Scripta Met. 9 p.723 (1975).

h) J. Masounauve and J.P. Bailon, Scripta Met 16 p.165 (1970).

i) J.P. Benson, Met. Sci. J. 13 535 (1979).

j) A. Otta and E. Sasaki, Eng. Frac. Mech. 9 p.307 (1977).

k) E.K. Priddle, Scripta Met. 12 p.49 (1978).

TABLE 3

The predicted opening loads, Q^1 from Equation 26 and Q^2 from equation 29 compared with the observed opening loads Q^3. The results were obtained from a CTS, B=13 mm, W=26 mm, G=77 GNm^{-2} and E=200 GNm^{-2}.

a/w	C μm	L μm	b μm	Q^1_{open} kN	Q^2_{open} kN	Q^3_{open} kN
.39	15	.100	9	3.23	2.75	1.86
.41	16	.100	9.5	2.90	2.36	1.96
.44	28	.125	11	2.51	2.14	2.01

Table 4: Published threshold data for various metals and alloys determined by ultrasonic resonance test methods

Material	Mode	Test conditions R	Environment	Temp.	Young's modulus	ΔK_{th} at $MN.m^{-3/2}$	da/dN m/cycle	Remarks	Reference
Al	Axial	-1	Oil	293 K	?++)	1,0	$8x10^{-13}$		a
Al	Axial	-1	Air	20 C	69700 - 72000	1,33	$1x10^{-13}$	Grain size and cold work effects	b
AlMg5	Axial	-1	Oil	293 K	?	1,4	$3x10^{-13}$		a
AlZnMg1	Axial	-1	Oil	293 K	?	1,9	$7x10^{-13}$		a
Cu	Axial	-1	Oil	293 K	?	2,7	$4x10^{-14}$	Comparison with NaCl-solutions	a
			Liqu.N_2	77 K	?	2,5	$4x10^{-14}$		
Cu	Axial	-1	Air	20 C	122000 - 126000	1,4-2,0	$1x10^{-13}$	Grain size effect	c
					126000 - 126500	1,4-2,6	$1x10^{-15}$	Cold work effect	
					138000 - 164000	1,6-2,3	$1x10^{-13}$	Single crystals	
Low-C steel	Axial	-1	Oil	293 K	?	3,8	$6x10^{-14}$	Comparison with NaCl-solutions*)	d
			Liqu.N_2	77 K	?	5,3	$9x10^{-14}$		
Low-C steel	Axial	-1		-20 K	?	7,2	$1x10^{-10}$	4,1 $MN.m^{-3/2}$ for 20 Hz	e,f
AISI 304	Axial	-1	Oil	293 K	?	7,0	$5x10^{-13}$	Comparison with NaCl-solutions	d
			Liqu.N_2	77 K	?	8,5	$9x10^{-13}$		
X10Cr13	Axial	-1	Oil	23 C	219600	6,7	$6x10^{-14}$		g
34CrMo4	Axial	-1	Air	20 C	196200	2,45	$1x10^{-12}$		h
C45	Axial	-1	Air	20 C	196200	2,44	$1x10^{-12}$		h

Table 4: Continued

Material	Mode	Test conditions R	Environment	Temp.	Young's modulus N/mm^2	K_{th} at $MN.m^{-3/2}$	da/dN m/cycle	Remarks	Reference
PM-Mo	Axial	-1	Air	20 C	322000	4,8-5,2	$1x10^{-13}$	Grain size effect	i
PM-Mo-0,8W	Axial	-1	Air	20 C	318000	5,8	$1x10^{-13}$		i,j
PM-Mo-1,5W	Axial	-1	Air	20 C	322000	6,6	$1x10^{-13}$		i,j
PM-Mo-Ti-Zr	Axial	-1	Air	20 C	324000	7,0	$1x10^{-13}$		i,j
PM-Nb	Axial	-1	Air	40 C	95500	1,8	$1x10^{-13}$		i,j
PM-Ta	Axial	-1	Air	40 C	179000	3,7	$1x10^{-13}$		i,j
A286	Axial	-1		20 C	?	13,0	$3x10^{-12}$		a
IN-738	Axial	-1	Air	20 C	200000	3,13	$1x10^{-12}$		k
IN-792	Axial	-1	Air	20 C	206600	4,48	$1x10^{-12}$		k
U-700 s.c.	Axial	-1	Air	20 C	?	no threshold down to 10^{-11}			
INCO.800	Transv.0,1-0,3		Air	20 C	?	approx.4	$1x10^{-13}$	+)	e
HASR.X	Tranc. 0,1		Air	20 C	?	no threshold down to 10^{-10}		+)	e
IN 600	Transv.0,3		Air	20 C	?	approx.5	$1x10^{-11}$		

+) Including comparison with low frequency test data

++) ? ... not reported

(a) E. Tschegg et al., US-methods for determination of near threshold FCGRs, Stockholm, S, June 1981, A. Blom Ed.

(b) M. Mullner et al., The effect of microstructure on the FCG behaviour near threshold in Cu and Al. This conference, 1981.

(c) M. Mullner et al., The effect of microstructure on the fatigue threshold in Cu Stockholm, S, June 1981, A. Blom, Ed.

(d) S. Stanzl et al., Influence of environment on FCG in the threshold region. Acta Met. 29, 1981, 21, DGM annual meeting, 1980.

(e) A. Puskar and D. Bokuvka, Kovove materialy 5, 1979, 570.

(f) A. Puskar and D. Kalocova, Kovove Materialy 2, 1981, 186.

(g) M. Speidel, Ermudung von Stahl X20Cr13, Z. Werkstoffkunde 2, 1980, 305.

(h) R. Stickler, Fracture mechanics data and determination for technical alloys, Final report 79-ARGE-BM-B1, 1979.

(i) B. Weiss et al., High cycle fatigue and threshold behaviour of pm Mo and Mo-alloys Fat. Eng. Mat. Struct. 2, 1979, 73.

(j) B. Weiss et al., ΔK_{th}-values for the Ni-base superalloys IN-792 and IN-738 Report COST-50/I, 78-UW-COST-B2, 1978-10-10.

(k) W. Hoffelner et al., Resistance to crack growth under conditions of fatigue, creep, corrosion, COST-50/II, Final Report, March 1981.

(l) W. Hoffelner, Fatigue crack growth at 20 kHz - a new technique, J. Phys. E: Sci. Instr. 13, 1980, 617.

TABLE 5

INFORMATION RELATING TO FIGURE 33 (86)

Material	σ_u MPa	σ_y MPa	Elongation %	Reduction in area %	K_{th} MPa$\sqrt{m}$
Mild Steel	335	242	-	76.3	7.45
Austenitic 0.45C Steel Alloy	750	550	40	25.0	5.0
Al-Mg-Mn	340	180	10	-	2.7

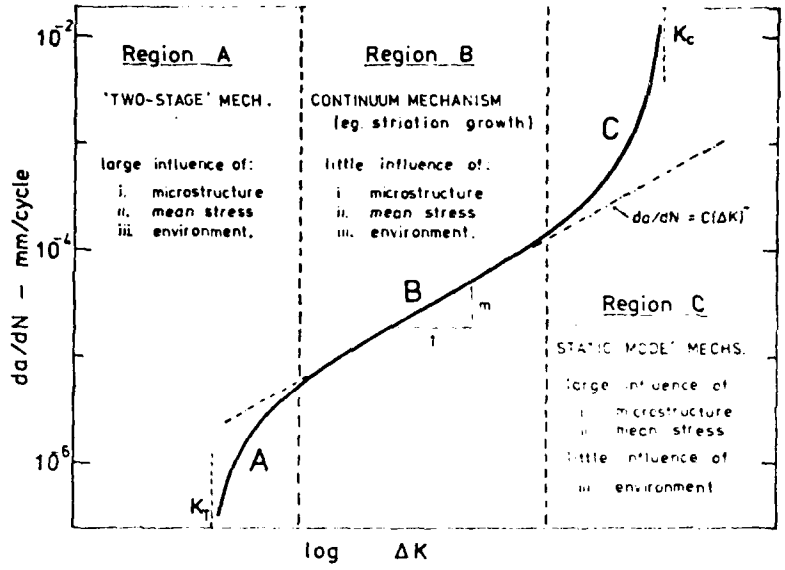

Figure 1 The characteristic log ΔK versus log da/dN response of metallics.

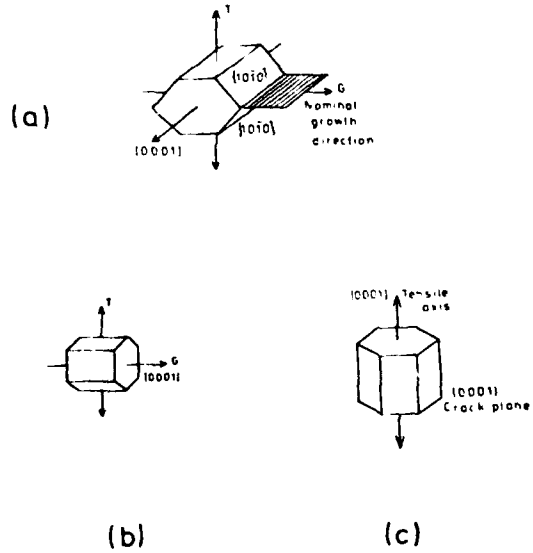

Figure 2 The three principal grain orientations that can be present in the crack tip region of an α-titanium specimen (2).

Figure 3 Striations on the fatigue fracture surface of a grain of orientation (a) in Fig. 2 contained in specimen of α-titanium, $\Delta K \simeq 16$ MNm$^{-3/2}$ (2).

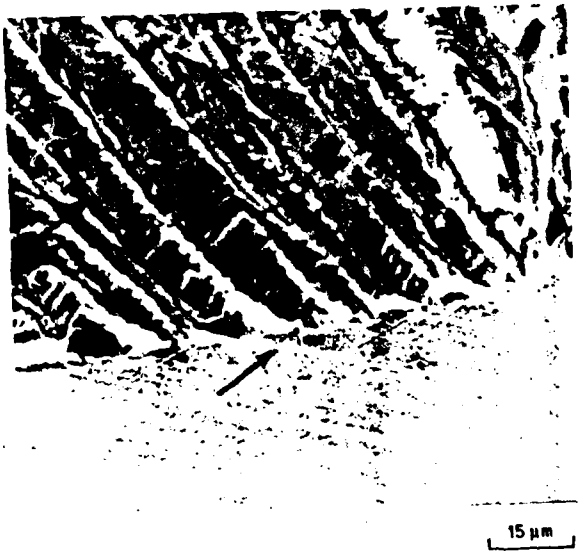

Figure 4 Furrow mode fcg in a grain of orientation (b) in Figure 2, contained in a α-titanium specimen, $\Delta K \simeq 16$ MNm$^{-3/2}$ (2).

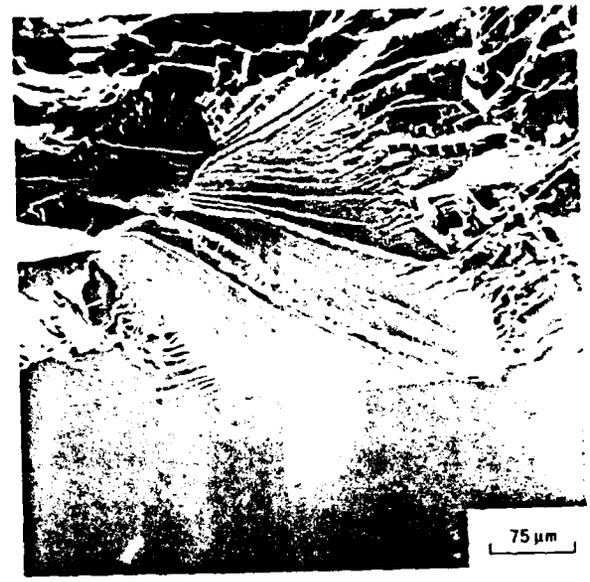

Figure 5 A fatigue facet formed in a grain of orientation (c), Figure 2 during fcg in α-titanium, $\Delta K \simeq 8$ $MNm^{-3/2}$ (2).

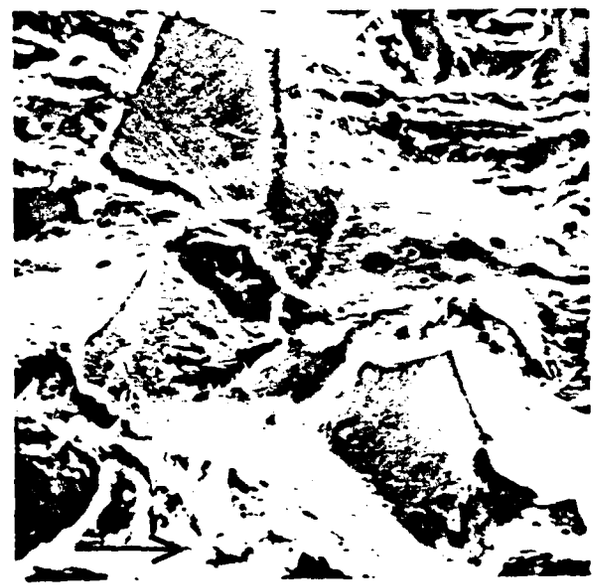

Figure 6 Intergrannular and ductile separation on the fatigue fracture surface of a quenched and tempered low alloy steel (6). x 1,000.

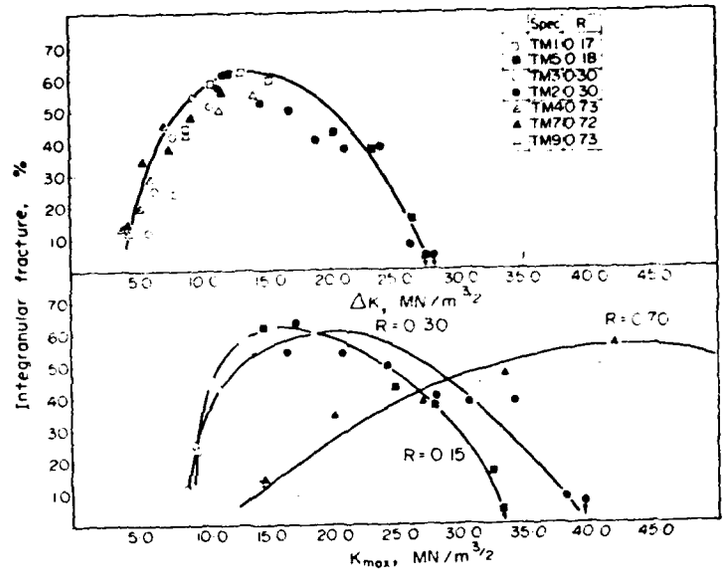

Figure 7 The variation of intergrannular failure as a function of ΔK and K_{max} for a low alloy steel tested in air (6).

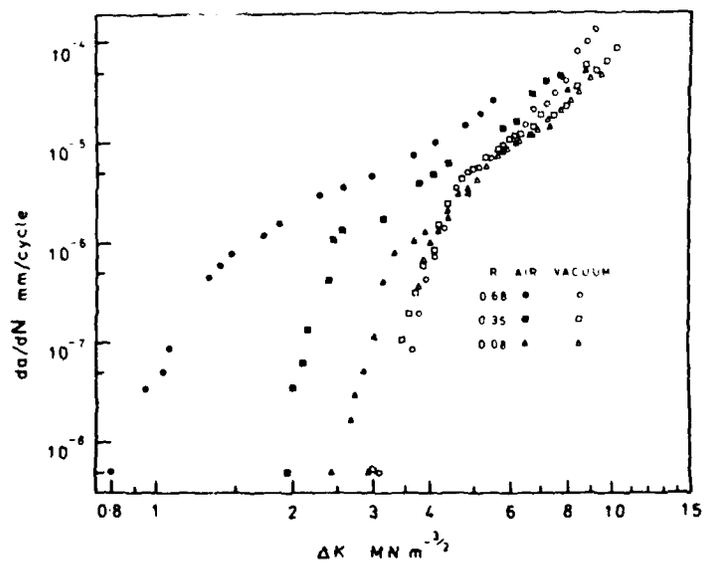

Figure 8 The influence of R ratio in air and vacuum on fcg rates in an aluminium 7075-T 7301 alloy (8).

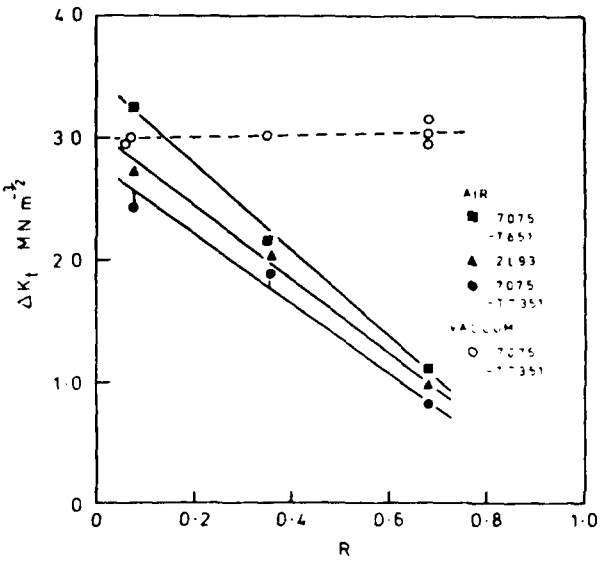

Figure 9 The influence of R ratio on ΔK_{th} for high strength aluminium alloys in air and vacuum (8).

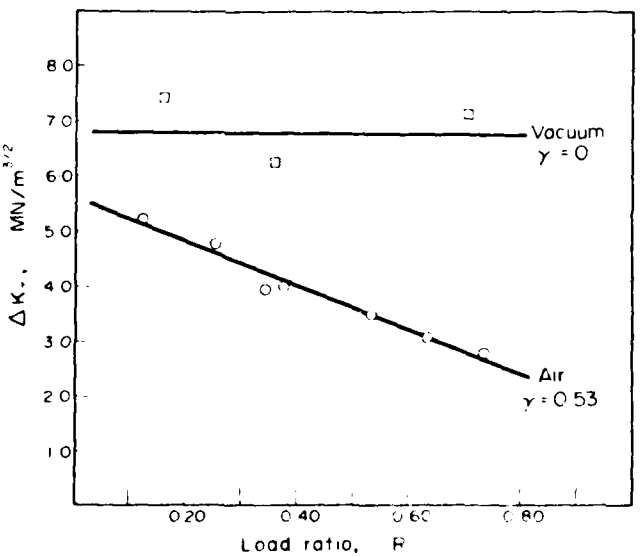

Figure 10 The influence of R ratio on ΔK_{th} for a quenched and tempered Ni-Cr-Mo steel (6).

AD-A128 721 A REVIEW OF FATIGUE CRACK GROWTH IN METALLICS AT LOW STRESS INTENSITIES(U) FINMET CONSULTANTS EDGBASTON (ENGLAND) C J BEEVERS 01 JAN 83 EOARD-TR-83-10

2/2

UNCLASSIFIED F49620-82-C-0088 F/G 20/11 NL

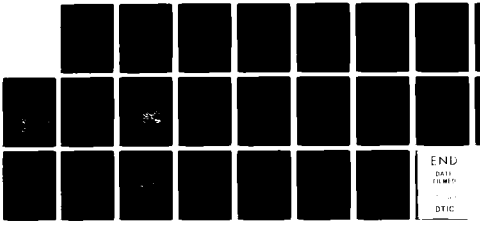

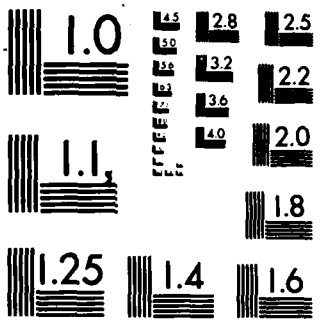

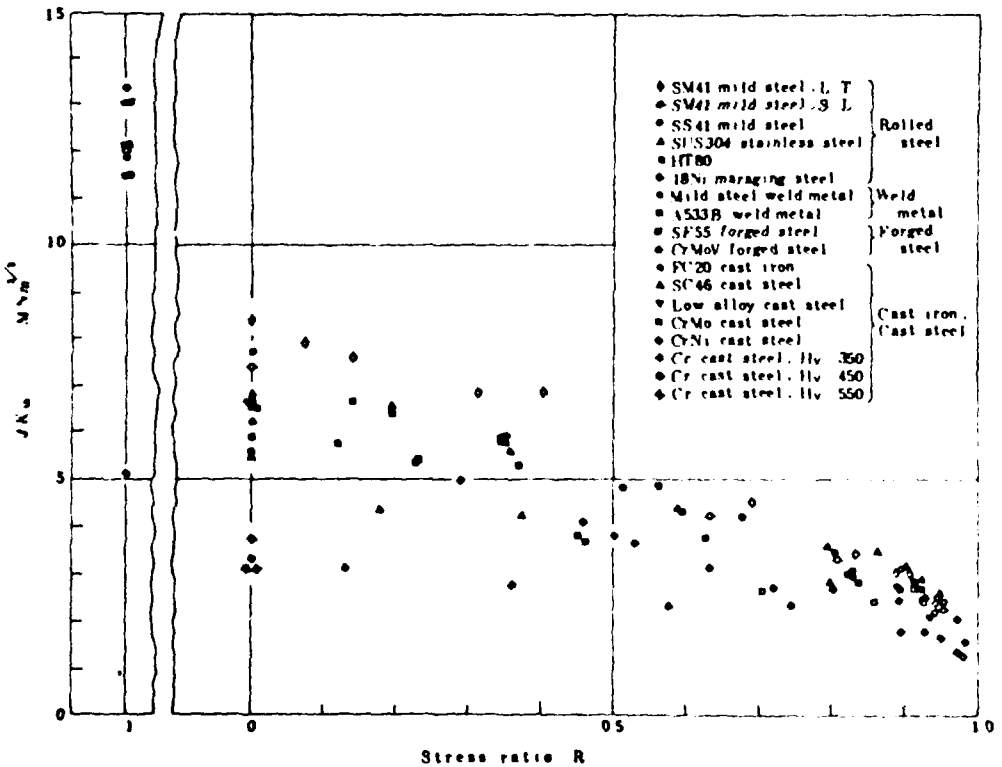

Figure 11 The variation of ΔK_{th} for a wide range of steels over the range R = -1 to 1, (19).

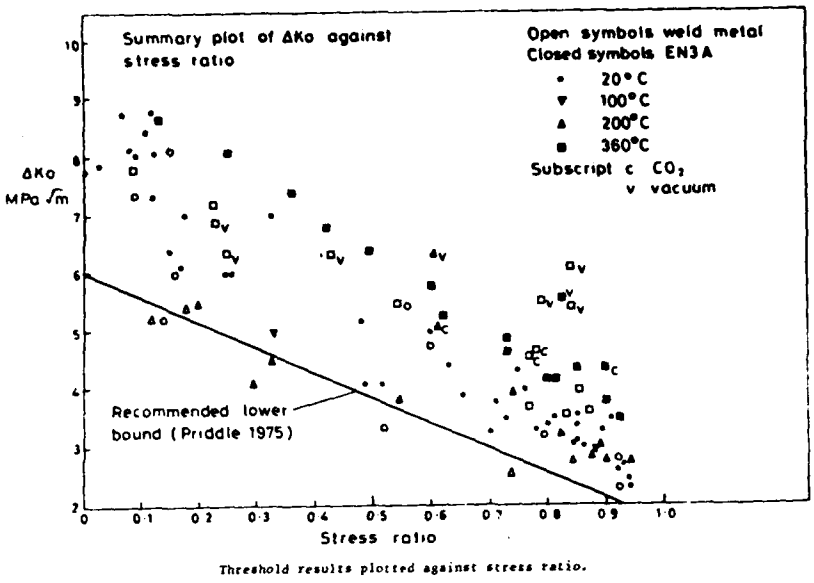

Threshold results plotted against stress ratio.

Figure 12 Influence of R ratio on ΔK_{th} for mild steel tested in a range of environments (20).

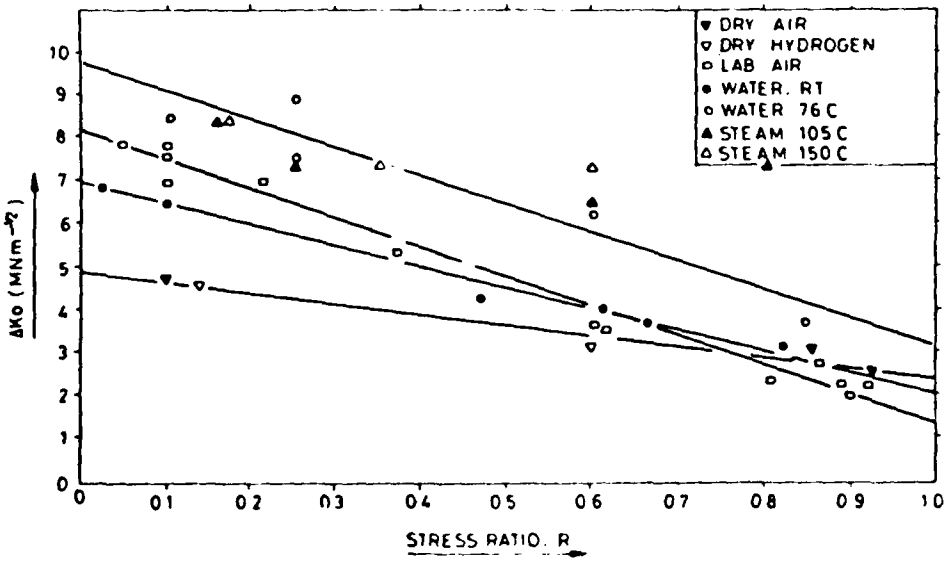

Figure 13 The influence of R ratio on ΔK_{th} for a steel tested in a range of environments (21).

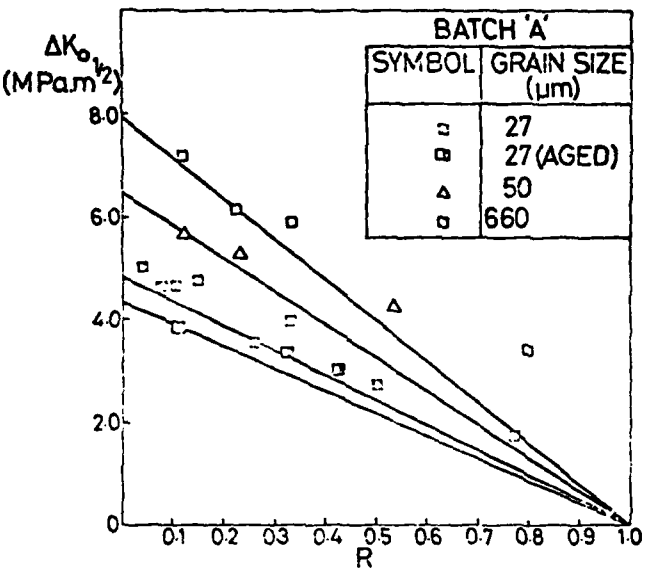

Figure 14 The R dependence of ΔK_{th} for an AISI 316 steel with a range of grain sizes tested in air at room temperature (22).

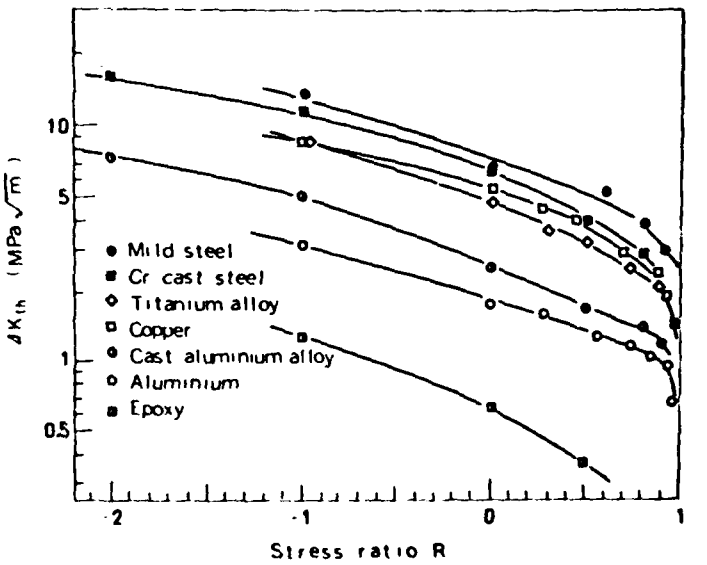

Figure 15(a) The variation of ΔK_{th} with R for a wide range of materials (19).

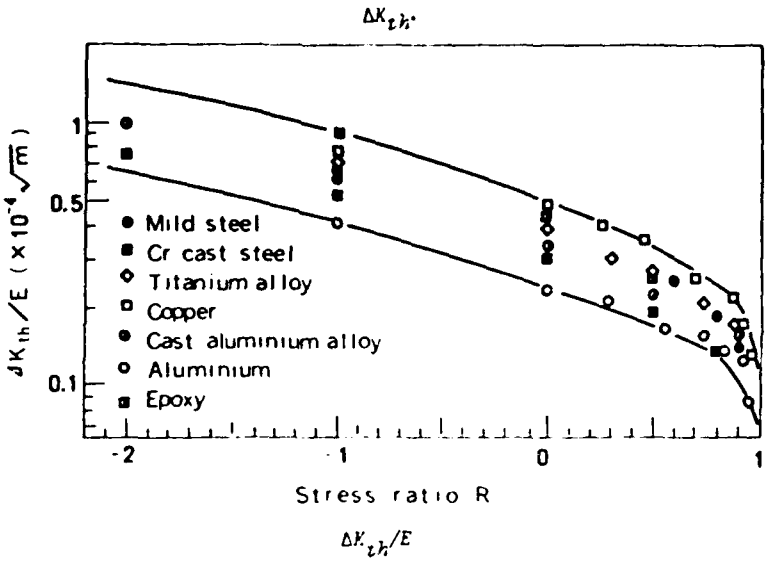

Figure 15(b) The variation of $\Delta K_{th}/E$ with R ratio for a range of materials (19).

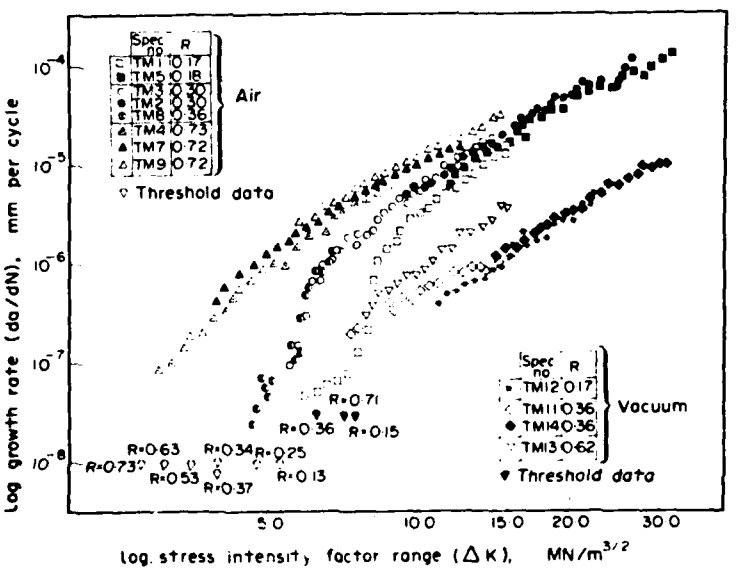

Figure 16 The fcg curves for a high strength steel En 24 tested in air and vacuum over a range of R values (6).

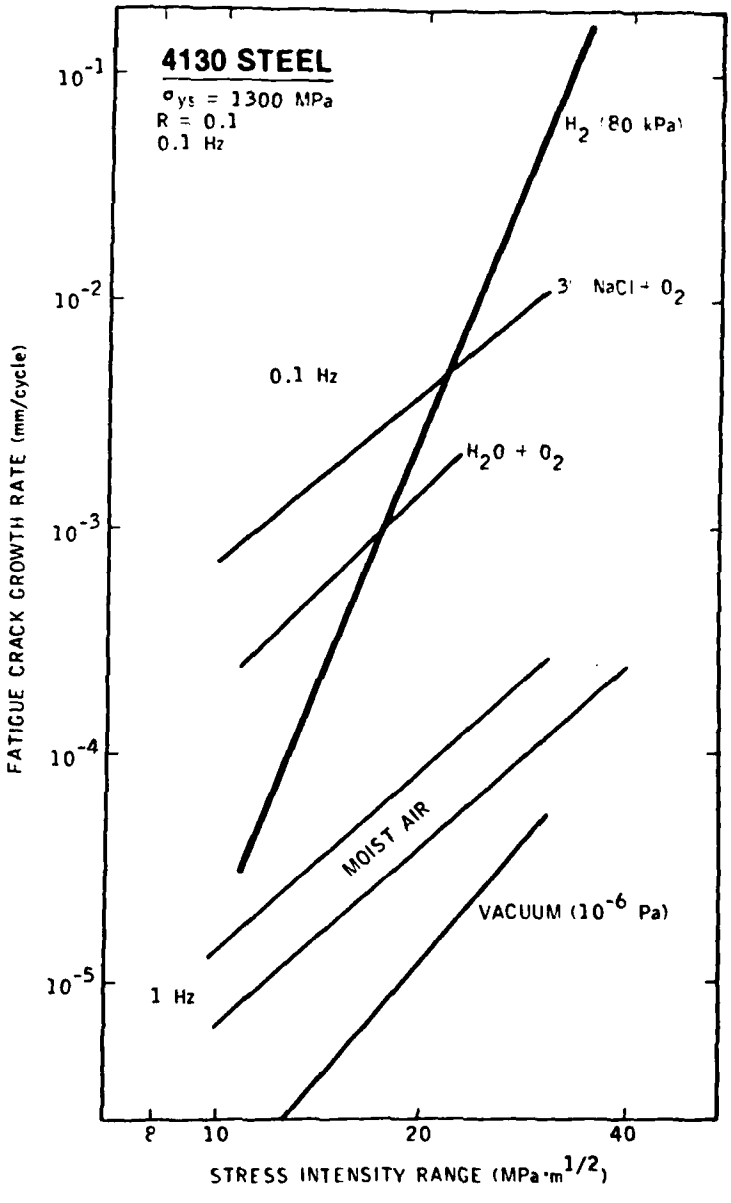

Figure 17 The influence of environment on the fcg behaviour of a 4130 steel (29).

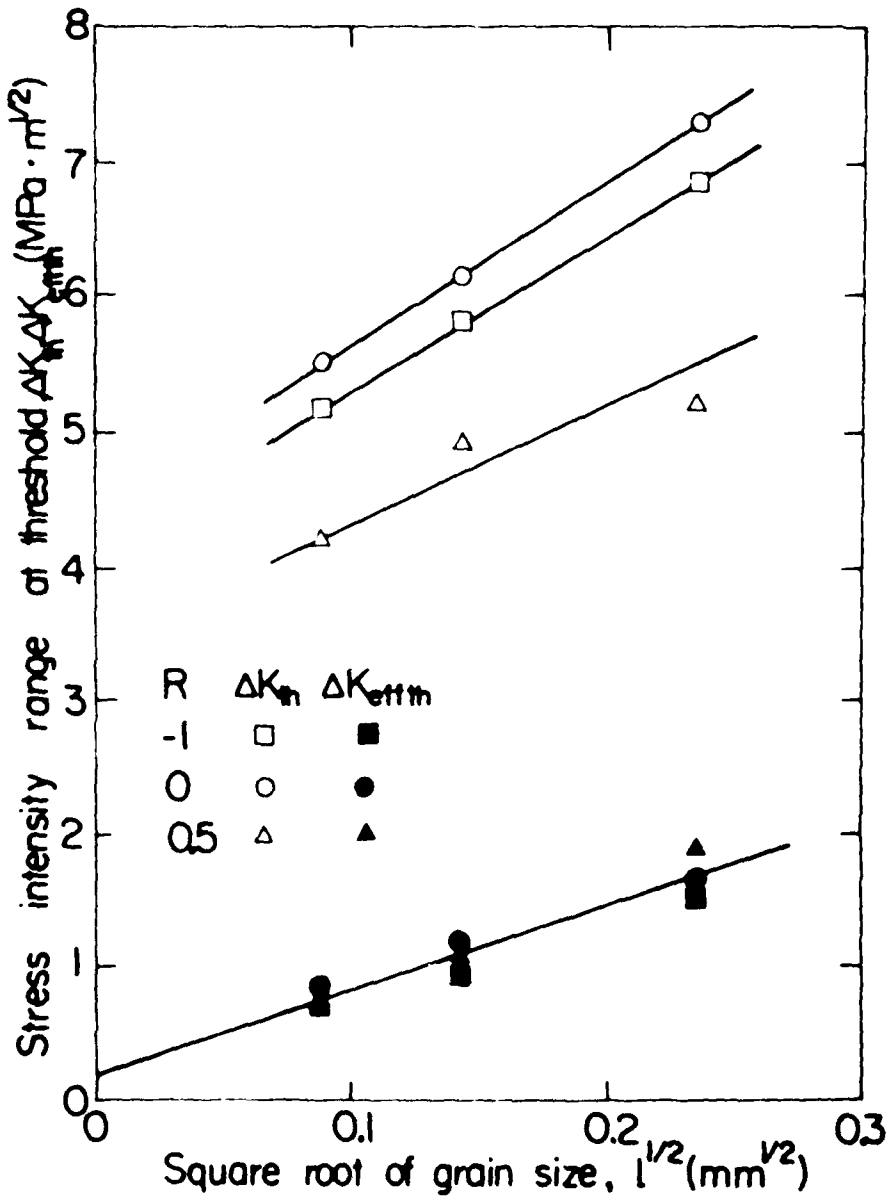

Figure 18 The variation of ΔK_{th} and ΔK^{i}_{th} (ΔK_{effth}) with grain size for a mild steel (34).

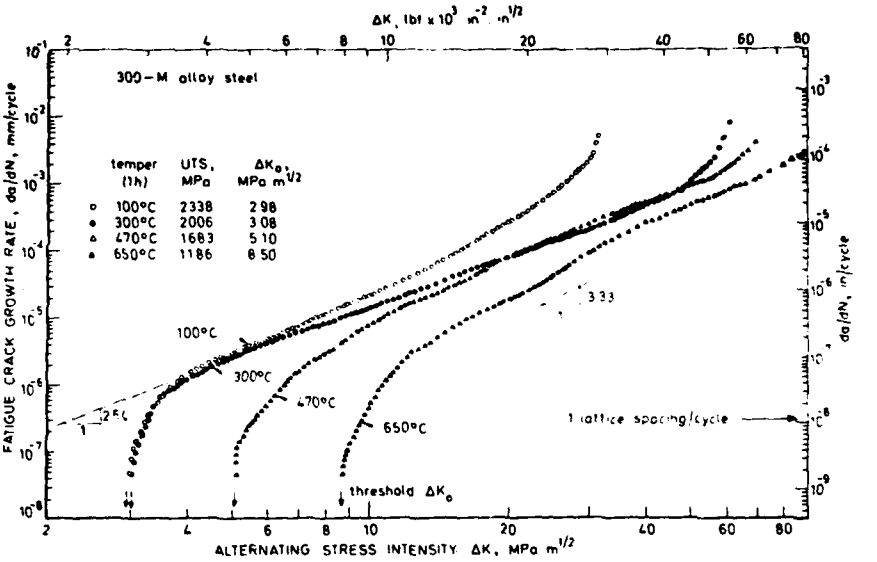

Figure 19(a) Fcg behaviour of 300 M steel as influenced by tempering temperature R = 0.1 (35).

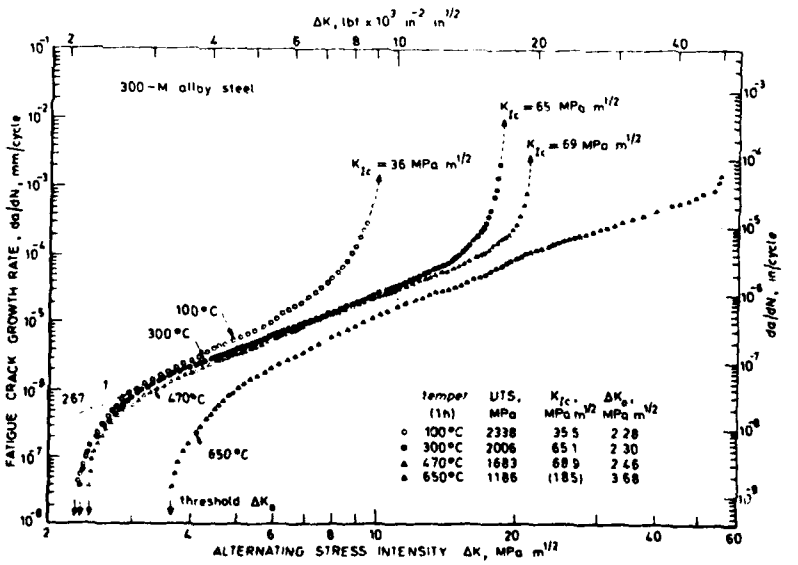

Figure 19(b) Fcg behaviour of 300 M steel as influenced by tempering temperature R = 0.7.

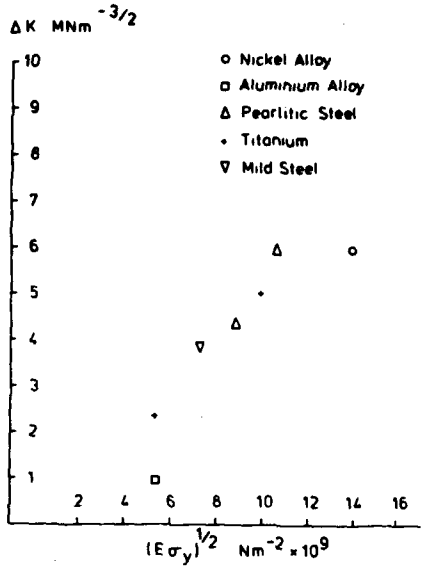

Figure 20 The influence of $(E\sigma_y)^{\frac{1}{2}}$ on ΔK^i_{th} for a range of metals and alloys exhibiting dominantly transgranular fcg (41).

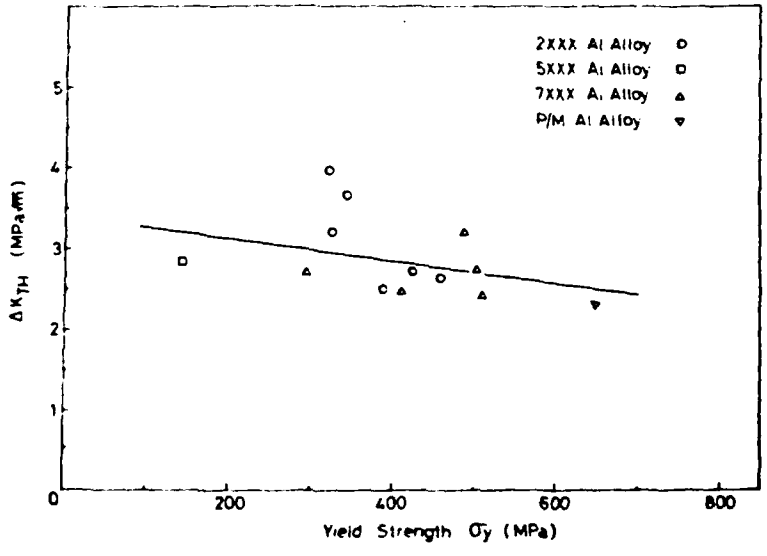

Figure 21 The influence of yield strength on ΔK_{th} for a range of high strength aluminium alloys (43).

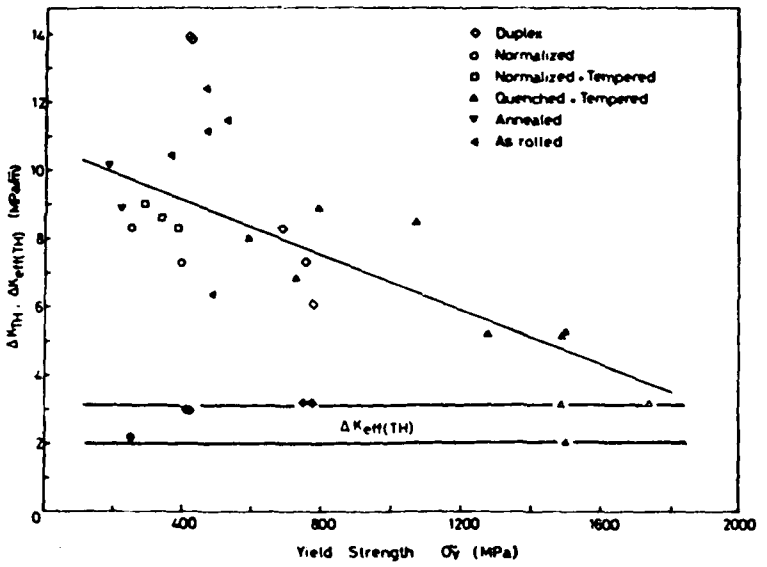

Figure 22 The influence of yield strength on ΔK_{th} for a range of steels (43).

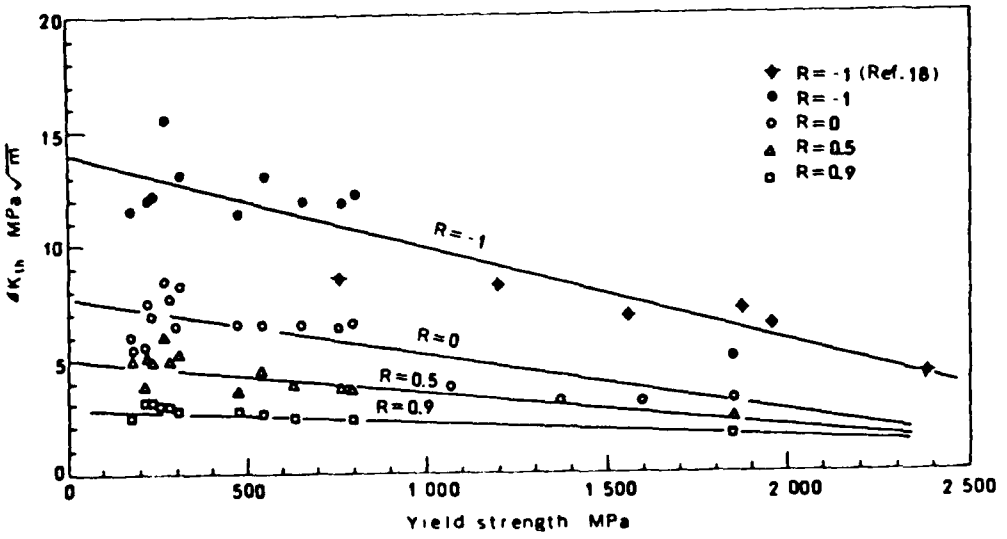

Figure 23 The influence of yield stress on ΔK_{th} for a range of mean stress in steels (19).

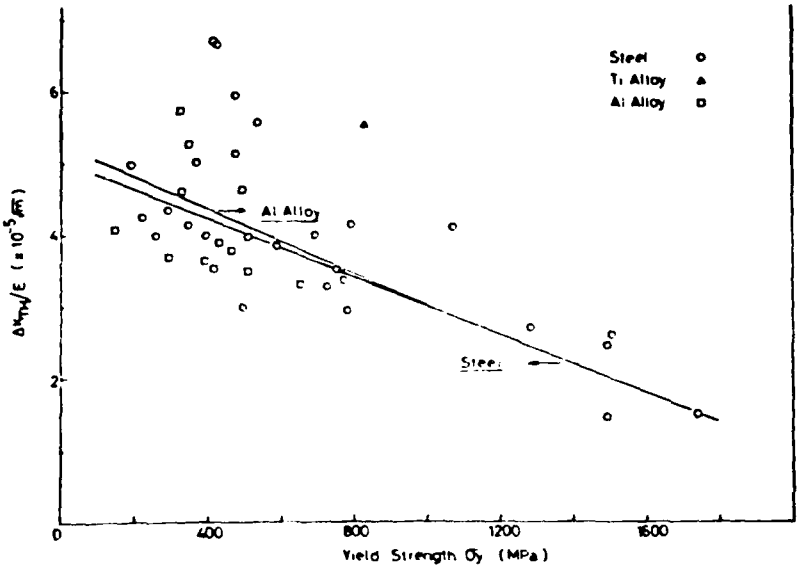

Figure 24 The influence of yield strength on ΔK_{th} for steels, titanium and aluminium alloys (43).

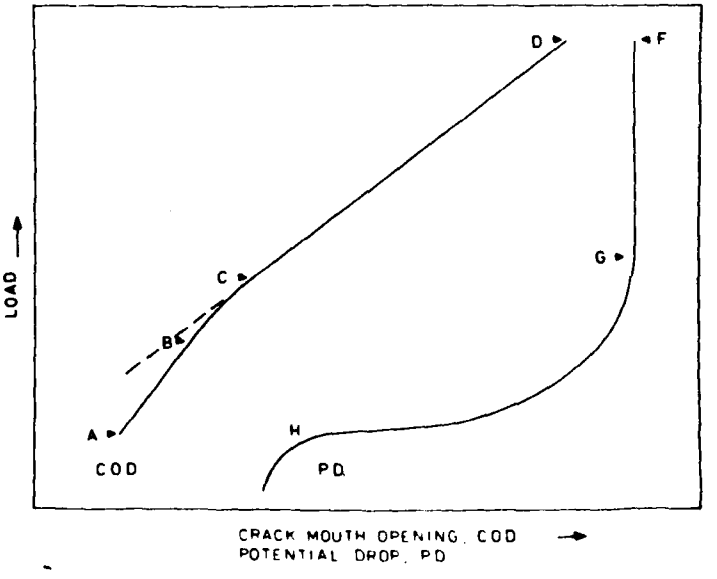

Figure 25 A schematic of the COD and potential difference response in the presence of crack closure.

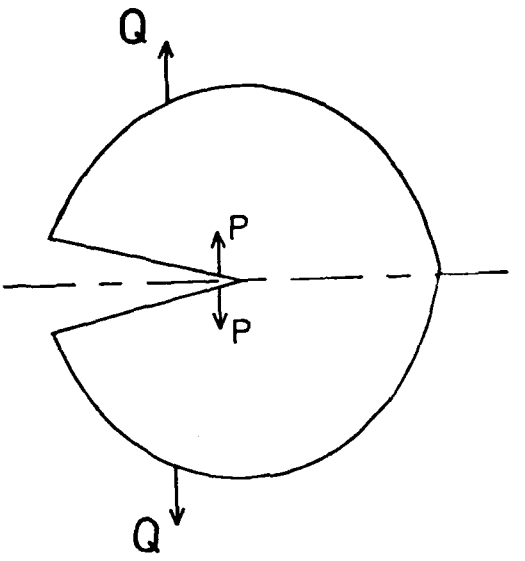

Figure 26(a) External and crack tip loading.

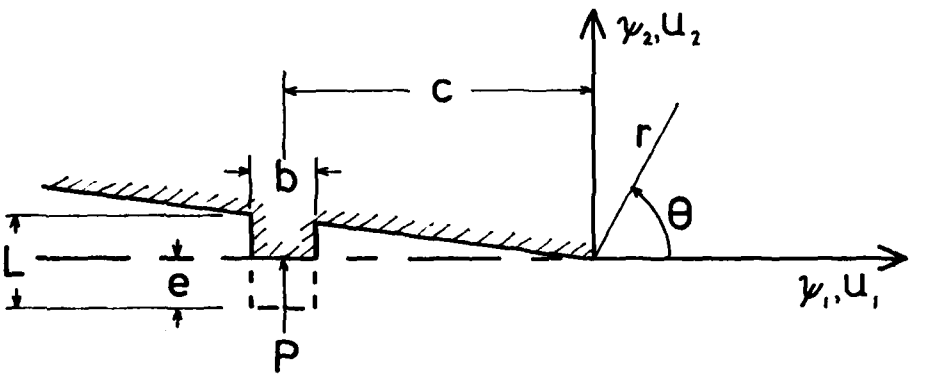

Figure 26(b) Upper crack face loading.

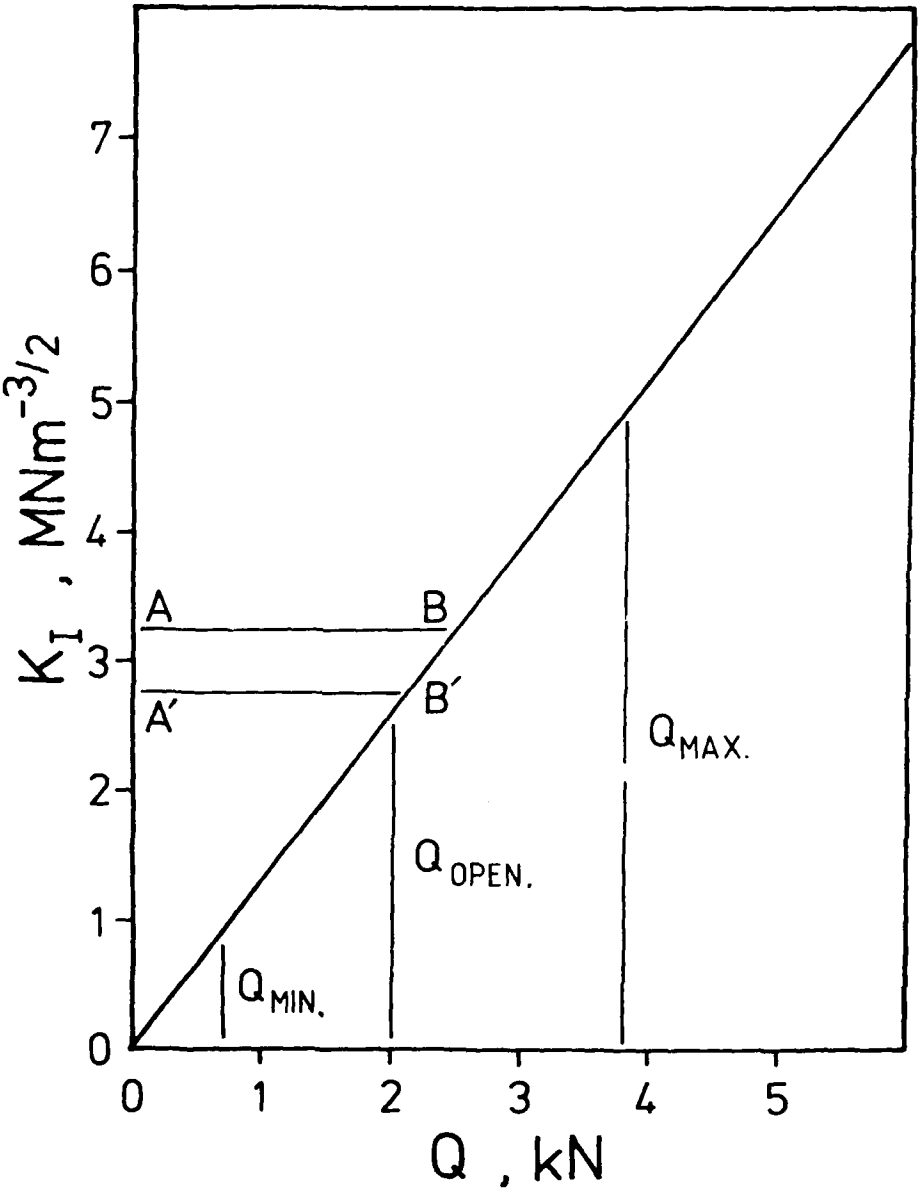

Figure 27 Stress intensity factor versus load for a CTS specimen, B=13 mm, W=26 mm, a/w=0.44, C=28 μm, L=0.125 μm, G=77 GNm^{-2} and E=200 GNm^{-2}.

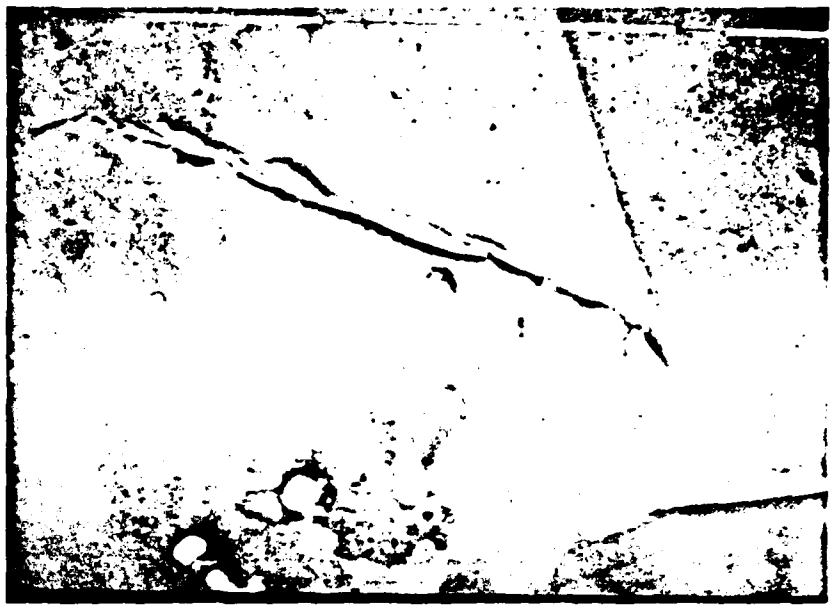

Figure 28 The crack tip region of a nickel CTS specimen showing the closure of the crack faces. x 2,500

Figure 29 Scanning electron micrograph of the fatigue fracture surface. R=0.1, ΔK=13.2 $MNm^{-3/2}$. x 320

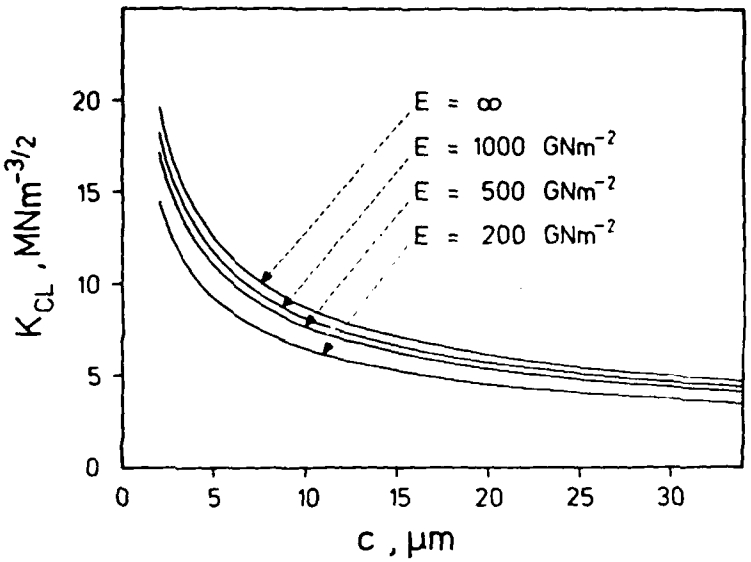

Figure 30 The influence of C and the rigidity of the asperity on K_{CL}, for L=0.2 μm, b=0.5 μm, G=77 GNm^{-2}, ν=0.3.

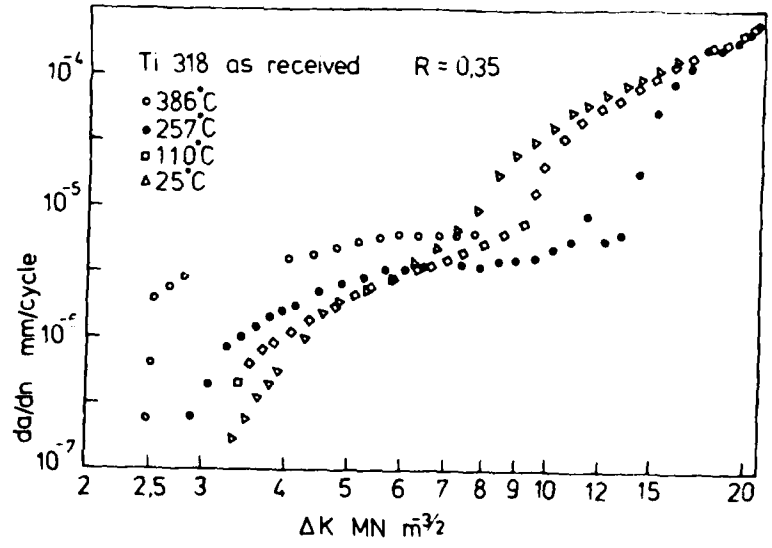

Figure 31 The influence of test temperature on fcg rates in a mill annealed Ti-6Al-4V alloy (71).

Figure 32 The fracture surface of a Ti-6Al-4V sample fatigued at 257°C showing facetted regions extending over several α grains (71). x 2,000

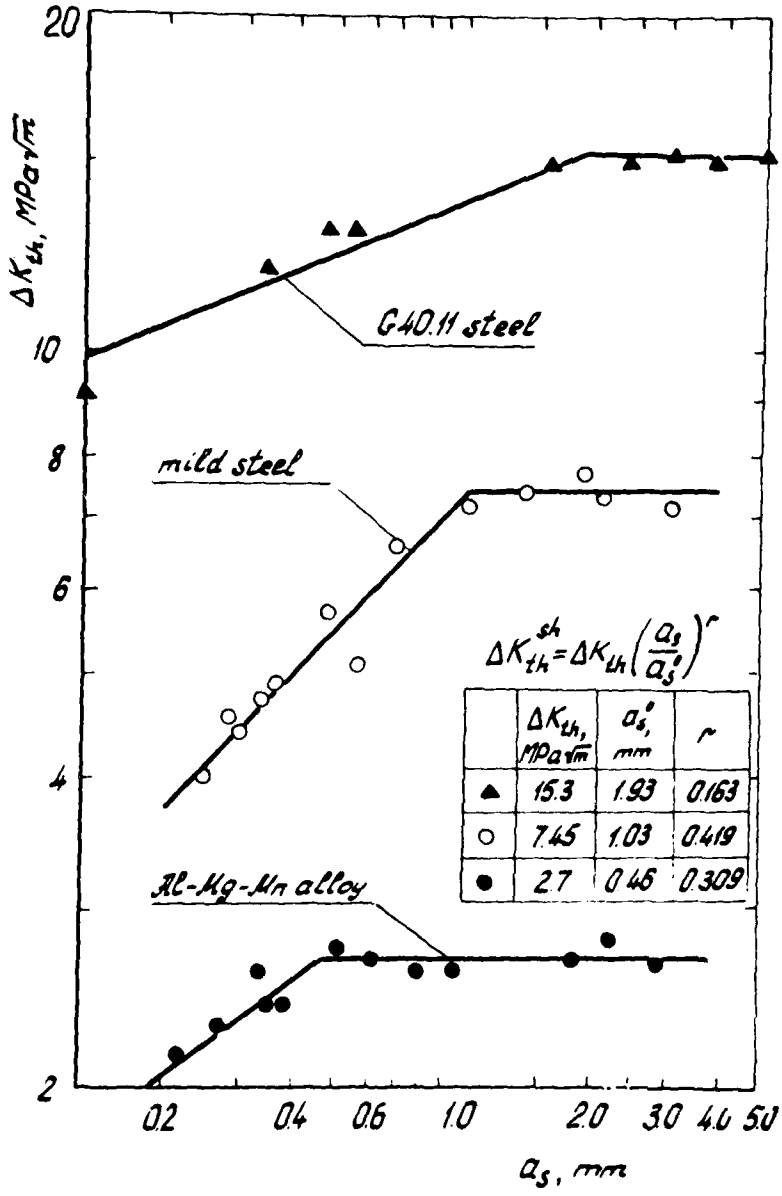

Figure 33 Influence of crack length on ΔK_{th} for an austenitic steel, mild steel and an aluminium alloy (86).

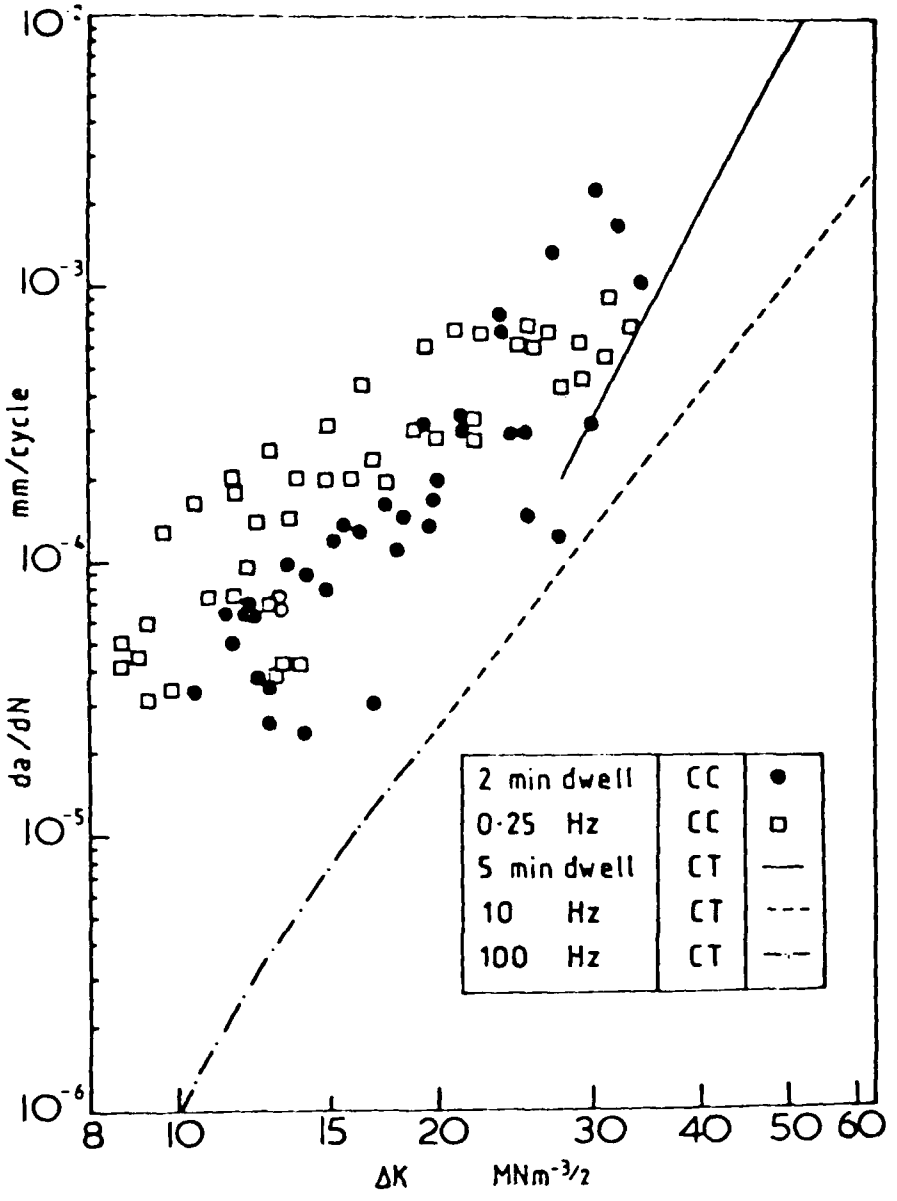

Figure 34 The effect of dwell at maximum load on fcg rates in IMI 685.
CC - corner cracked specimens.
CT - compact tension specimens (87).

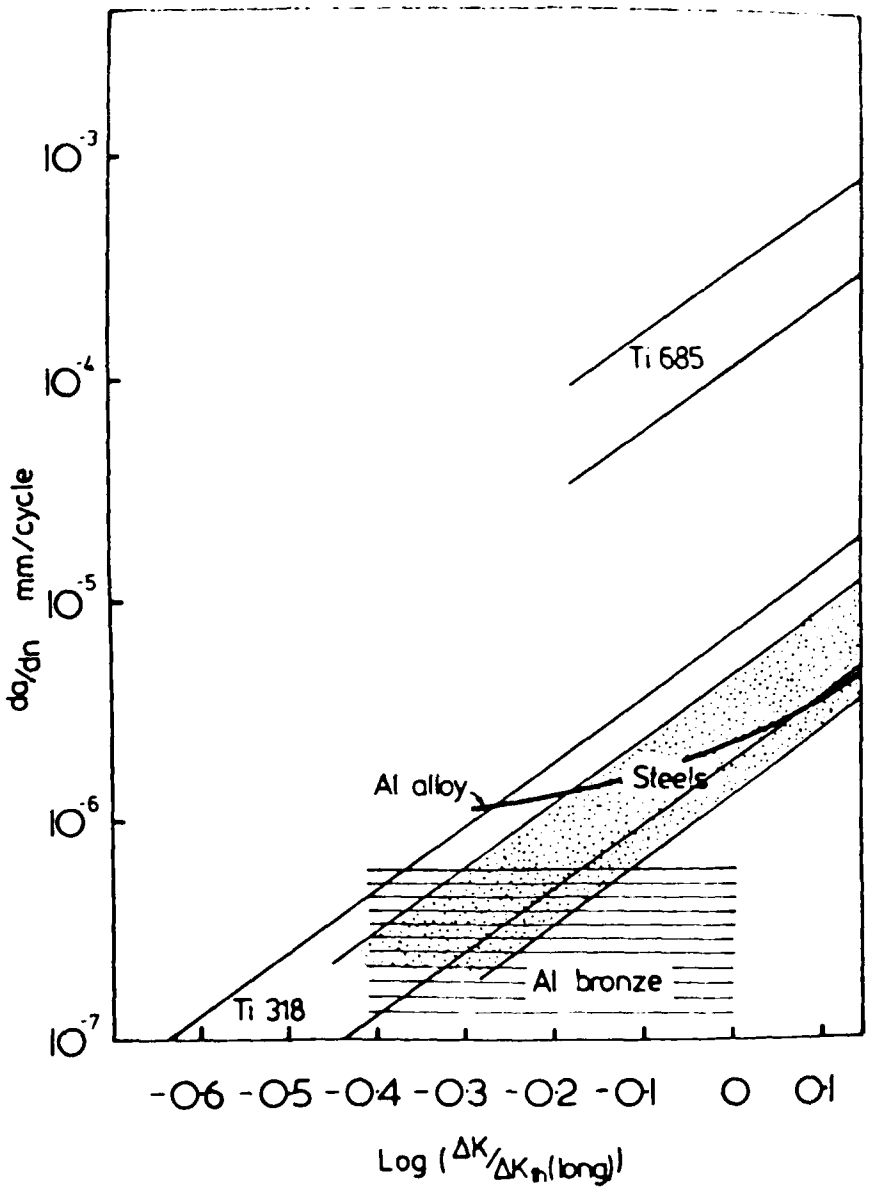

Figure 35 A normalised plot of short fcg data for a range of materials (87).

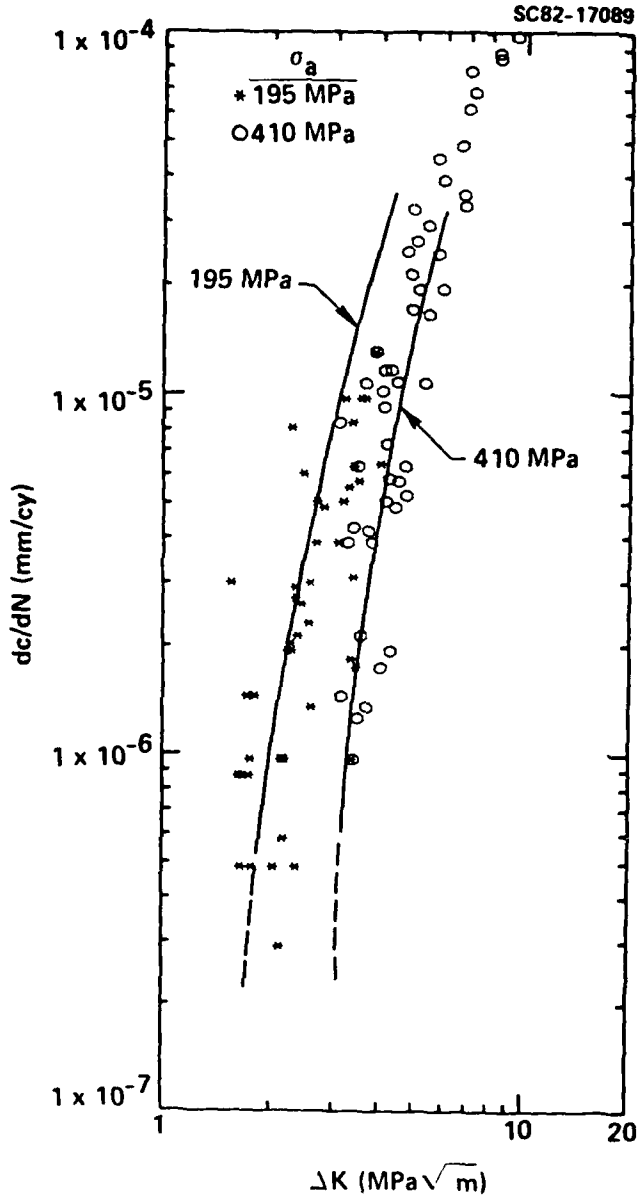

Figure 36 The observed and predicted (full line) fcg rates for short cracks in an Al 7075-T6 alloy (91).

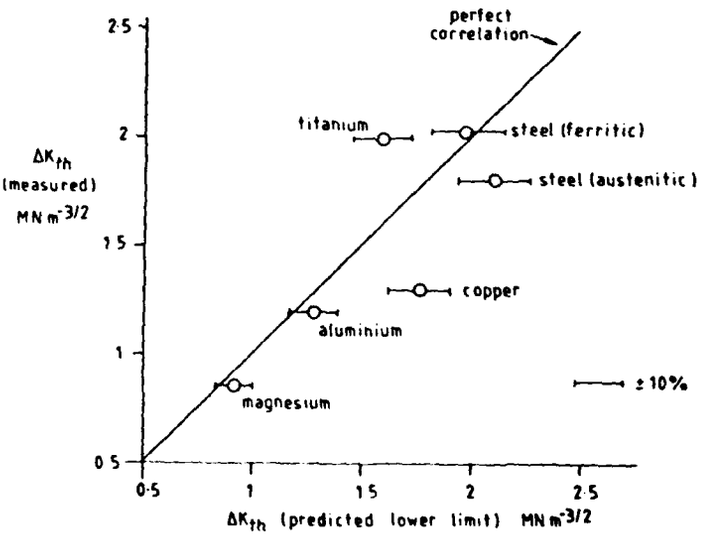

Figure 37 A comparison of observed and predicted values of ΔK_{th} (96).

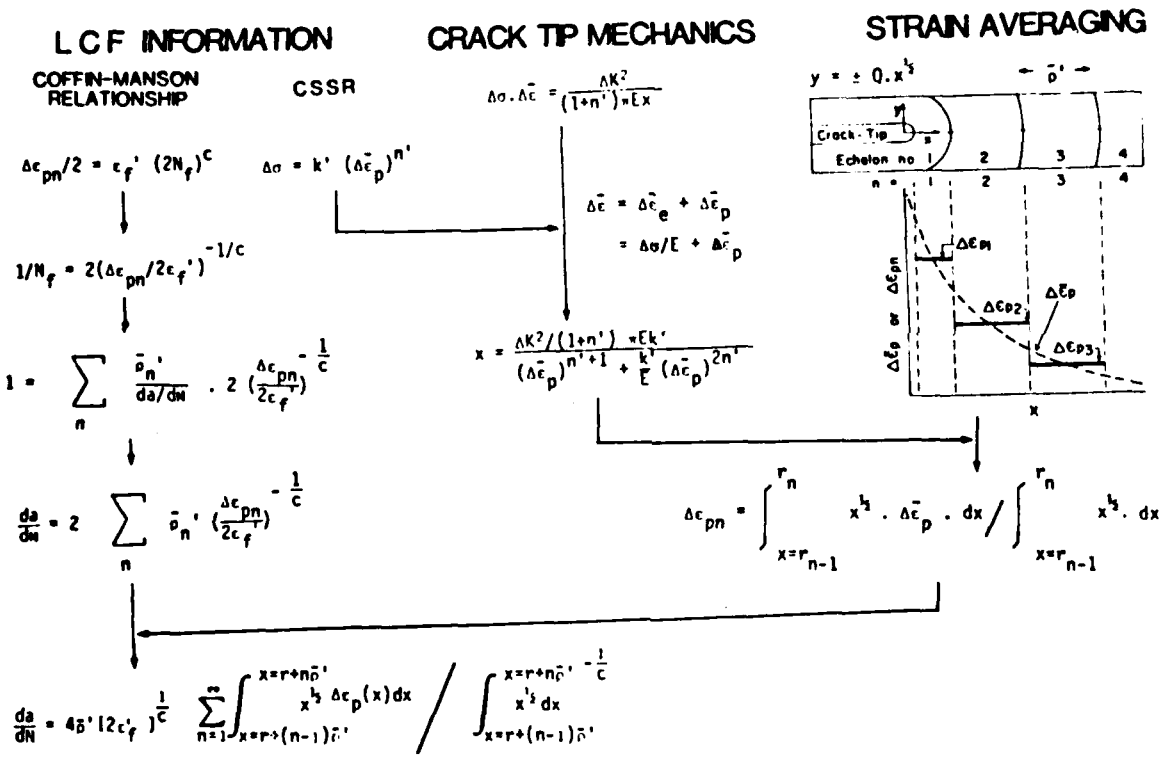

Figure 38 The Chakraborty Model for predicting fcg rates (109).

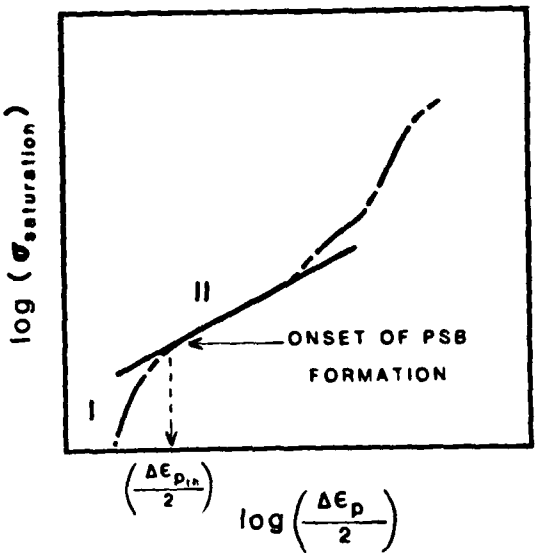

Figure 39 Cyclical stress response of metals and alloys indicating the strain range required for the formation of persistent slip bands (PSBs) (110).

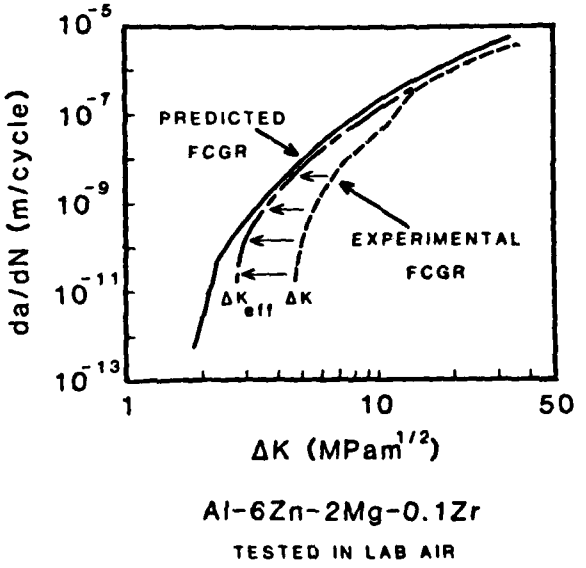

Figure 40 The application of the modified Chakraborty model (109) to an aluminium alloy (110).

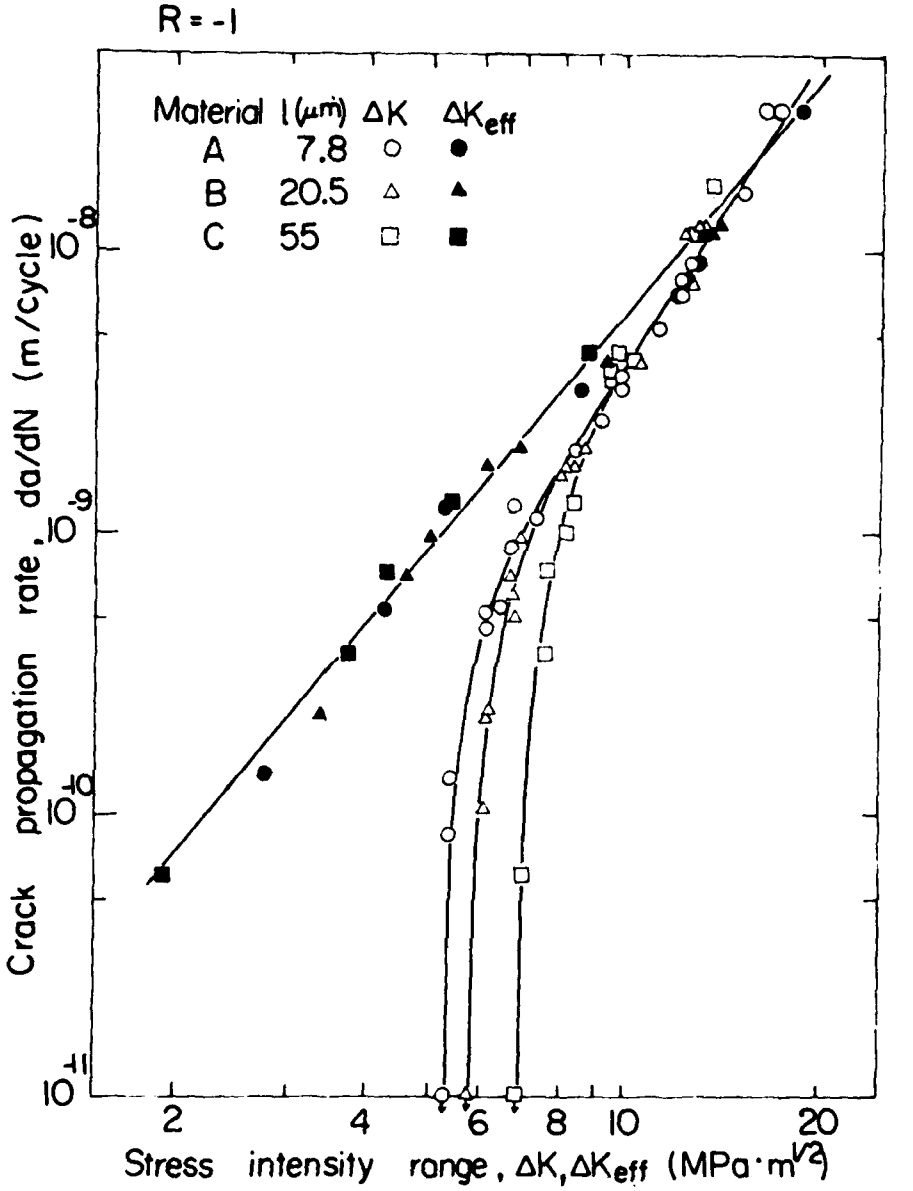

Figure 41 Log ΔK and ΔK_{eff} plots versus log da/dN for a low carbon steel R = -1 (34).

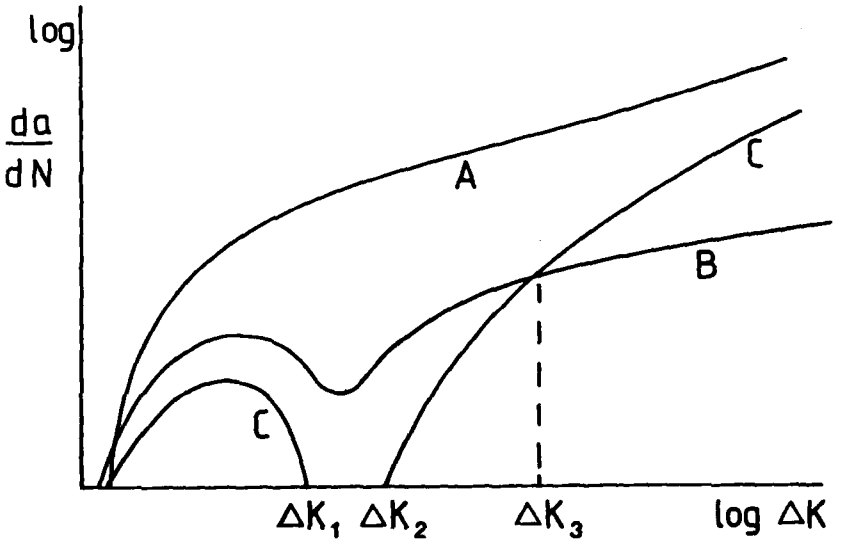

Figure 42 Projected fcg/ΔK response for cracks initiated in single crystals or single grains. A, single crystal, B, intermediate grain size, C, fine grain size, $\Delta K<\Delta K_1$, short crack arrested at grain boundaries. $\Delta K>\Delta K_2$ arrested cracks recommence growth. $\Delta K>\Delta K_3$ fatigue crack closure builds up from the presence of dominantly elastic asperities.

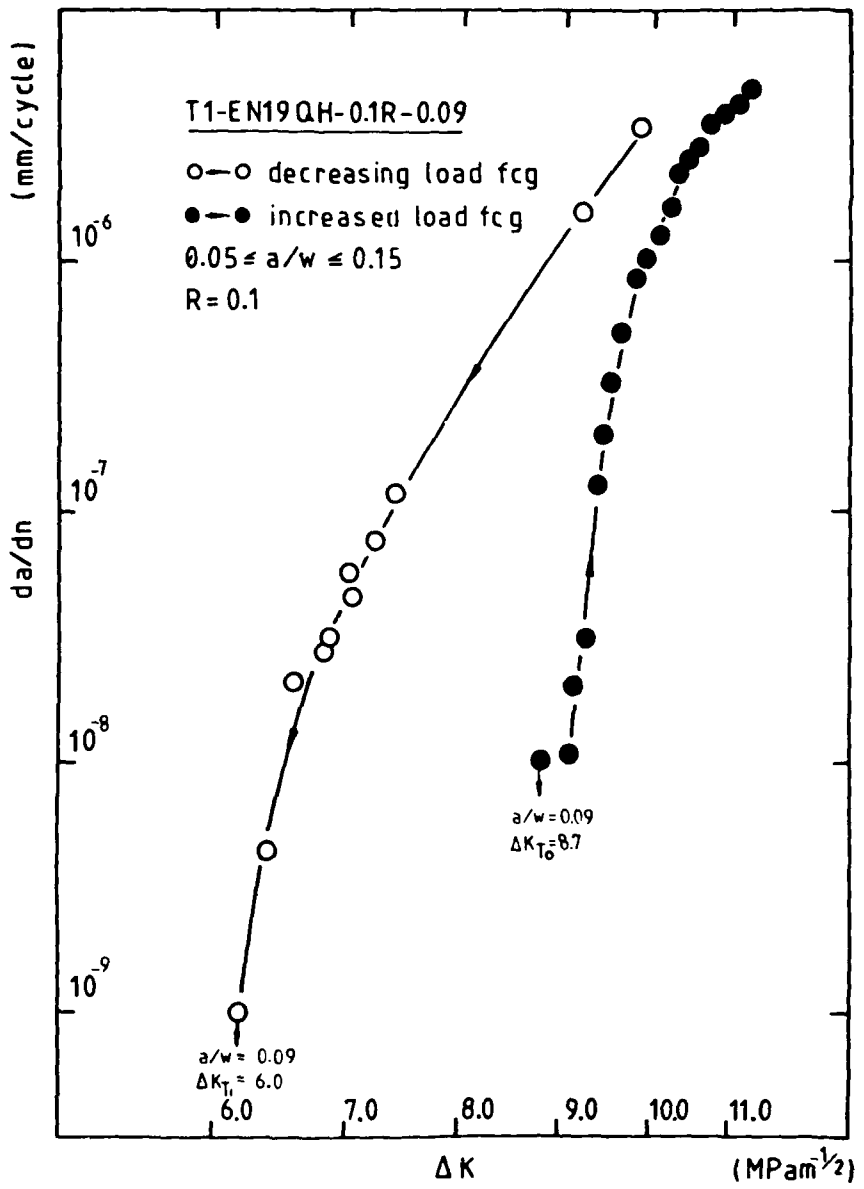

Figure 43 The influence of load decreasing and load increasing test procedures on da/dN and ΔK_{th} for a low alloy steel (114).

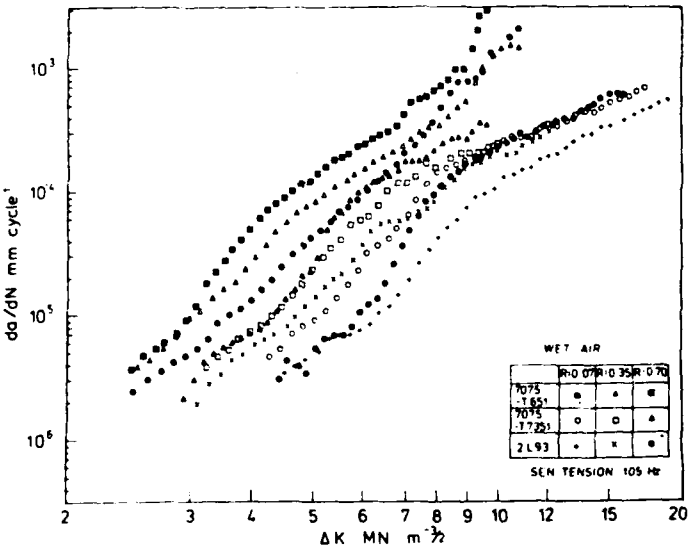

Figure 44 The fcg characteristics of aluminium alloys 7075-T651 and 7075-T7351 and 2L93 tested in wet air, at R=0.07, 0.35 and 0.7 (115).

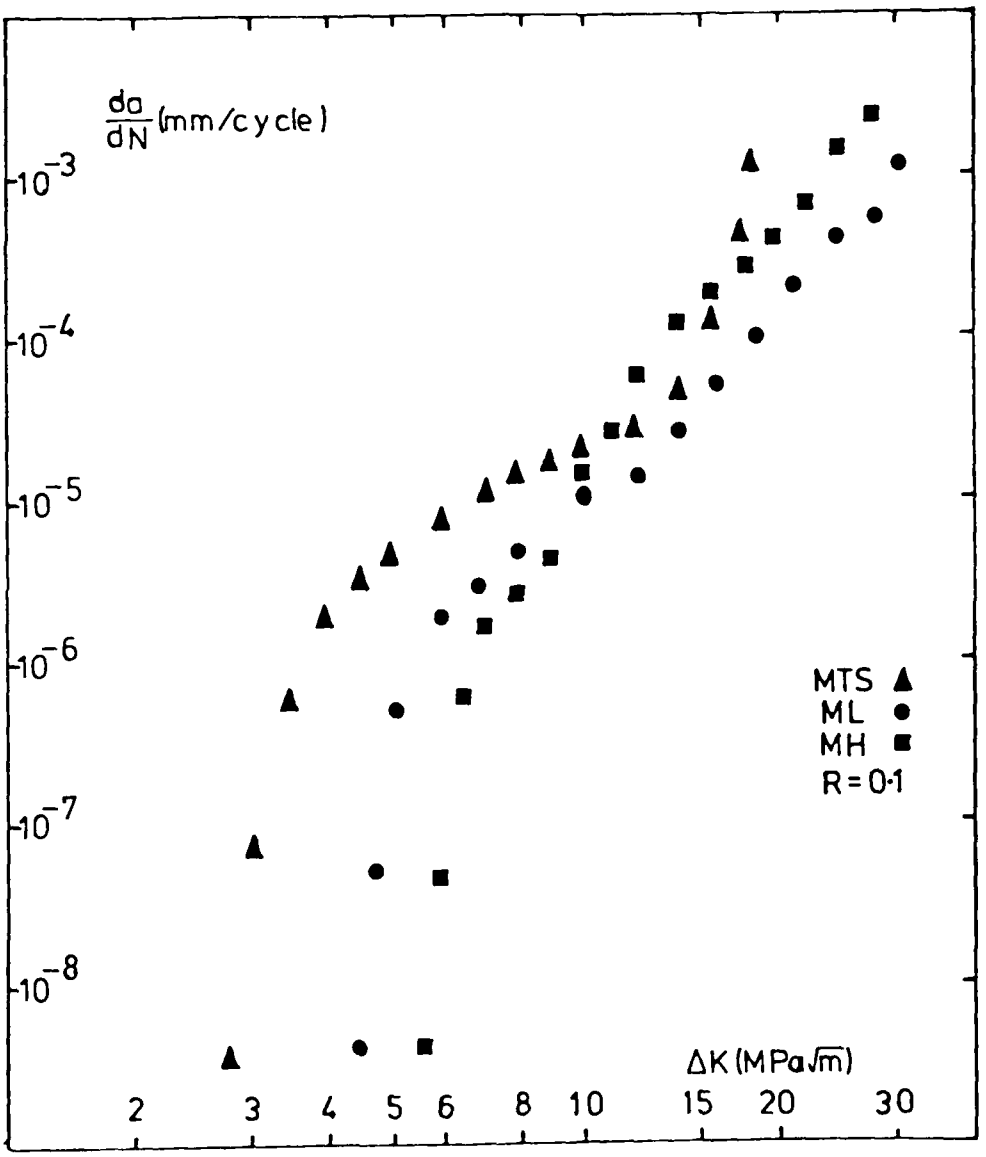

Figure 45 The log ΔK v log da/dN curves for an Al/Mg/Si alloy with Mn additions. The alloy MF has the largest vol. fraction of Al_2Mn_3Si dispersoids (118).

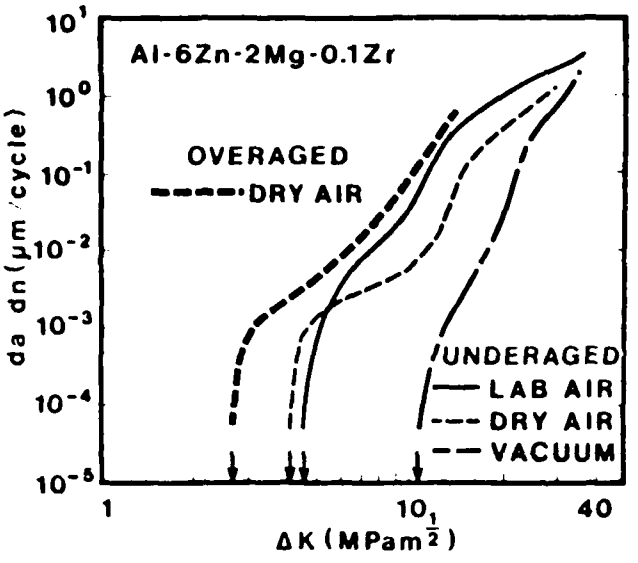

Figure 46 The influence of ageing conditions and environment of the fcg characteristics of a 7XXX series alloy (121).

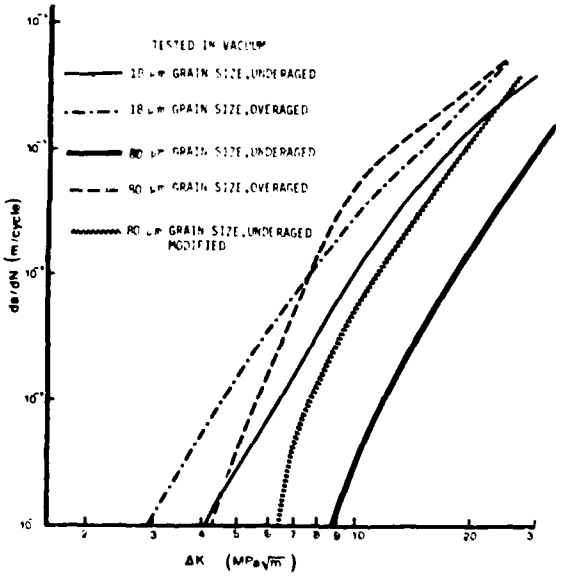

Figure 47 The fcg curves for a 7475 aluminium alloy tested at R=0.1 in vacuum (after E.A. Starke et al.).

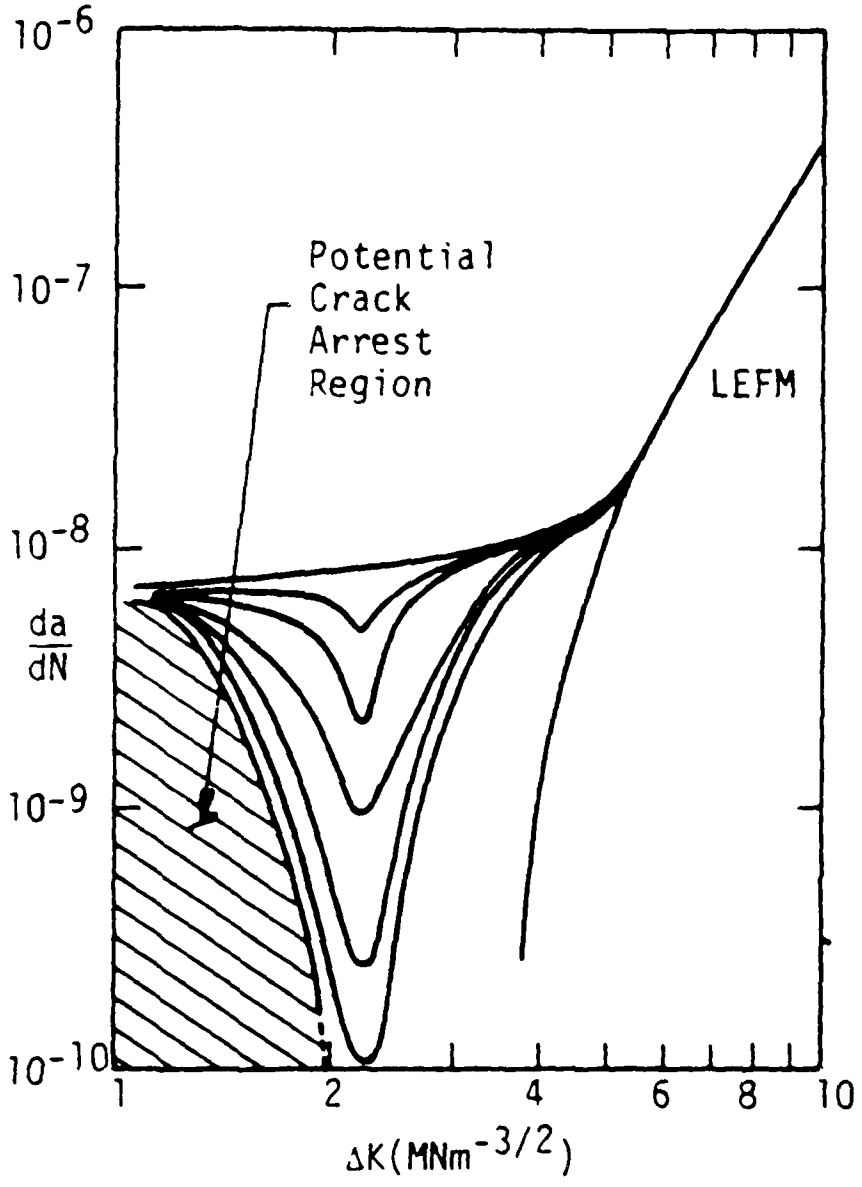

Figure 48 Fatigue crack growth of short cracks in 7075 T6 alloy ($\Delta K < 2\ MNm^{-3/2}$) compared with the growth of long cracks (LEFM) $\Delta K > 2MNm^{-3/2}$ (124).

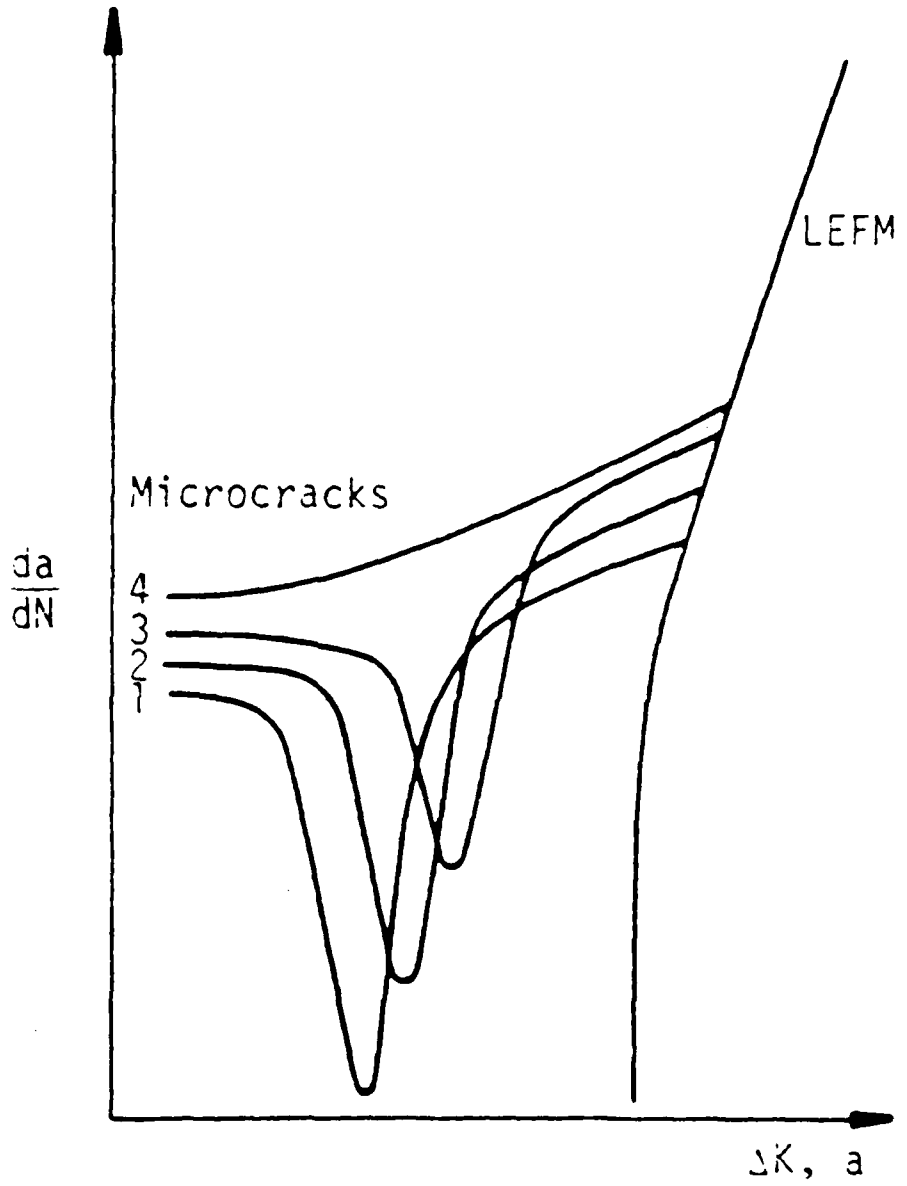

Figure 49 Schematic of the fcg of short crack (microcracks) and long cracks (LEFM) as influenced by grain size (GS) GS 1<2<3<4 (124).

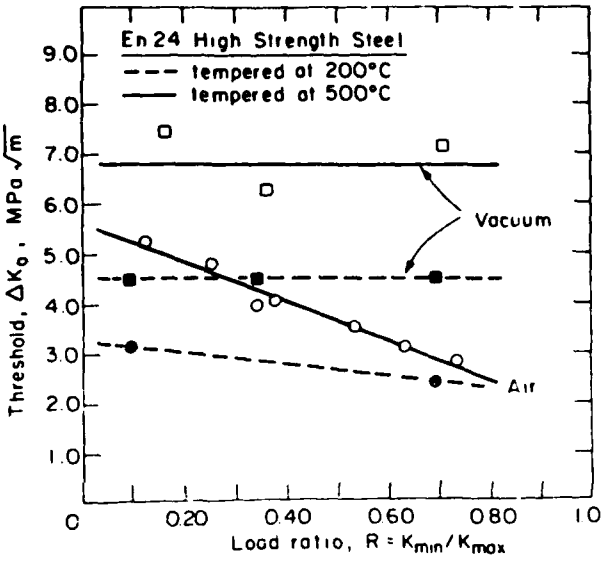

Figure 50 The influence of environment on the fatigue threshold of an En 24 steel at ambient temperatures (6,125).

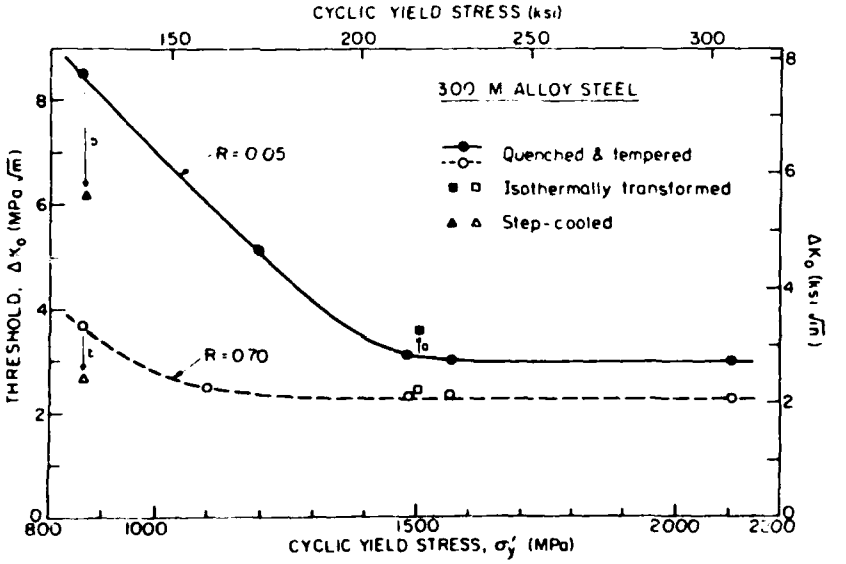

Figure 51 The variation of ΔK_{th} with cyclic yield stress for 300 M steel tested in moist air at ambient temperatures (35).

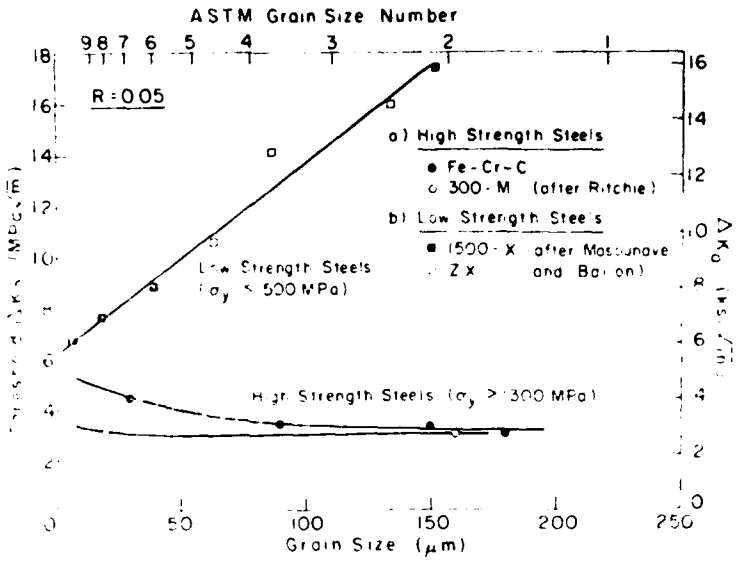

Figure 52 A comparison of the effects of ferrite and prior austenite grain size on ΔK_{th} (35).

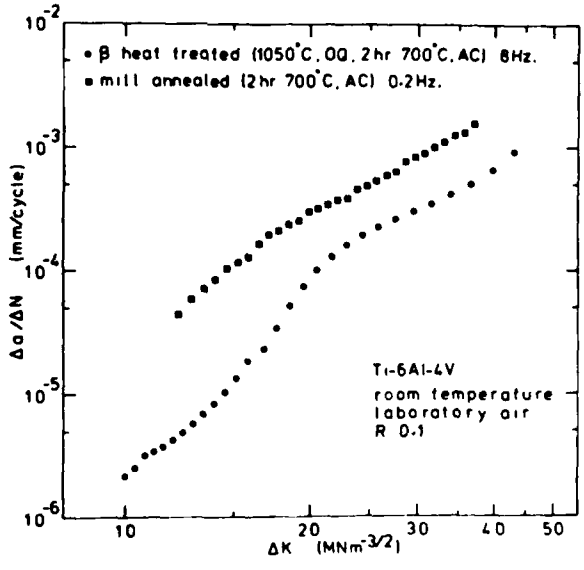

Figure 53 The fcg response of β heat treated and mill annealed Ti 6Al-4V (31).

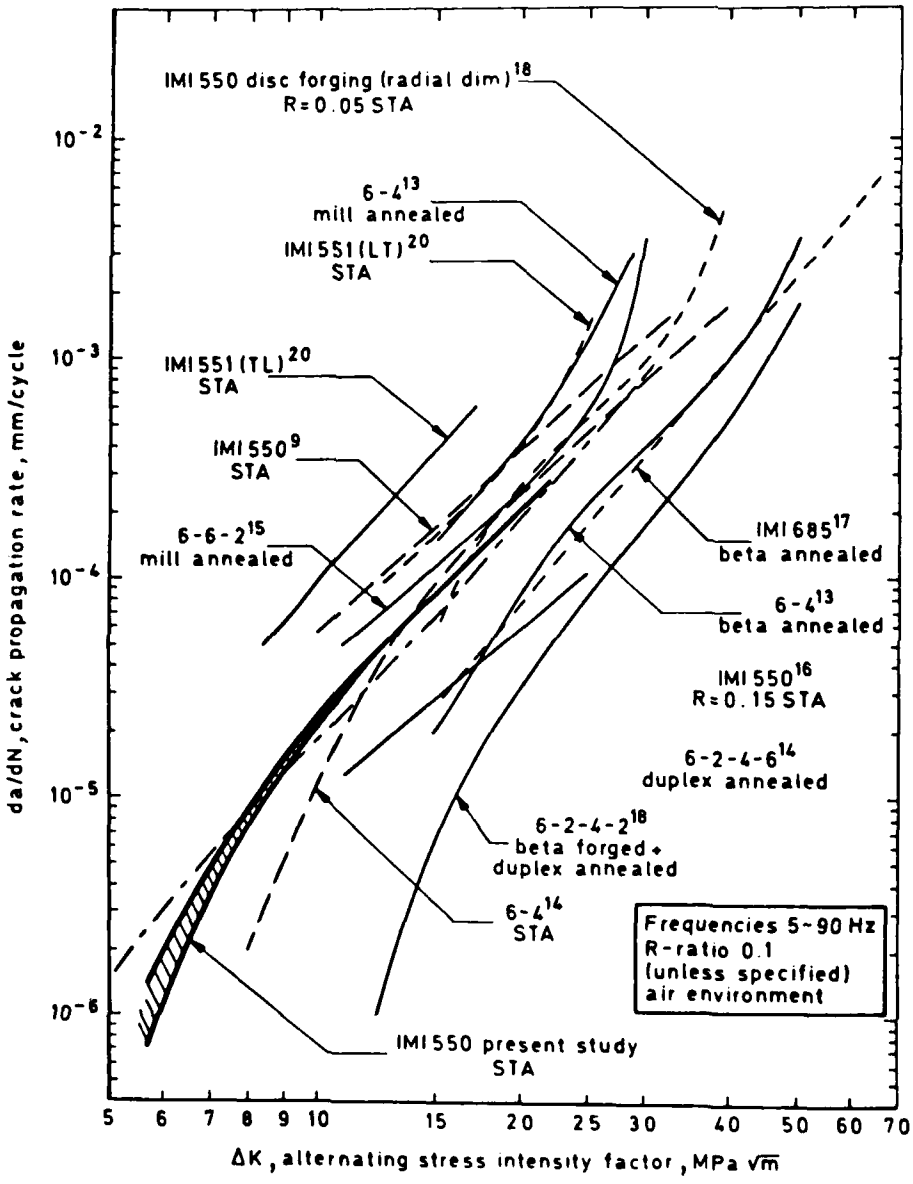

Figure 54 Comparison of the fcg response of a range of titanium α/β and near α alloys (143) after C.M. Ward-Close TR 81079 RAE Farnborough.